Fault rock assemblages and fault architecture in the Møre-Trøndelag Fault Complex

By

Marit Stokke Bauck

27-May-10

Norwegian University of Science and Technology
Faculty of Engineering Science and Technology
Department of Geology and Mineral Resources Engineering

Abstract

The Møre-Trøndelag Fault Complex (MTFC) is a major fault zone, extending along the coast of mid-Norway. It has a prolonged history of reactivation. Three outcrops along parts of the MTFC, known as the Tjellefonna Fault have been described in this study. The focus has been the study of fault architecture and the related fault rocks.

At Vik, more than three sets of fault lenses have developed, bounded by numerous faults in a complex pattern. The faults here are cutting the foliation at a high angle, resulting in the complex fault architecture. For the other localities of Rød and Mulvik, the faults are partly reactivating the Caledonian foliation, making the fault architecture more regular and systematic.

All fault rocks sampled in this study are brittle, and are suggested to have formed at crustal depths of 9 km and shallower. The matrix of the fault rocks is dominated by elongated laths of zeolite. These are torn off from the crystals along the cleavage. At least 3 generations of zeolite are found at Vik and Mulvik. The first generation pre-dates a zeolite-dominated cataclasite. At Mulvik this was followed by another generation of zeolite, two generations of cohesive breccia and a third zeolite generation. One of the last generations are found to be steep sets of extensional fractures filled with zeolite. This zeolite is analysed by XRD and found to be laumontite.

The last activity of faulting is thought to be represented by the uncohesive breccia found at Mulvik. This is related to shears, interpreted as R-shears indicating an overall “northwest side down” sense of movement of this last activity along the fault.

Table of contents

Preface

This work is part of an ongoing project along the Møre-Trøndelag Fault Complex (MTFC) supported by Norwegian University of Science and Technology, University of Uppsala and the Geological Survey of Norway.

I am grateful to my supervisor at NGU, Dr. Per Terje Osmundsen, who has inspired and contributed through field-work, lab-work and discussions. He and his colleague Dr. Thomas Fitzmaurice Redfield have briefed and helped me in field. My supervisor at NTNU, Professor Stephen J. Lippard has been helpful through discussions and giving feedback in the writing process.

For the LIDAR acquisition and processing, I will thank Dr. Aline Saintot and NGU for possessing the instrument and the associated software. She, Martina Bøhme and Dr. Catarina Melchiorre have been helpful during the processing and modelling of the LIDAR data.

Arild Edin Monsøy at the lab at NTNU has prepared the thin sections. Bjørn Willemoes-Wissing at the SEM-lab at NGU have helped and briefed us in the SEM work. The XRD analysis was carried out at the lab at NTNU by Kjell Reidar Kvam.

Trondheim, May 2010

Marit Stokke Bauck

1 Introduction

The Møre-Trøndelag Fault Complex (MTFC) (Figure 1-1) is a major fault complex in Mid-offshore and onshore Norway. It is found at a longitude between 1˚- 12˚E and latitude between 61˚- 64˚N. On satellite photographs and digital elevation models (Figure 1-1), the fault zone is clearly seen, as lineaments, stretching along and defining the coastline of mid-Norway.

The MTFC was established as a sinistral shear system during early Devonian (Watts, 2001). It has experienced several phases of activity after this; involving sinistral transtension, dextral strike slip and dip slip faulting (Grønlie and Roberts, 1989; Grønlie, et al., 1991; Redfield, et al., 2004; Osmundsen, et al., 2006). Parts of the MTFC were active during formation of the offshore Møre Basin in Triassic, Jurassic and Cretaceous time (Gabrielsen, et al., 1999). Major strands of the MTFC, described in detail by Grønlie et al. (1991) are the Hitra-Snåsa and the Verran Faults (Figure 1-1). The lineament described in this study is found further south, and closer to the alpine inland of Møre og Romsdal. It is called the Tjellefonna Fault Zone (TFZ) hereby referred to as the Tjellefonna Fault (Redfield and Osmundsen, 2009). It strikes ENE-WSW and is sub-parallel to Langfjorden (Figure 1-1).

In western Norway, the Tjellefonna Fault of the MTFC constitutes the NW border of the high alpine landscape of Møre og Romsdal County, and the hilly lowland bordering the coastline. The fault zone appears as a pronounced boundary in the landscape. The great contrast in elevation across the lineament may indicate that the fault has been, and probably still is an important factor controlling the landscape of the region (Redfield, et al., 2005, Redfield and Osmundsen, 2009). The mountains are an uplifted fault-block. It has been suggested that the most recent phases of activity along the Tjellefonna Fault should be considered as causal on the landscape-formation of the region. Sea-level apatite fission track (AFT) age patterns indicate that this differential uplift occurred in the Late Cretaceous and/or the Cenozoic (Redfield, et al., 2004).

As displacements have accumulated along the faults in the MTFC, it is probable that assemblages of fault rocks that form are weak relative to the host rock (Watts, 2001). High fracture densities in the damage zones of faults also contribute to the weathering of the fault. Rock slope

failures are likely to occur along such weak zones. The Langfjorden area has experienced one of the largest rockslides recorded in Norway. It took place at Tjelle (Figure 1-1), along the trace of the Tjellefonna Fault in 1756. As earthquakes are recorded in the region, Redfield and Osmundsen (2009) speculated whether the rock slide at Tjelle was triggered by an earthquake.

It is important to understand and learn how the fault has been active. The local communities want to know whether and how rockslides may occur in the future. The rock slide at Tjelle can be related to the fault structures in the area, and it is speculated that it was triggered by an earthquake. Therefore it is important to understand whether the fault will be active in the future, and if and how weak the fault zone is.

It is important to consider the role fault zones has in landscape formation and possible geohazardous impact on the surrounding communities. Understanding the mechanisms and processes acting in these zones is of importance. To better understand the impact the faulting has on the strength of the rock, and to learn whether or not a fault is presently active, will help predicting its prospective potential instability.

This thesis presents detailed descriptions of fault architecture and brittle fault rocks at three localities along the Tjellefonna Fault. It should be considered as a detailed contribution to geophysical NGU project, trying to image the MTFC at depth.

During four weeks of fieldwork in the Langfjorden/ Tjelle/ Rød/ Tingvoll area, the fault architectures and fault rocks were studied in detail at the three localities. Two of the localities are scanned with Light Detecting and Ranging (LIDAR), and the data were processed and interpreted. Detailed line drawings and figures were prepared to improve our understanding of the fault architecture and its development. In addition, brittle fault rocks from the three fault localities were sampled and analysed in the optical microscope, the Scanning Electron Microscope (SEM) and an X-Ray Diffractometer (XRD).

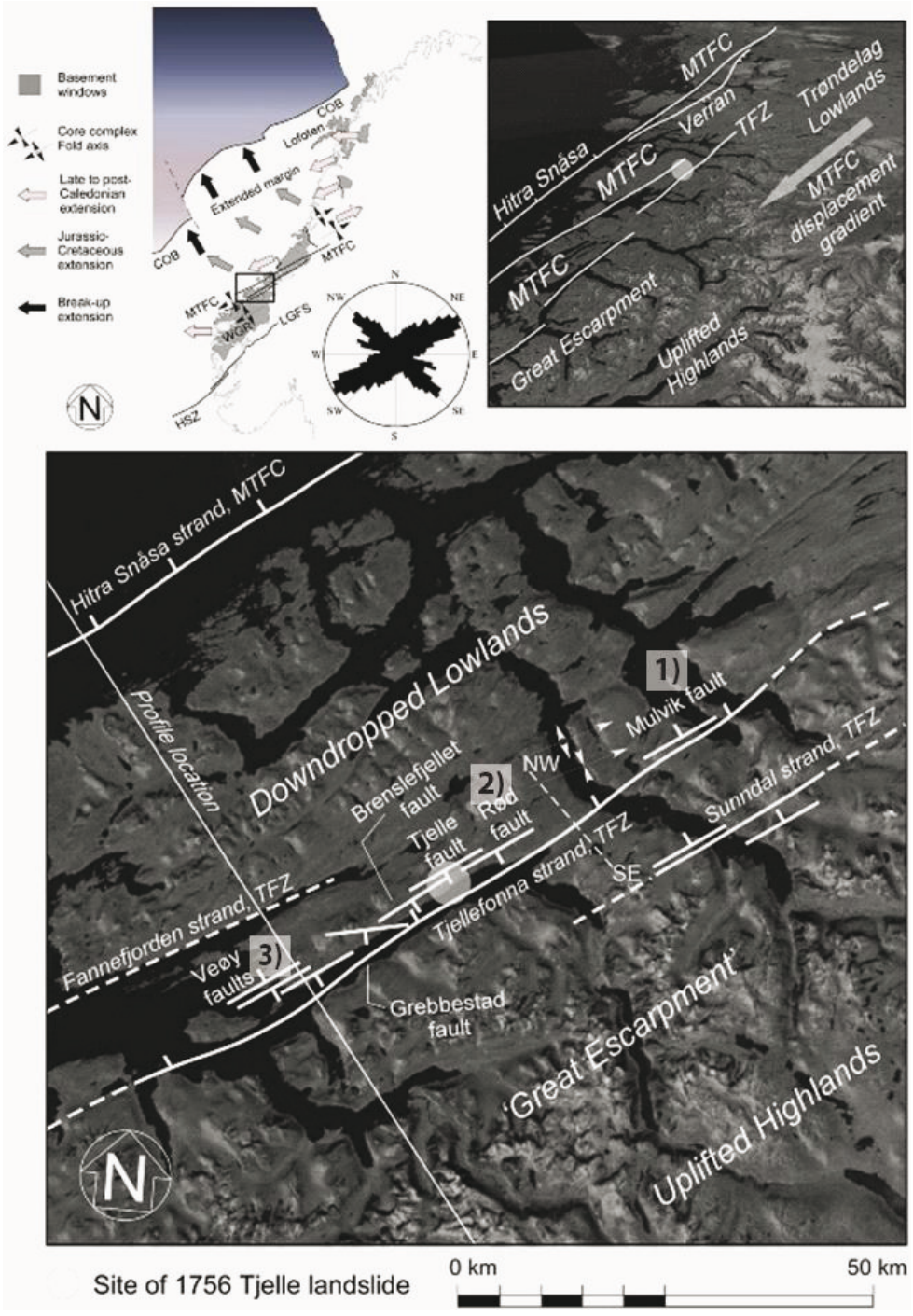

Figure 1-1: Showing the location of the three localities found along the Tjellefonna zone in Møre og Romsdal from Redfield and Osmundsen 2009. Locality 1) Mulvik fault, locality 2) Rød fault and locality 3) Vik fault, close to Veøy fault. The additional locality of Tjelle fault are found close to Rød fault, and the site of the Tjelle landslide are marked wih a white circle

2 Background

2.1 Regional geology

2.1.1 Bedrock geology

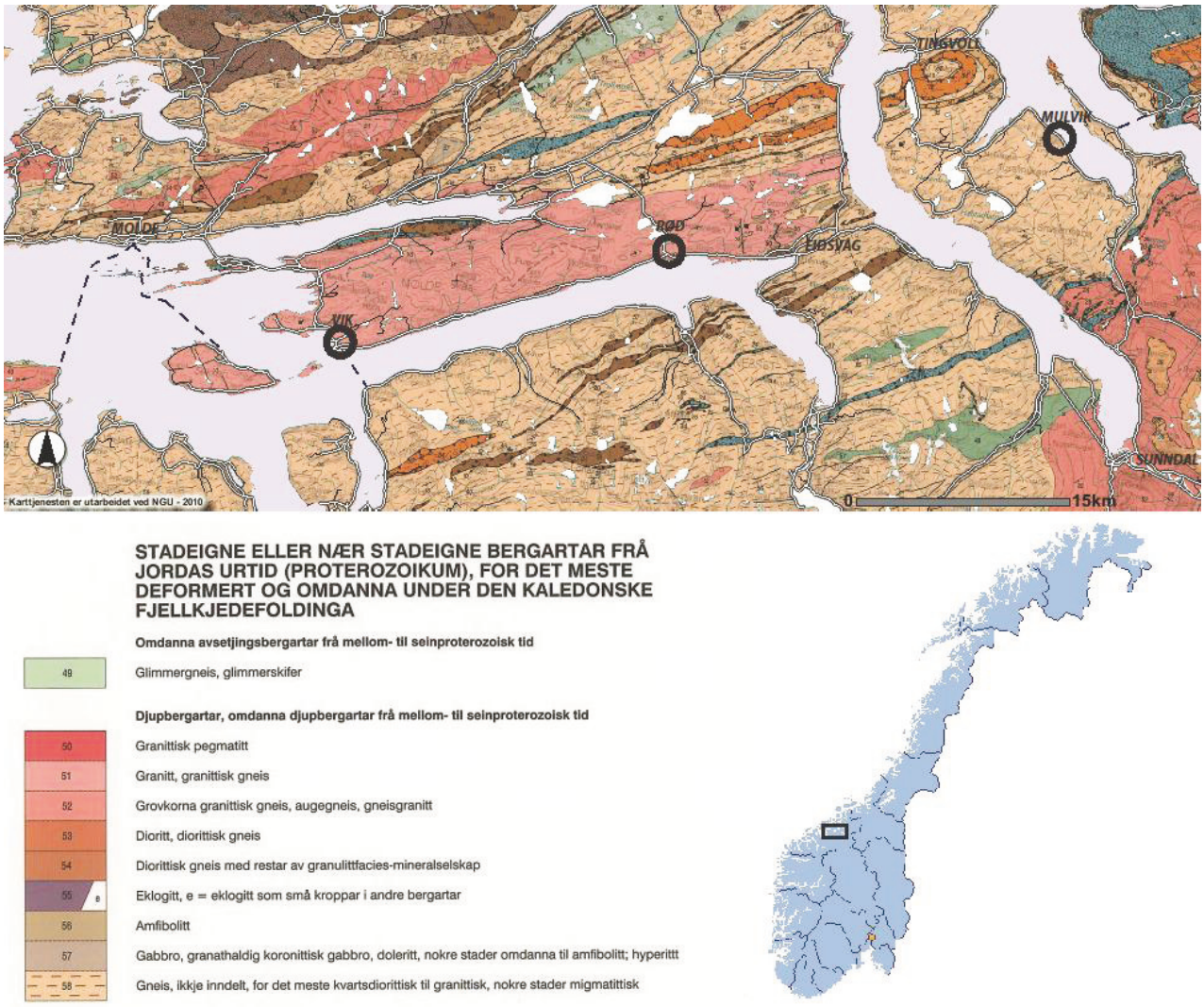

Figure 2-1: The geological map of the field area, prepared by NGU, N250 Berggrunn (www.ngu.no/no/hm/Kart-og-data/). Granitic gneiss and gneiss are the dominating bedrocks.

Chapter 2

Large parts of north-western Norway consist of a Precambrian bedrock-province called the Western Gneiss Region (WGR), seen on the upper left part of Figure 1-1.The eastern part of the WGR is dominated by felsic intrusives and gabbros (Koenemann, 1993). The localities described in this study are in an area, where there are some minor Sveconorwegian intrusions of gabbro and granite, but in general, the bedrock of the study area is plagioclase-rich gneiss. On the lower part of Figure 1-1 and in Figure 2-1, the location of the studied localities, 1) Mulvik, 2) Rød and 3) Vik are displayed. From the geological map of 1:250 000, shown in Figure 2-1, the bedrock of the field area is granitic gneiss and gneiss. More detailed mapping are done in the 1:50 000 map sheet of Stangvik (Krill, 1987) where the bedrock at locality 1) Mulvik is granitic to granodioritic gneiss, and the 1:50 000 map sheet of Tingvoll (Bryhni, et al., 1991), granitic gneiss is registered at locality 2) Rød without further classification.

2.1.2 Location of the study area and the 3 main localities

The Tjellefonna Fault is a part of the MTFC. The master fault is suggested to be located in the fjord of Langfjorden (Figure 2-2) (Redfield and Osmundsen, 2009), with a steep dip towards the north. The three fault outcrops studied here are found in road cuts along the Tjellefonna Fault. An overview of the following localities is displayed in Figure 1-1.

1) The outcrop at Mulvik (8˚25’ 36’’ E, 62˚51’ 39’’ N) in Ålvundfjorden displays a 140 m long road section with faulted rocks. It has several fault cores, and three of these were described. The largest exposed fault core is approximately 6 m wide, displaying a rich ensemble of fault rocks. This fault core probably represents the master fault or an important fault strand of the Tjellefonna Fault, as suggested in Figure 2-2. The faults found at Mulvik are close to vertical with a slight dip towards the north. The main fault core has an orientation of approximately 250/80.
2) The outcrop at Rød (7˚53’ 36’’ E, 62˚46’ 4’’N) is close to Tjelle along road 62. Its core consists mainly of protobreccia cut by zeolites in an extensional duplex. This core is defined by a zone of crushed and partly incohesive gouge and fault breccias, below and above the extensional duplex. Orientation of the fault is 086/66 +58, which is sub-parallel to the host rock foliation.

3) This outcrop is in the opening of Vik tunnel on road 64 by the mouth of Langfjorden (7˚27' 15''E, 62˚41' 26''). The outcrop exposes the main fault plane, dipping towards the south, and several antithetic and synthetic faults. The outcrop gives a 3-dimensional impression of the fault architectures, with several fault cores, that are bounding sets of fault lenses. One of the antithetic faults has a well developed fault core, displaying rotated fault lenses. The master fault at Vik has an orientation of 087/ 80.The most developed fault core at Vik is of an antithetic fault with an orientation of 239/70.

In addition, one fault outcropping close to the Tjelle (7˚52' 17'' E, 2˚46' 2'' N) rockslide is described. Its location relative to the Rød fault are shown in Figure 1-1, and in the conceptual block diagram of the area, by Redfield and Osmundsen (2009), in Figure 2-2. The fault shows similar architecture, orientation and fault rocks as the three main localities. This fault has an orientation of 063/80.

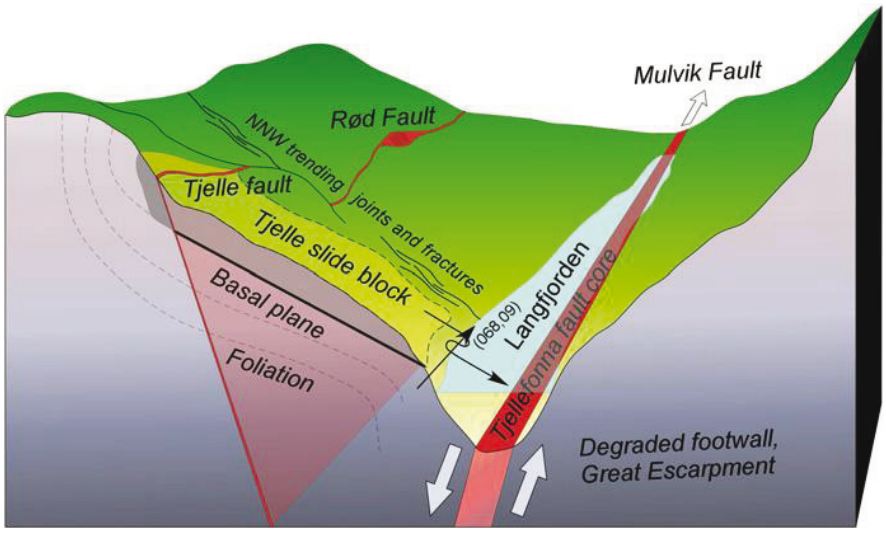

Figure 2-2: A conceptual model of the Tjellefonna Fault, displaying locality 1) Mulvik, 2) Rød and the Tjelle fault behind the Tjelle rockslide. (From Redfield and Osmundsen, 2009).

2.1.3 The Møre-Trøndelag Fault Complex (MTFC)

The MTFC is a regional-scale set of lineaments with a prolonged history of deformation. The complex consists of several fault strands that commonly reactivate the flanks of upright folds (Seranne, 1992). It can be traced from Snåsa to Stadt in a NE-SW direction, and it defines the

coastline in parts of Møre and south-Trøndelag. It has been tectonically active in several stages, starting with ductile sinistral shear in late Silurian to early Devonian, followed by several periods of brittle faulting (Late Devonian/Early Carboniferous, Permo-Carboniferous, Post-Mid-Jurassic, Late Jurassic to Early Cretaceous and Late Cretaceous). Permo-Carboniferous sinistral transtension resulted in the formation of cataclasites and pseudotachylyte, and established a set of N-S trending fractures (Watts, 2001). In post-Mid Jurassic there was dip-slip faulting, followed by dextral strike-slip faulting (Grønlie, et al., 1991; Watts, 2001). This event was the main period of hydrothermal faulting related to zeolite mineralizations (Grønlie, et al., 1991). During Late Jurassic to Early Cretaceous, dip-slip normal faulting is documented in a WNW-ESE extension (Bering, 1992). In the Cenozoic, the extension direction has changed to NNW – SSE, giving a total change of 90˚ compared to the late to post Caledonian extension. The latest extensional direction (marked with black arrows in upper parts of Figure 1-1) is therefore at a high angle to the fold axis of the Caledonian folds.

The brittle faults of the MTFC partly coincide with the flanks at steep Caledonian folds (Seranne, 1992, Osmundsen, et al., 2006). This is the case in the studied area of Langfjorden, where a Caledonian anticline, running parallel to the fjord, is reactivated by the brittle faulting (Redfield and Osmundsen, 2009). Some activity along the MTFC has been associated with pulses of hydrothermal activity, particularly in post-Mid Jurassic (Grønlie, et al., 1991).

A recent publication by Redfield et al. (2005), show how apatite fission track data indicate that the MTFC has been active as a normal fault in or after the Late Cretaceous. It may be active today, as 280 earthquakes on the magnitude of 1.1 to 4.6 Mw (moment magnitude) are registered in Møre og Romsdal (Redfield and Osmundsen, 2009). In theory these earthquakes could be a triggering factor for rockslides, albeit this remains a speculation.

2.1.4 Fault control on topography

Redfield et al. (2005) observed that the high topography in Møre og Romsdal is bounded by the strands of the MTFC. These authors further suggested that both the sea-level AFT age-patterns and the large-scale topography could be explained by Late Cretaceous or younger faulting in the MTFC, with increasing displacement towards the southwest.

In Møre og Romsdal there is a great contrast between, the high alpine landscape of Romsdalen, south/south east of Tjellefonna strand (Figure 1-1), and the more gentle topography to the north/north-west. The Tjellefonna Fault has been interpreted to be a tectonically defined boundary (Osmundsen, et al., 2010), where the southern part represents an uplifted and glacially eroded fault block. The hanging wall is in the north, and is represented by gentle lowlands. This contrast in landscape across the Tjellefonna Fault indicates that the active normal faulting affected the landscape evolution of the region. An ongoing project at NGU has tried to detect the Tjellefonna Fault, using different geophysical methods, including gravity and magnetic measurements, refraction seismic and 2D resistivity imaging.

2.1.5 Tjelle rock slide 1756

In February 1756 a major rockslide fell into Langfjorden from the hill of Tjelle. The Tjelle rockslide released 15.7 million Cubic metres (Redfield and Osmundsen, 2009) of rock, resulting in several tsunamis that washed out the surrounding settlements, killed 38 people and destroyed several houses and boats. Along the slide-scar, steep sets of fractures, as well as the penetrative main foliation, are dipping towards Langfjorden. A fault is also found in the bedrock, close to the top of the avalanche, showing similar fault rocks and orientations as the 3 main outcrops of this study. This is described informally as the Tjelle fault (Chapter 4.4).

Western Norway has experienced several similar events in the past, in Loen (1905 and 1936), Tafjord (1934) and Skafjellet (1731) (Redfield and Osmundsen, 2009). In order get an overview of future hazards, it is important to investigate and try to understand the mechanisms and physical behaviour of such weak fault zones, and to understand, to what degree these mechanisms controls rock slope failure. Fault zone microstructures and associated fault rocks can be directly related to the probability of rockslides (Henderson, et al., 2010).

2.2 Fault architecture and fault products

As approximately 90% of the released energy of an earthquake goes into rock deformation (Sibson, 1977) a prominent transformation of the involved rocks will take place. Once formed, a fault zone is often active through long periods of time at different crustal depths. One should be aware that the exposed fault structures and fault rocks are probably dominated by

the most recent events of faulting, which often in exposed outcrops have occurred at relatively shallow crustal depths. Products from these events tend to dominate and overprint older products.

2.2.1 Fault mechanisms

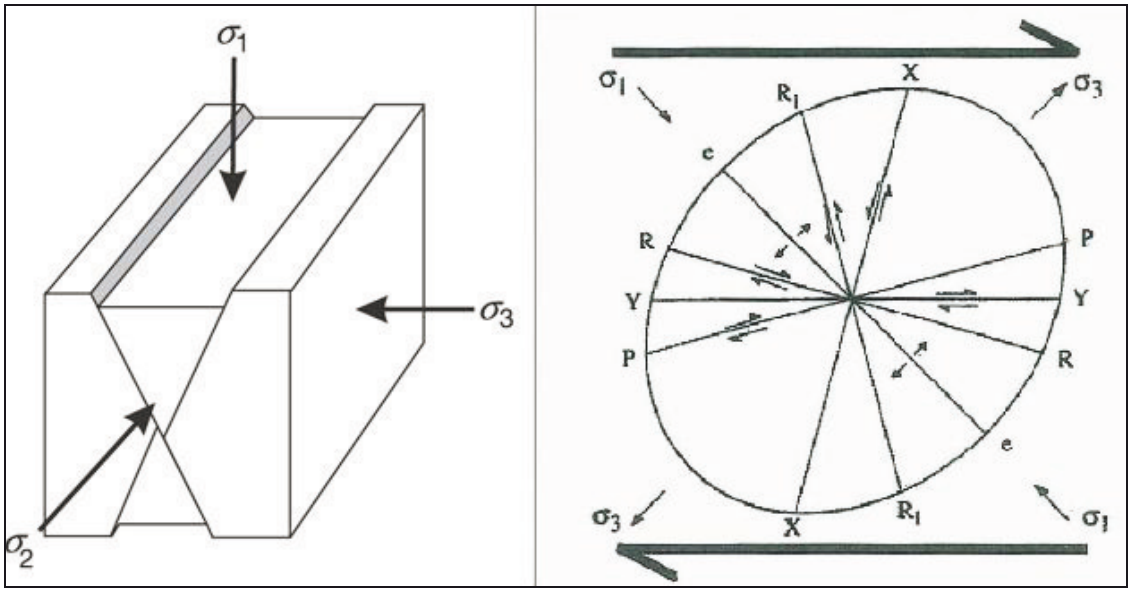

Figure 2-3: To the left: Principal stress axes in a normal fault. (From Healy et al., 2006). To the right: Displaying principal shears that develop in a simple shear system (Watts, 2001). Being R and R_1 Riedel-sears, P-shears, X-shears, Y-shears and e, which is extensional joints.

Stress in a rock is defined along three orthogonal principal stress axes, which together defines the stress ellipsoid. The three stress axes are the maximum (σ_1), intermediate (σ_2) and minimum (σ_3) stresses (left part of Figure 2-3). In normal faults, the maximum stress axis is vertical, as shown in the left part of Figure 2-3. Mechanisms that can produce kinematic heterogeneity are: anisotropy reactivation (for example reactivation of the foliation), triaxial deformation, strain compatibility constraints and/or multiple deformations (Marrett and Allmendinger, 1990).

Grain size reduction

When faulting occurs in the Elastico-Frictional regime, the protolith will experience different processes due to frictional flow (Henderson, et al., 2010). Three processes can lead to grain size reduction (GSR): 1) Feldspar alteration, 2) constrained comminution and 3) selective fracturing of larger particles (Blenkinsop, 1991). The latter author suggested that, the dominating particle

size reduction process in Cajon Pass drillhole is alteration by laumontization of feldspars. This resulted in larger particles than deformation by shearing.

Mechanism leading to GSR are 1) intra-granular or 2) a process of particle abrasion (particle-margin fracturing) (Henderson, et al., 2010). According to these authors, intra-granular fracturing of a grain results in 2 particles of equal size. Abrasion leads to a bimodal distribution of grains, where the matrix consists of elongated particles and larger grains will be more rounded. The two processes do not necessarily occur separately, but compound in complex ways.

2.2.2 Kinematics

Kinematics is the study of the movement of the rock from undeformed to deformed state. Sense of shearing can be reverse, normal, strike-slip or oblique slip. The kinematics of a fault can be revealed by kinematic evidence for movement direction that were made under deformation. Brittle and ductile kinematic indicators are somewhat different.

The type of shears and fractures created in relation to faulting are defined by Riedel, (1929). They are seen in the right part of Figure 2-3. These shears are applicable at all scales. Three sets of synthetic shears are defined, being P-shears, Y-shears and R-shears. Their angle to the main fault, depend on the mechanical strength of the rock. R-shears are common in normal faults. They are usually at an approximate angle of 15˚ to the imposed fault. P-shears are at an approximate angle of 10˚ to the fault, whilst Y shears are close to parallel to the fault. R_1 and X-shears are antithetic shears. R_1-shears are conjugate shears, at an approximate angle of 75˚ to the fault. Extensional fractures are commonly filled with minerals, and they are orientated at a high angle to σ_1 (Figure 2-3). The orientation of all the fractures seen in right part of Figure 2-3 can give an indication on relative movement of the fault.

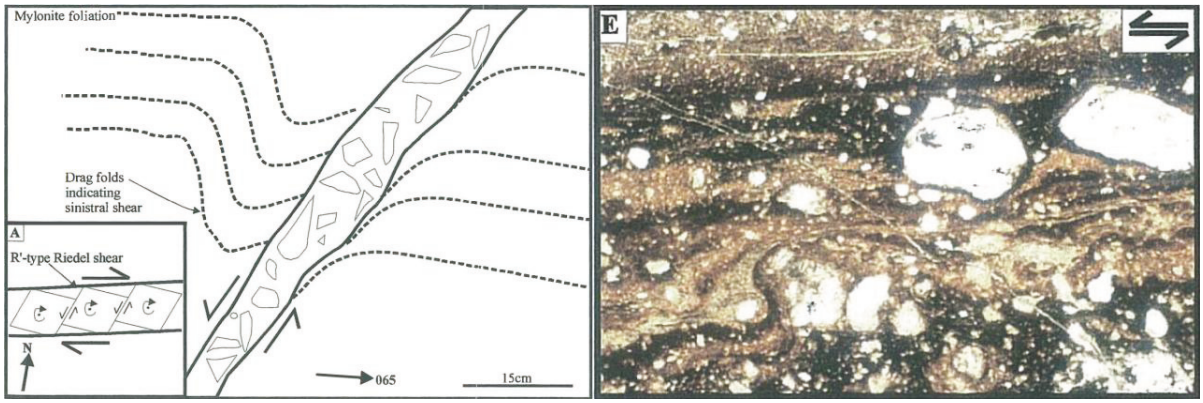

Figure 2-4: Examples on kinematics from Watts (2001), Figure 6.38, to the left: Plan view sketch of a zeolite and calcite mineralised breccia from Verran Fault Zone. The foliation rotates towards the fault core indicating sinistral shear. Inset A) shows that the breccia fragments within the fault core have synthetically rotated R_1 type Riedel shears, formed during a period dextral strike slip movement of the fault. To the right: Plate 7.6 E: Compositional banding of pseudotachylyte. It is folded in a sinistral-verging fold.

At the macroscopic scale, kinematic indicators include rotation of the foliation towards a zone of intense deformation/comminution. This is seen in the example from Watts (2001), seen in Figure 2-4, where the rotation of the foliation indicates a sinistral strike slip movement. On this figure another kinematic indicator can be seen within the fault core, where the breccia fragments are faulted by R_1 shears. The breccia clasts are synthetically rotated during dextral strike slip movement, differing from the sinistral strike slip post-dating and dominating this outcrop. Other macroscopic shear sense indicators can be vein asymmetry or fold overturning. Shear indicators can be slickenlines, grooves, etc.

In this study the evident deformation seen is mainly brittle, and the main kinematic indicators are mainly geometries, fracture geometries and slickenlines. Slickenlines are tectonic striations or fibre lineations found on a fault plane. Fibre lineations are made when minerals are growing on a surface, as it is opened (Fossen and Gabrielsen, 2005). The minerals will then grow in a preferred direction. If the fracture is an extensional fracture, the mineral prefer growing at a high angle to the surface, or obliquely if the fracture has opened obliquely. When striations are evident in a fracture plane they are called slickenside. Brittle deformation on microscopic scale may result in rigid faulting of the porphyroclasts in synthetic shears or also result in domino-faulting of the porphyroclasts.

Parts of the brittle deformation might be vulnerable to more intense deformation, and may therefore show kinematic indicators associated with viscous deformation, like in the left part of Figure 2-4, where the banding is folded. It is important to look for general indicators on a rock-mass, and not misinterpret such local structures to be key structures for the whole rock mass.

Viscous creep result in a more deformed rock, and shear sense indicators include: S-C and S-C[1] fabrics, σ-type, δ-type porphyroclasts, asymmetric myrmekite, quarter mats and folds, mica-fish, garnet spirals, pressure shadows and fibres (Watts, 2001). All these are shown in an overview figure in (Watts, 2001), but will not be described any further here.

2.2.3 Fault architecture

The architecture of a fault zone is controlled by lithology, pre-existing structures, magnitude of displacement and degree of strain localization (Caine, et al., 1996 and Faulkner, et al., 2008). Other controlling factors can be through-going fluids, and the chemistry of these.

Faults are rarely continuous planes; they are complex zones of deformed material that vary in three dimensions (Wibberley, et al., 2008). If the deformation is strain-softening, prolonged faulting tends to occur along older fault planes, often by asperity bifurcation faults (Figure 5-1). Wibberley et al. (2008) suggested that a seismogenic faults width is defined in the beginning of evolution of a fault. If the fault products in the fault core are weaker than the surrounding protolith, the zone of deformation may narrow, as the fault develops and new periods of faulting occur.

The structural elements in a fault system are the fault core/fault rock lenses/pockets or layers, other fault lenses, slip surfaces, shear fractures, extension fractures and contraction features. Deformation bands are commonly developed in porous sedimentary rocks (Fossen, et al., 2007). These structural elements are divided into different zones of the fault zone, such as fault core, damage zone and transition zone (Figure 2-5). The damage zone can be further divided into subzones based on fracture density (see below) (Braathen and Gabrielsen, 2000).

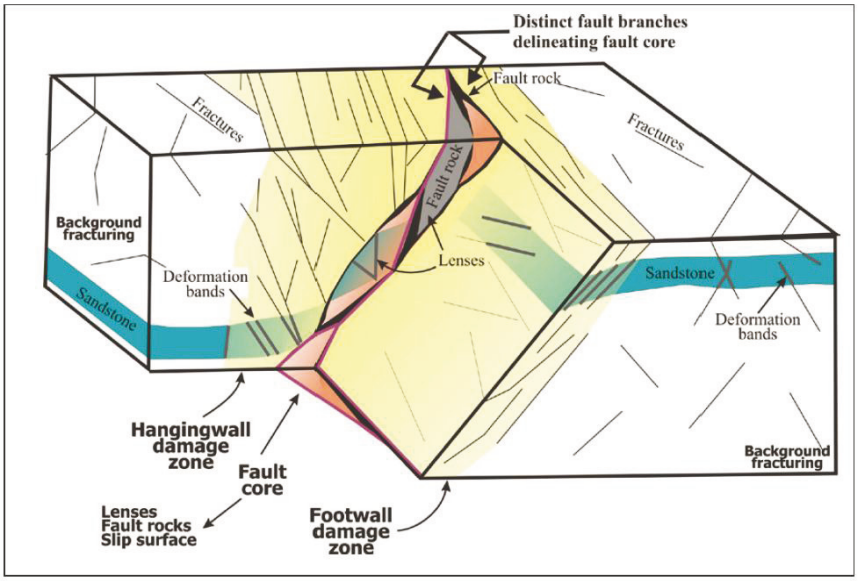

Figure 2-5: Conceptual model of structural elements in a normal extensional fault from Lindanger et al. (2007) which has modified it from Berg (2004). This is for sedimentary rocks. Apart from the deformation bands, similar structures are found in crystalline bedrock.

Fault core and damage zone

A fault zone is an approximately planar zone which has displacement along it. It normally consists of a fault core and a damage zone. Chester et al. (2004) defined the fault core as a narrow and tabular zone of fine-grained fault rocks, while the damage zone is a wide fractured zone of faulted rocks. The fault core can be from less than 1 mm to several metres, depending on the amount of displacement along the fault. Several fault cores can appear in the same fault zone.

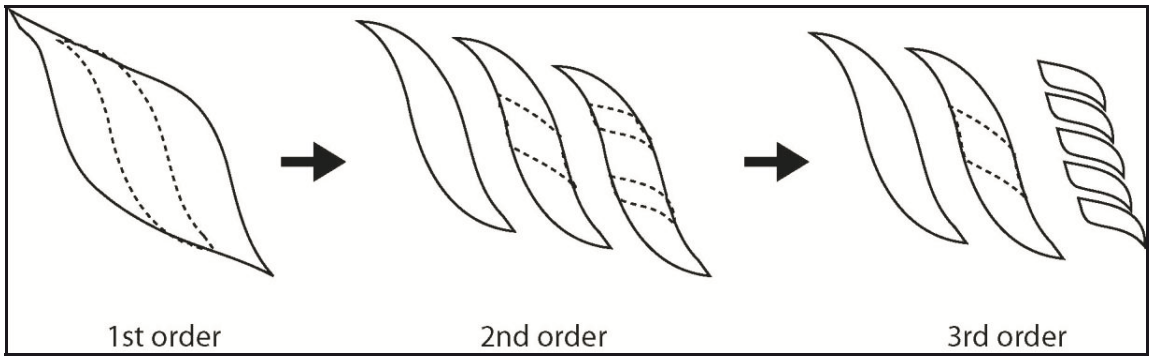

Figure 2-6: Shows how a 1st order fault lens may break down into several fault lenses. From Lindanger et al. (2007).

A feature found in both fault core and damage zone in most fault zones is fault lenses (Figure 2-5). In the literature they can also be referred to as horses. Fault lens will be the term used in this study. As indicated by the name they are generally lens and lozenge-shaped features and bounded by faults and fractures. The shape and internal structures of fault lenses can vary. When several parallel lenses occur in a system they can be referred to as duplexes.

When a fault lens is first established, new periods of deformation tend to make 2nd, 3rd and higher orders of fault lenses within the already established fault lens, as shown in Figure 2-6.

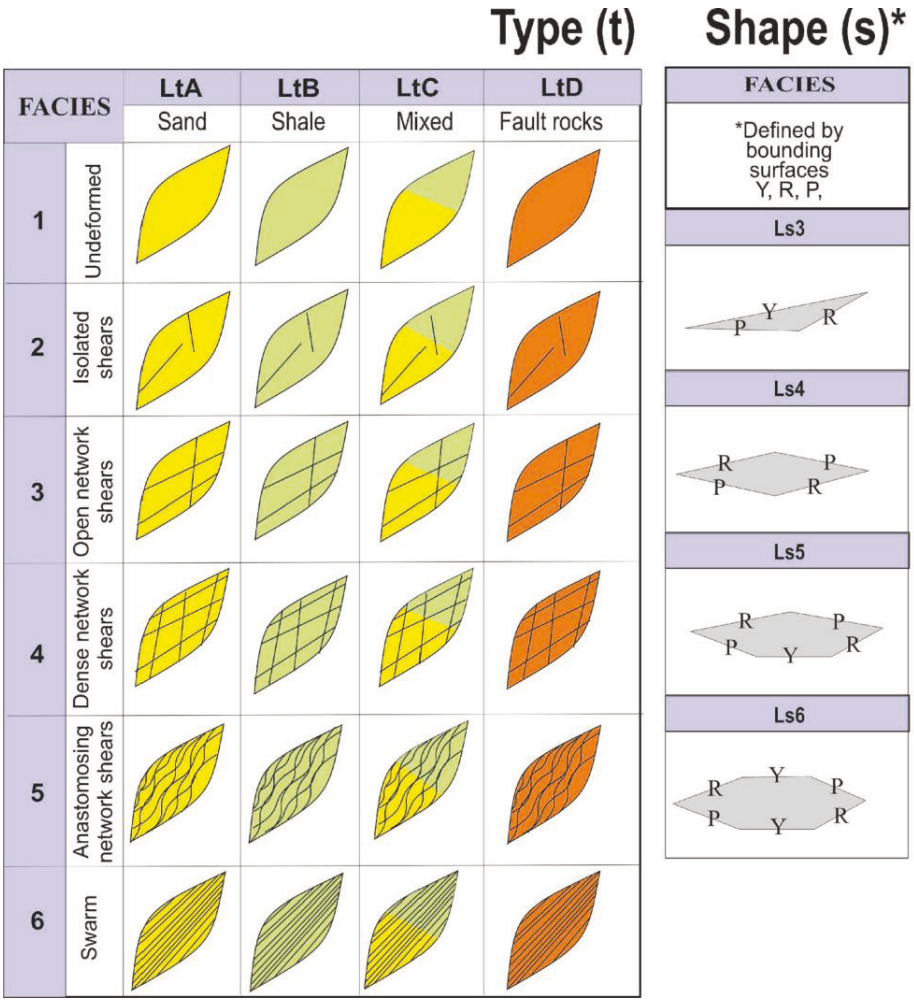

Figure 2-7: Fault lens facies from (Braathen, et al., 2009). I have neglected the sand/shale classification, and used this for describing shapes of lenses, and the type of fracturing within a fault lens.

Braathen et al. (2009) suggested a fault facies classification scheme, shown in Figure 2-7. Here the shapes of the fault lenses are classified after the type of bounding surfaces. The number of bounding surfaces can vary from three to six or more. The surfaces are called R-shears, P-shears and Y-shears (Chapter 2.2.2) depending on their angle the surface has to the fault. The "Type"-part of this classification is mainly for sedimentary rocks, and is therefore not used in this study. The type of internal shearing however is used. It can vary from undeformed lens, through isolated shears, open network shears, dense network shears, anastomosing network shears to a swarm of shears.

Permeability and fluid flow

The fault architecture and related permeability-structures control the fluid-flow in brittle fault zones in the upper crust. Fluids will influence the mineral precipitation, and as the chemistry of the fluids varies, the nature of the cementation varies. This is important as it is a part of fault rock evolution, and may result in weakening or strengthening of the fault zone.

Another aspect is the ability of a fault zone to transmit fluids and whether it makes connections between source and reservoir rock, which is fundamental in the oil industry. Reservoir quality will be affected by the deformation bands, and formation of fault rocks, as faults tend to decrease the porosity and permeability of porous sandstones (Fossen, et al., 2007, Heynekamp, et al., 1999). Faults can also have a sealing affect, and may confine an oil reservoir.

Faulting may affect the host rock differently, depending largely on lithology. For crystalline rocks the porosity will usually increase due to faulting, as it is initially non-porous. Therefore such the fault cores often conduct fluids. The pore-pressure is therefore increased, resulting in a decrease of the rocks shear-strength (see Figure 5-4).

Fracture density

Normal faults are commonly dominated by shear fractures and layers/ pockets or lenses of fault rocks, but tensional fractures occur. There are usually more fractures in the hanging wall than in the footwall (Figure 2-8). Braathen and Gabrielsen (2000) suggested fracture density in the different zones of a fault to be as follows: (in fractures/metre)

Fault core:	5 – 100
Damage zone A:	2 – 10
Damage zone B:	2 – 3
Transition zone:	1 – 3
Unaffected host rock:	1.5 – 2.5

In the fault core the fractures are usually parallel to the fault zone. In the damage zone the fractures tend to be sub-parallel or up to 30˚ to the strike of the main fault. Orientations of fractures in the transition zone are highly variable.

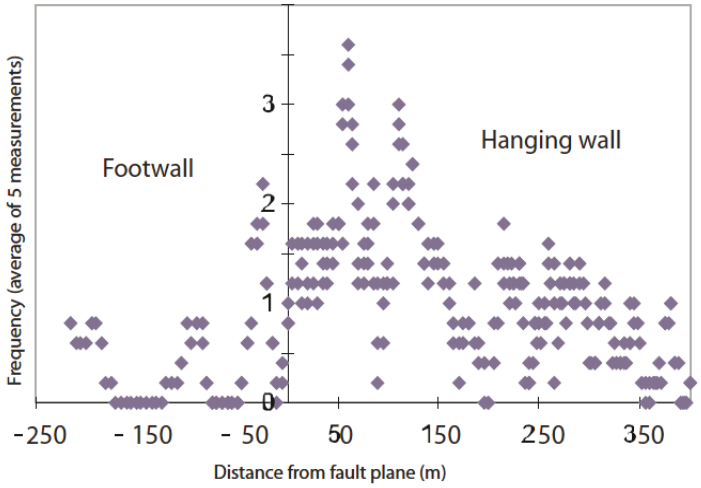

Figure 2-8: Fracture density measured across 20 bigger normal faults by (Braathen, et al., 1998). The plot shows a clear asymmetry with a higher fracture density in the hanging wall.

2.2.4 Fault rocks

Fault rocks are usually made under concentration of stress along planes or tabular zones (Braathen, et al., 2004). Temperature and pressure changes occur, and fluids might be present. Fault rocks were first described by Lapworth (1885). He described mainly mylonites. Later Waters et al. (1935) introduced the term cataclasitic rocks including breccias, fault gouge, cataclasites and mylonites. This was not an ideal way to describe the fault rocks, as they are made by different processes, not only by cataclasis. Cataclasis involves brittle comminution of mineral-grains, rotation of fragments and frictional grain-boundary gliding and dilation. The first classifi-

cation of fault rocks was suggested by Sibson (1977), (Figure 2-10). He focused on the distinction between mylonites and cataclasites, where mylonites have foliations and cataclasites have random fabrics.

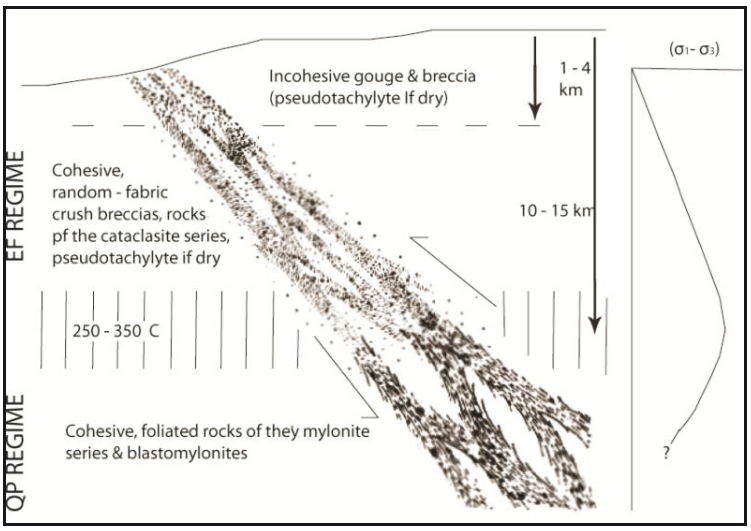

Figure 2-9: Brittle fault rocks form in Elastico-Frictional (EF) regime, Mylonites form in Quasi-Plastic (QP) regime (Sibson, 1977).

By faulting at different crustal depths the host rock will be deformed and different assemblages of fault rocks will develop. This led Sibson (1977) to correlate fault rock texture and deformation environment, seen in Figure 2-9. Mylonites and blastomylonites form in the Quasi-Plastic (QP) regime at higher temperatures (>350˚C) and pressures, by ductile deformation. Above the brittle-ductile transition (250˚- 350˚C), in the Elastico-Frictional (EF) regime, crush breccias, cataclasites and pseudotachylyte are created. At shallow crustal depths (1-4km) the deformation is brittle, and the fault rocks are incohesive breccias and gouges (Figure 2-9).

Sibson's classification can be seen in Figure 2-10. It is often used as the basis for fault rock classification, although with minor adjustments as the profession has developed. The fault rocks of this study are mainly cataclasites and breccias, although the breccias are mainly cohesive. In the Sibson (1977) classification (Figure 2-10) only crush breccias are described as cohesive breccias. A need for distinguishing between cohesive and incohesive breccias give the basis for supplement the classification with parts of the Braathen et al. (2004) classification, seen in (Figure 2-11).

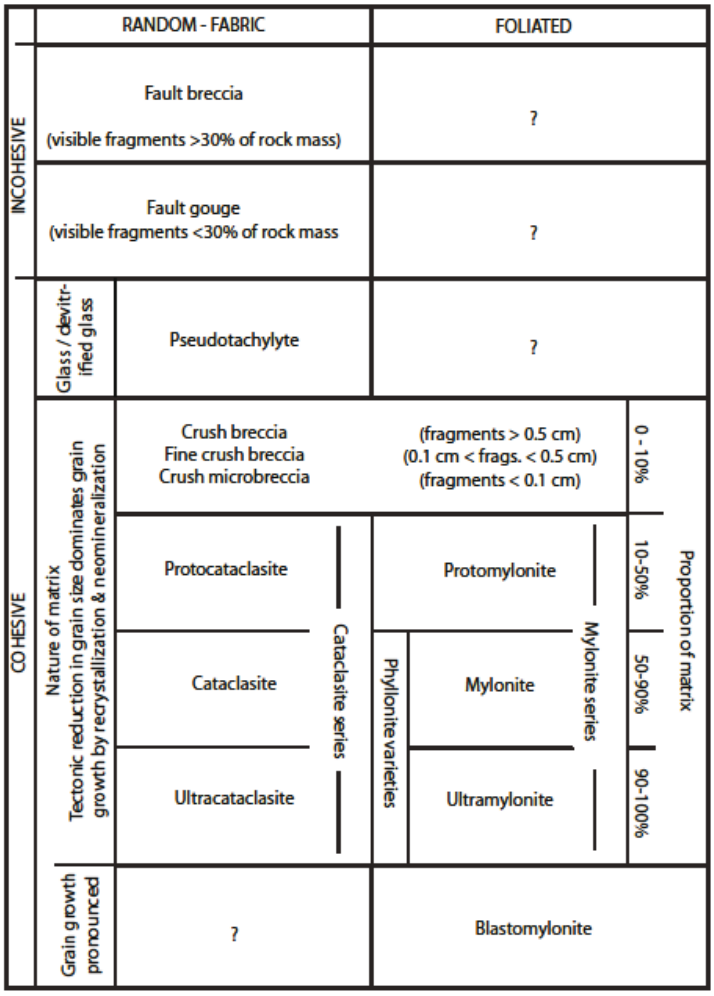

Figure 2-10: Sibson (1977) classification of fault rocks. Primarily divided into foliated and random fabric fault rocks.

This classification is developed under a study of the Nordfjord-Sogn detachment zone in Western Norway. The scheme is made based on deformation mechanisms, deformation style and cohesion during formation. A separation of fault rocks with primary cohesion, like mylonite and cataclasite from fault rocks with no or secondary cohesion, like breccias is suggested. If the rock has primary cohesion, the cohesion is preserved during formation. The cohesive breccias can be either cemented or indurated, where cemented consolidation will occur by mineral precipitation in the pores of the matrix and indurated means consolidation by compaction due to direct pressure, annealing by recrystallization of grains or neomineralization (Braathen, et al., 2004).

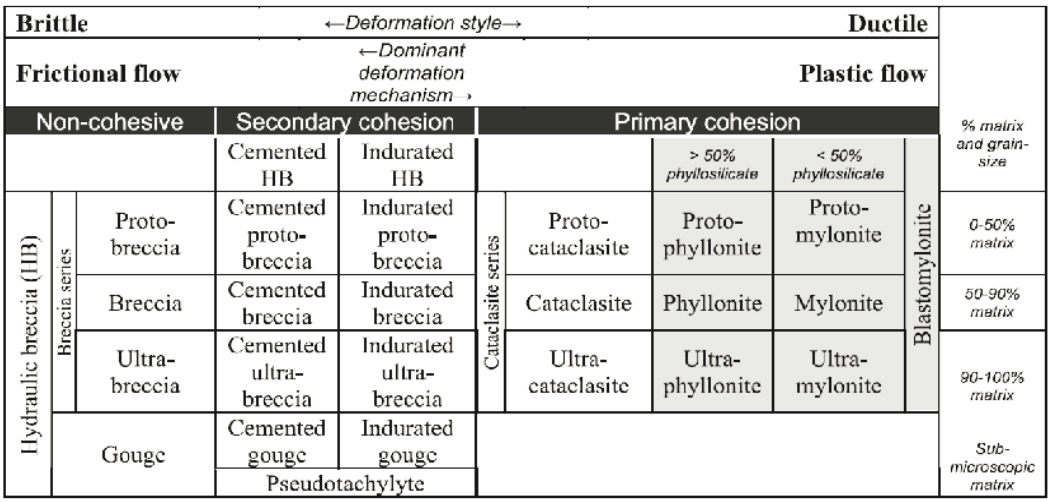

Figure 2-11: Fault rock classification from Braathen et al. (2004), where the deformation styles are ranging from brittle to ductile, and the deformation mechanism is by frictional to plastic flow. The main characterisation extracted from this classification is the separation between cohesive and incohesive breccias.

The focus of this study has not been to distinguish between these, but deciding whether the breccia is cohesive or incohesive. A combination of the two classification schemes is therefore used.

Brittle Fault rocks

The strength of brittle fault rocks will usually increase with depth during formation (Faulkner, et al., 2008). Incohesive breccias are incohesive rocks with angular, non-oriented clasts formed by mechanical comminution. They become cohesive by cementation or induration. The matrix can be secondary cemented by for example by quartz, carbonate or zeolite. If they are cemented by carbonate or zeolite, there have probably been fluids involved, and mobile fault rocks may be injected into fractures.

In the classification by Braathen, et al. (2004), cohesive brittle fault rocks are either cataclasites, with primary cohesion or breccias, with secondary cohesion. When cataclasites, cohesive breccias and incohesive breccias have 0-50% matrix, the prefix proto- is added. Similarly for 90-100% matrix, the prefix ultra- is added. The matrix of gouges and pseudotachylyte is submicroscopic. Pseudotachylyte is glass to devitrified glass formed under dry seismic slip or at the base of a rockslide (Grønlie, et al., 1991; Fossen and Gabrielsen, 2005).

If a fault has been reactivated, the most recent fault structures will overprint older ones and a complex assemblage of fault-rocks may develop. In such an assemblage young breccias can contain clasts of older fault rocks. This provides a chance to establish a fault-rock chronology and to distinguish between different phases of movement along the fault.

Grain size

The classification from Braathen and Gabrielsen (2000) is used:

Mega-breccia:		> 0.5 m
Breccia:	0.5 m	- 1.0 mm
Micro-breccia (fine-grained):	1.0 mm	- 0 .1 mm
Gouge:		< 0.1 mm

As most of the fault rocks of this study are in the breccia class between 0.5 m and 1 mm. The terms fine-grained and coarse breccia are added to the classification, with intervals from Brattli, (1992):

Coarse breccia:	0.5 m	- 5.0 mm
Medium-grained breccia:	5.0 mm	- 1.0 mm

To describe the roundness of the clasts the terms: angular, sub-angular, sub-rounded and rounded, are used, following the standards given in Boggs (2006).

Host rock minerals and mineral processes

Gneisses can have an igneous (I) or a sedimentary paragenesis. The amount of calcium (Ca) can give you a hint of what its origin might be. An indication of igneous origin may be given by a high content of calcium and aluminium (Al) (Hine, et al., 1978), and low sodium (Na)/potassium (K) content. Common minerals in igneous gneisses are green/brown biotite, sphene, allanite and hornblende.

Deformation under metamorphic conditions in a fault zone cause different secondary minerals to form. At lower temperatures minerals can be fractured, kinked or transformed to other minerals by various processes. Myrmekitization, saussuritization, sericitization and chloritization are commonly found granitic gneisses, like the host rock of the study area. Alteration of rock will

continue through faulting and cataclasis. Below, Allaby (2008) have been used to describe some alteration processes that may have relevance to this study:

Saussuritization is a common process under low-grade metamorphism. It is seen in the microscope as 'diffuse' plagioclase. Ca-rich plagioclase is altered and replaced by an aggregate of secondary minerals like sodium-rich plagioclase, muscovite, calcite, scapolite, epidote (zoisite) and zeolites. Sericitization is another feldspar alteration process. Muscovite or paragonite appear as small scales or aggregates on the feldspar. It is formed by hydrothermal alteration or by weathering at a later-stage.

Intergrowths of plagioclase in potassium-rich alkali feldspar are called perthite, whilst exsolution of alkali feldspar in plagioclase is called antiperthite.

Epidotization is a hydrothermal alteration process in rocks with albitized plagioclase. Epidote and zoisite may replace feldspars, micas, pyroxenes, amphiboles, garnets and other minerals. They are often associated with chloritization in rocks with a high content of ferromagnesian minerals (Braathen, et al., 2004).

Chloritization of biotite is often related to sericitization. Kinked biotite is common in fault rocks and altered host rocks. Other mineral processes can be silicification and muscovitization. The first will result in very hard fault rocks.

Zeolites have been identified in localities along the MTFC. These are hydrated alumino-silicates and are common in altered igneous rocks, cavities in igneous rocks and veins. They are usually secondary minerals commonly formed through alteration of plagioclase. In the MTFC, north of the study area, in the Verran and Rautingdal faults stilbite, prehnite and laumontite were identified by Grønlie et al. (1991). Prehnite is found as groundmass material; while the laumontite mineralization evidently is from the latest extensional activity, as it cuts the older fault rocks, both mylonites, crush breccias and cataclasites.

3 Methods

The fault localities have been described in detail in field. Line-drawings and LIDAR-scans are used as aid for modelling and describing the fault architecture. This gives a better overview for understanding where and how the different faults and fault rocks have developed. Readings of kinematic indicators and fracture density was performed at all localities. The fault rocks were investigated in more detail using optical microscopy of thin section, Scanning electron microscopy (SEM) of polished thin sections, and X-ray diffraction (XRD) analysis of the vein and matrix minerals. This enables detailed descriptions of the fault rocks at different scales, which in turn provide a fundament for interpretation of faulting mechanisms, temperatures, pressures and succession of faulting events.

3.1 Fieldwork

4 weeks fieldwork was carried out during the summers of 2008 and 2009, partly supported by NGU personnel.

Strike and dip readings were made with a Silva Ranger Compass and a Built-In Clinometer, using right-hand rule. At each location, fault planes, fractures and slickenlines together with ductile structures such as main foliation and mineral lineations, were measured. Where mineral lineations are evident, they have been measured. The program 'Stereo' have been used to make the following stereo-plots:

- Slip-linear plot
- Poles to the planes, contours of the poles and rose diagram for the fractures
- Mean great circle for the foliation

3.1.1 Description of the 3 localities in outcrop-scale

Outcrop-scale descriptions at the 3 main localities were made by a combination of line-drawings made on location, photography-aided line-drawings, and Light-detection and Ranging (LIDAR) scanning.

1) To make a good line drawing of the fault core at Mulvik I made a grid of 50 cm intervals. On a drawing of 1:5. Fractures have been plotted and the various fault rocks are drawn. Points of samples are also registered. Later the drawing was carefully redrawn in Adobe Illustrator on top of a photo-stitch.
2) At Rød the locality is more complex and some parts are inaccessible. Thus the line drawing is less detailed. I have tried to distinguish between extensional fractures with zeolite growth and other fractures. There are a lot of fractures in the fault core, and the relationships between them have been investigated and were described.
3) The most complex fault architecture is observed at Vik. Several smaller fault cores and one bigger fault core are displayed in a 50 m wide outcrop. An overview line drawing is made and several detailed line drawings that show details of the fault cores when present.

3.1.2 Light Detection And Ranging (LIDAR)

Methodology of terrestrial LIDAR scanning

Terrestrial LIDAR scanning obtains high resolution point clouds on the scanned outcrop. A laser pulse of 1500 nm is sent put from the device (Oppikofer, et al., 2009). When it meets an object it is reflected as a back-scatter and registered on the LIDAR. The time of flight for this laser pulse to and through the device is converted to the distance between the objects. This results in a high resolution point cloud. To get a good 3D model this must be done with three (or more) different angles to the outcrop.

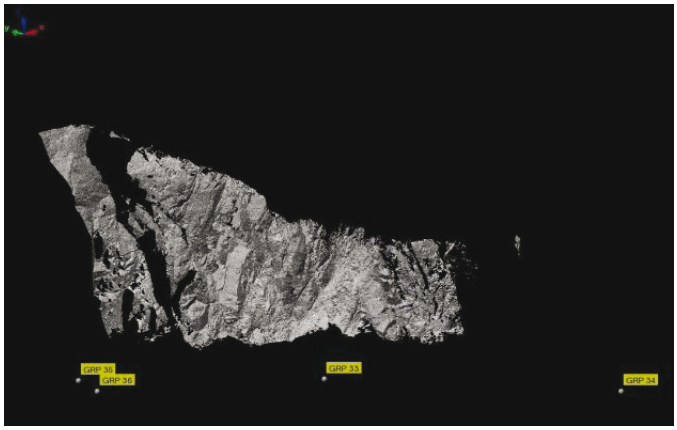

Figure 3-1: LIDAR model of Vik, illustrating the location of the device at each scanning point. The final models can be seen in Figure 4-21, and in Appendix 2.

Scanning and processing

Parts of the localities at Rød and Vik are inaccessible. Thus terrestrial LIDAR scanning was made to construct a detailed 3D model of the whole outcropping fault core and obtain measurements of the fracture planes surrounding it. The terrestrial LIDAR-scanning was made with the Optech IRIS-3D terrestrial LIDAR scanner, on the fault outcrops at Rød and Vik in the end of May 2009, facilitated by NGU and carried out by Aline Saintot and myself.

SCAN INFORMATION		SHOTS			GPS COORDINATED		
Name	Date	Number	Spacing [mm]	Distance [m]	Easting	Northing	Altitude
fault1_task104_section1	28.05.09	3688603	7.4	26.39	443492	6960287	120.5
faults 2_task101_section1	28.05.09	3651515	5.3	18.92	443504	6960287	119.5
faults 3_task101_section1	28.05.09	3938568	5.2	18.39	443517	6960285	118.7
faults 4_task101_section1	28.05.09	4218686	7.7	25.66	420866	6952070	14
faults 5_task101_section1	28.05.09	4151214	7.1	29.54	420882	6952065	12
faults 6_task101_section1	28.05.09	3950691	5.3	20.46	420860	6952092	13.5
faults 7_task101_section1	28.05.09	1902805	6.6	21.95	420860	6952080	13

Table 1: Displaying the characteristics of the 7 scans.

Three scans from three different positions were done at Rød with 5.3, 7.4 and 5.3 mm between the points respectively, resulting in approximately 11.3 million points. It was raining at the time of scanning, so we expected some noise in the data. Some points were lost, as the light is more scattered when the rock is wet. At Vik 4 scans were made. The locations of the device are shown in Figure 3-1. Here the scans are done with 6.6, 7.1, 5.3 and 7.7 mm between the points, resulting in 14.2 million points.

The terrestrial LIDAR scan result in different point-clouds with associated pictures. The Polyworks software was used to process and analyse the data.

To prepare the scans they are parsed in a program called ‘Parser’. In this first step we made an IXF file with 8-bit scaling and without any picture draped on the point clouds. To achieve the

best resolution of the scan an external camera was used, as the internal cameras resolution is poor. Each external picture is manually matched to each point cloud in 'MatchView' software. After opening this IXF-file and the external picture in 'MatchView' the matching can start. For each of the scans I have found points that can easily be recognised at both the point cloud and the picture. This should be done accurately on multiple recognisable points, like sharp corners, in order to get a good fit. I have fitted between five and eight points on each scan.

The result is a calibration file, which is used in Parser for the next step. The quality of the calibration file is defined by a RMS (root mean square) value. This value should be less than 2 for a good calibration, and a value between 2 and 8 is acceptable. In my dataset the rms values are between 2 and 4, and the alignment should be good.

A new Parsing is then done in order to get a PIF-file with colours. The external picture with the new calibration files, (one for each of the 7 scans) are draped on the different scans. Then the scan must be cleaned for any redundant data, like trees, road and cars. This is done in PIFEdit. Care was taken to avoid removing data from the outcrop itself.

After cleaning the scans from each locality they can be opened in Polyworks: a LIDAR software for aligning, inspecting, extracting information and modelling the data. First I aligned the three scans from Rød. This is done using 'N-pair alignment'. Recognisable points at two scans are picked. When they are aligned they are frozen and the third scan aligned to them. The same technique is used for Vik. Geo-referencing is done in the Polyworks software IMAlign using the measured GPS points at each position of the scanning device. As the accuracy of the GPS was ~5 ms. The positions were corrected using a geo-referenced high-resolution ortho-photo layer in ArcGIS from (www.norgeibilder.no) on which the exact position of the LIDAR device could be set.

In the Polyworks software IMInspect I have extracted the important fracture planes at Vik. As the scan is Geo referenced, the software calculated the orientation of the main fractures in the locations. This is useful, as the fracture pattern define the geometry and architecture of the fault lenses.

To create the planes I used the method 'fit to elements', and the 'best fit method'. This will gives

the most accurate result. 123 planes were picked at Rød and 149 planes at Vik. The strikes and dips of the fractures are extracted and the results are plotted and compared with field measurements.

3.1.3 Sampling and measuring fracture density

The fault core exposure at Mulvik is the largest one in the study, and 16 oriented samples were collected here in 2008. These represent different generations and combinations of fault rocks. 7 samples from Rød were collected. These will help us to study the characteristic, red material associated with these fault cores. 7 samples were collected from the fault core in Vik. They represent fault rocks and the pink vein material. All 30 samples were prepared as polished thin sections in the lab at the NTNU for studies in the optical microscope (Chapter 3.2) and Scanning Electron microscope (SEM) (Chapter 3.3).

I have counted how many fractures and faults are found in one metre from host rock, through damage zones and fault cores. The counting was done along a scan line oriented approximately normal to the fault. In locality 1) Mulvik, fracture density was counted along a 135 m long section. From locality 2) Rød, which is the smallest of the three outcrops, 23 m long section was measured. At this locality, the hanging wall is not well exposed, and this should be considered when interpreting the results. At locality 3) Vik, the foot-wall is inaccessible, but the measurements of the 40 m of outcrop in the hanging wall was made at a high angle to the antithetic fault core. At Rød and Vik, the fault core is highly fractured with more than 1 fracture per cm. Therefore only an estimation of the fracture density is plotted in the fault core, where the fault core consists of cataclasitic rock.

3.2 Optical microscope

All thin sections have been studied in detail using optical microscope (Nikon Eclipse E200). The compendium of Brattli (1992) was used as a manual when describing the gneissic rocks. Sibson (1977)-classification, in combination with the classification of Braathen et al. (2004), have been used for fault-rock classification, as described in Chapter 2.2.4.

For the mineral descriptions, the following abbreviations have been used: quartz (qz), plagioclase (pl), alkali feldspar (kfs), orthoclase (ocl), microcline (mcl), biotite (bt), laumontite (la), zeolite (ze), hornblende (hbl), amphibole (abl), sphene (sp), apatite (ap), chlorite (cl), epidote (ep), garnet (gr), zircon (zr), spinel (sp). The micrographs shown in Appendix 1 are made by a simple scan at NGU. Photographs through the optical microscope were taken at the NTNU.

Modal analysis of the host rocks at each locality were performed with 400 points and a stage interval of 5. MB 14 from Mulvik, MBR 07 from Rød and MBV 07 from Vik were analysed.

3.3 Scanning Electron Microscope (SEM)

The fault rocks tend to have a very fine-grained matrix, which cannot be resolved in the optical microscope. To understand how the rock is formed it is important to know as much as possible about the mineral content and the form of the grains in the matrix. As the samples may represent several faulting events, the differences in matrix chemistry of different generations of fault rock are examined. The matrix chemistry and the size and shape of grains are investigated in SEM in several samples: 8 samples from Mulvik, one from Rød and three from Vik.

The electron microscope at NGU has been used. It is a 150VP scanning electron microscope from LEO Electron Microscopy Ltd. with an X-ray system from Oxford instruments and an energy dispersive spectroscopy (EDS) analyser of 128 eV resolution. On a polished surface the Backscatter Electron (BSE)-detector can be used to take good BSE-pictures. Minerals with high molecular weight are bright. In the backscatter image, we have made a chemical probe-analysis combined with an EDS analysis.

Appendix 6 in Jones (1987) has been used for temporary mineral-characterization.

3.4 X-Ray Diffraction (XRD)

XRD analysis gives detailed information on the crystal structure and chemistry. At all three localities fractures with secondary mineral growth are found. From observations in hand specimen and descriptions in Grønlie et al. (1991) it was suspected to be a zeolite, but in order to decide more accurately what minerals this is, XRD analysis was run on 3 different samples.

The mineral crystals from each sample are carefully scraped out and crushed in an agate mortar. To evenly distribute the fine powder on a glass slide, alcohol is added. The XRD used is a 'BRUKER D8 ADVANCE' with a 'Lynx Eye DETECTOR' and a CuKα radiation. For searching and matching the result with mineral-data the program Eva is used with a database called PDF 2+ (ICDD).

4 Detailed outcrop architecture and fault rock descriptions

In the following Chapter, each locality is described at different scales. An overview of the outcrops is give, supported by LIDAR-models and photographs. Then detailed photographs and line drawings from selected faults are described. Further the fault rocks are described, from hand specimen, at microscopic (mm) scale and in µm scale in the SEM backscatter images.

First Locality 1) Mulvik is described, concentrating on three fault cores. Following are localities 2) Rød and 3) Vik described. These are three-dimensional, and are therefore better for describing the fault architecture.

4.1 Locality 1) Mulvik

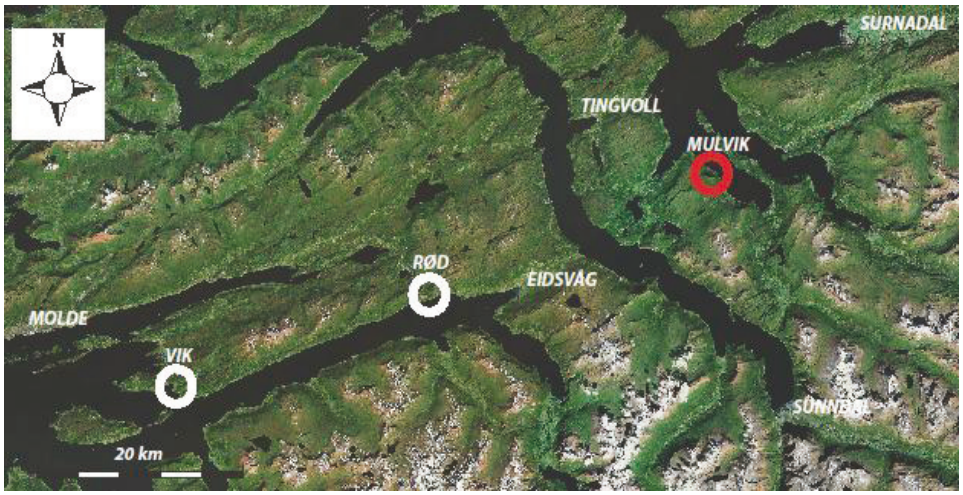

Figure 4-1: Red circle marks the location of locality 1) Mulvik (8˚25' 36'' E, 62˚51' 39'' N). Satellite-photo from www.gulesider.no/kart

At Mulvik (Figure 4-1), an approximately 140 m wide, two-dimensional exposure of faulted rocks (Figure 4-4) is found. It is only a few metres high, and it is therefore good for studying the distribution of fault-rocks and fractures in cross section.

Several fault cores with increased fracture density and zeolite-mineralized fault rocks are found. Their widths are varying from a few centimetres to six metres. Many of these fault cores are covered by superficial deposits and vegetation, and are therefore not discussed any further here.

However one large fault core and some smaller faults are well exposed. Three fault cores are selected here, A) the northern fault core, B) the southern fault core and C) the Mulvik fault core. The last one (C) is the main fault core (Figure 4-4), and shows the transition from pure granodioritic gneiss through highly fractured and lensed gneiss, and its further development into protobreccia and a rich assemblage of fault rocks in the fault core. One zone within this core consists of unconsolidated, dark red breccias, further described in Chapter 4.1.3.

As seen in the stereogram down to the right in Figure 4-4, the orientation of C) the Mulvik fault core is 250/80. It is close to vertical, with a steep dip to the north, so that the northern side of the outcrop is referred to as the hanging wall and the southern side as the footwall.

16 oriented samples were collected from Mulvik fault core, representing the different stages in fault rocks. These have been the fundament in fault rock descriptions at macroscopic, microscopic and μm scale, see Chapter 4.1.3.

Fault A) and fault B) are found tens of metres away from Mulvik fault core, in the northern (A) and southern direction (B), respectively.

4.1.1 Fault architecture

The foliation at Mulvik varies in orientation, but it is generally quite steep, with a mean of 245/75. Some zones of amphibolitic gneiss are found along the road cut, and faulting appear to have localized along the boundaries between these and the granodioritic gneiss, as the contact between them is weak.

A) The northern normal fault core of Mulvik

One fault core found north in the section is shown in Figure 4-2. As the split arrows indicate, it is a normal, brittle fault with multiple veins of zeolite growth (pink lines on the figure). The fault is splaying (Figure 5-1 E), and surrounds a fault lens of gneiss (coloured blue in the middle part of the line drawing). In the middle right part of the line-drawing, the fault is splaying, resulting in a fault lens, marked blue in the middle part of the line-drawing. This lens is probably continuing a few metres below the exposure. The splayed part of the fault is shown in close-up photographs of Figure 4-2 b and c, where large quartz crystals appear in relation to white zeolite growth. The

zeolite is growing in open extensional fractures .The gneiss bordering the zeolite veins have an orange to brick-red colour, probably due to feldspar alteration, whilst the unaffected gneiss is light grey.

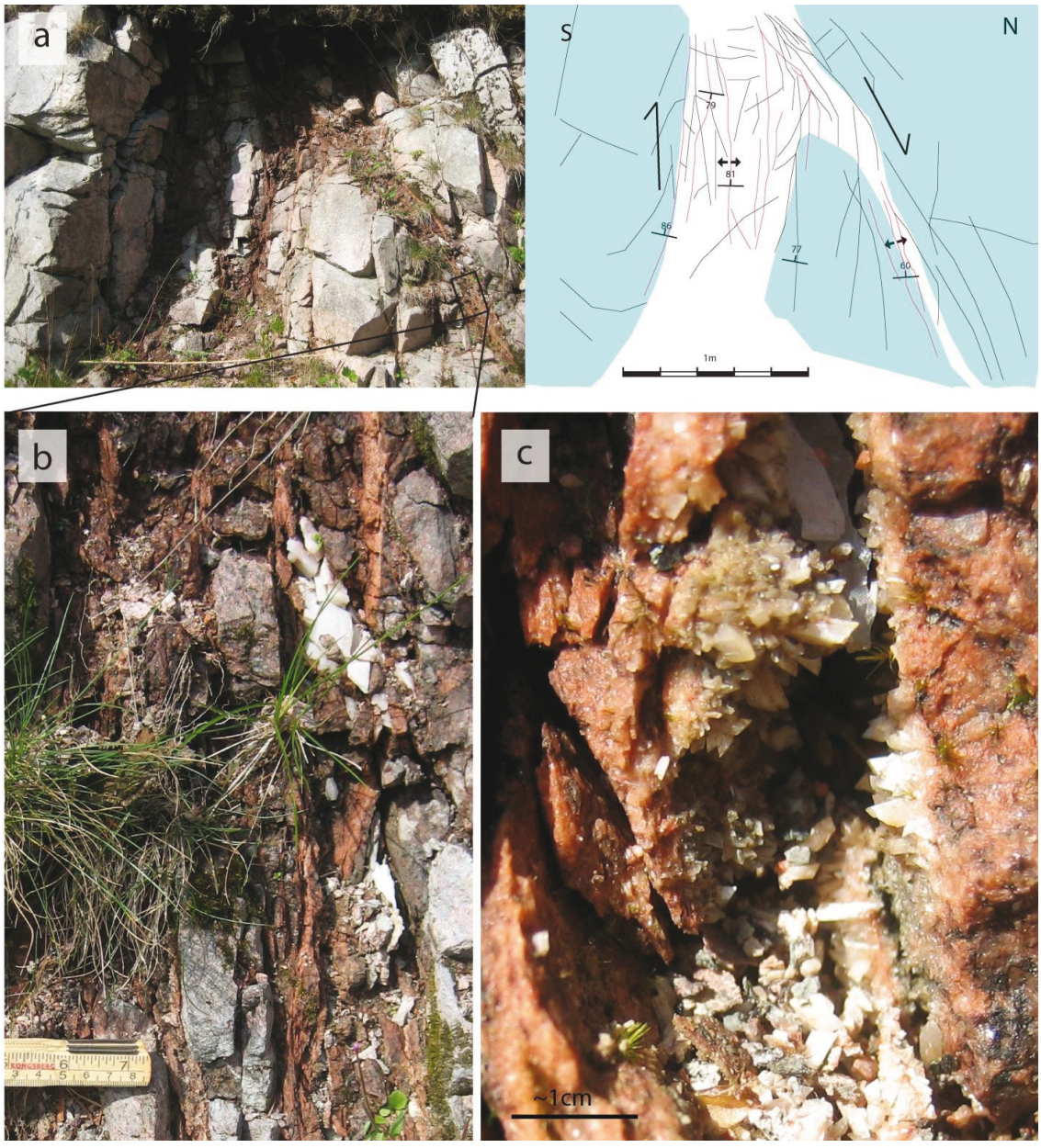

Figure 4-2: a) Photograph and appurtenant line drawing of a normal fault from the northern part of locality 1) Mulvik. b) and c) Display the extensional fractures which are filled with zeolite growth.

B) The southern normal fault core of Mulvik

To the south of the Mulvik fault core, another normal fault is found; the southern normal fault core of Mulvik (Figure 4-3). It is a steep fault with a northerly, steep dip, similar to the Mulvik fault core, and the northern fault core of Mulvik. It has anastomosing sheets of red zeolite, shown as pink lines stretching along the fault. The fault core is well defined in the gneiss, and is varying in width from 2 to 25 cm. The fault shows segment amalgamation (Figure 5-1 F) by R-shears, shown with an R in the upper right of Figure 4-3. These have an approximate angle of 40˚ to the fault. P-shears are marked with a P, and are found in the lower part of the fault core. They are oriented with an angle of ~20˚ to the fault.

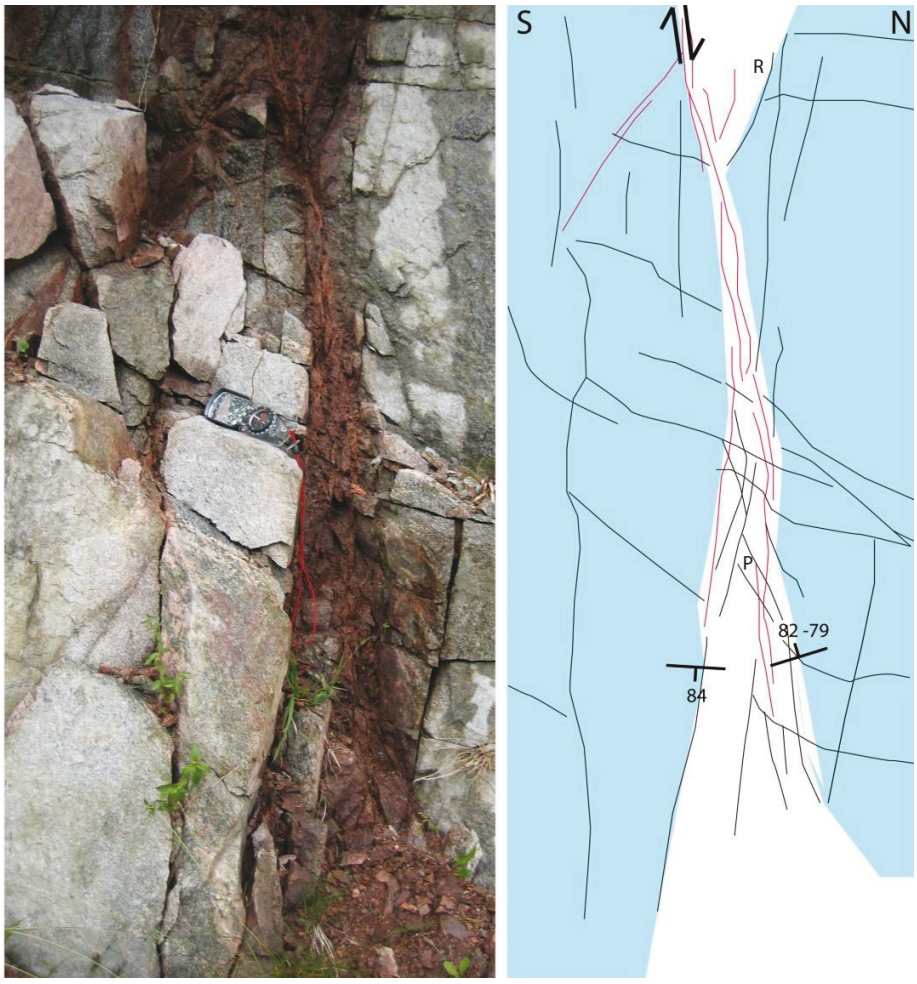

Figure 4-3: Photograph and appurtenant line-drawing of Mulvik southern normal fault core. It is from 2 to 25cm wide. Note the anastomosing red sheets of red material. The fracture density increases abruptly in the fault core. Compass for scale.

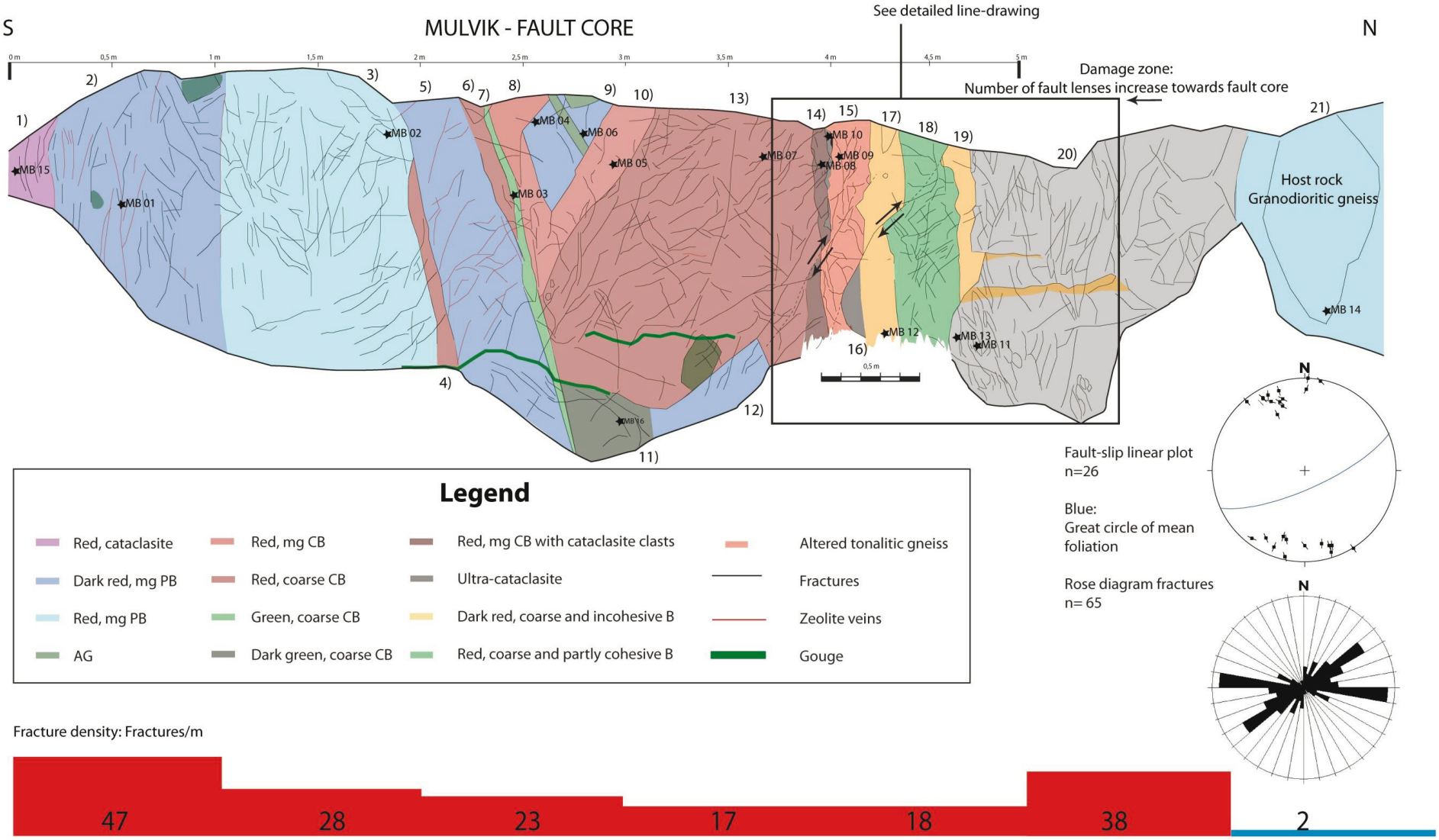

Figure 4-4: Fault core at locality 1: Mulvik. Abbreviations used are: CB – cohesive breccia, PB – proto-breccia, AG – altered gneiss, B – breccia and mg – medium-grained (1-5mm clasts). The different fault rocks are numbered from zone 1) to zone 21) from south to north. A detailed line drawing is made of the most complex part of the fault core, marked with a black square, see Figure 4-6. The histogram of the fracture density in the lower part of the figure is extracted from the fault core part of Figure 4-7. Fault-slip linear plot and rose diagram of measured fractures are shown down to the right in the figure.

A) Mulvik fault core

The Mulvik fault core is be divided into 21 zones of different fault rock, marked with increasing number towards north on Figure 4-4. These zones are in the following section grouped and described from south to north. The groups are zones 1) to7), zones 8) to 13) and zones 14) to 19). Zone 20) represents a 1.5 m wide damage zone on the northern side of the fault core, whilst zone 21) represents the unaffected host rock. The southern boundary between the gneiss and the fault core is abrupt, and no damage zone has developed here.

Zones 1) to 7):

The fault core starts abruptly from undeformed host rock to zone 1), which is a zone of elongated slivers of red cataclasite. This is a narrow zone between the protolith and the other fault rocks, with concentration of deformation. It is saturated with fault-parallel fractures with zeolite mineralizations. Further into the fault core, zone 2) is found. It consists of dark red protobreccia, with fault-parallel fractures. In the southern part of the zone the fractures are filled with zeolite, but towards the north the number of zeolite-filled veins diminishes, and the fractures begin to dip towards the north. The zone has some larger clasts (< 20 cm) of altered gneiss. The boundary between this dark red protobreccia to the aligned zone 3) of brighter red protobreccia is marked with a semi-continuous mineral filled fracture. Following to the north is another zone of protobreccia 5) which has an orientation of 246/68. It is similar to zone 2), and has anastomosing mineral-filled extensional fractures with a generally southerly dip. As an example, one vein has a strike/dip of 084/65, representing the extensional fracture set (Chapter 2.2.2).

Zone 5) is defined by zones of red, coarse cohesive breccia of zones 4) and 6) at each side. Further north, zone 7), an elongated sliver of green, coarse cohesive breccia, marks the end of the first group of fault rocks. These first 7 zones have close to parallel boundaries. Further into the fault core the fracturing and the changes of different fault rock assemblages appear more complex.

Zones 8) to 13):

Zones 8) to 10) appear together as a triangular pocket among the surrounding rocks. Zones 8) and 10) represent a zone of red medium-grained cohesive breccia. Captured within it is zone 9) a dark red protobreccia, similar to zones 2) and 5), containing altered gneiss clasts. Zones 11) and

12), which seem to be in the prolongation of the previous group 8) to 10), are composed of zone 11), dark green, coarse cohesive breccia and zone 12) a dark red protobreccia similar to 2), 5) and 9). This is also related to a clast of altered gneiss. Zone 13) is a large zone (~2m) of red, coarse cohesive breccia. It is displayed in photograph of Figure 4-5 a, and in the left part of Figure 4-5 b.

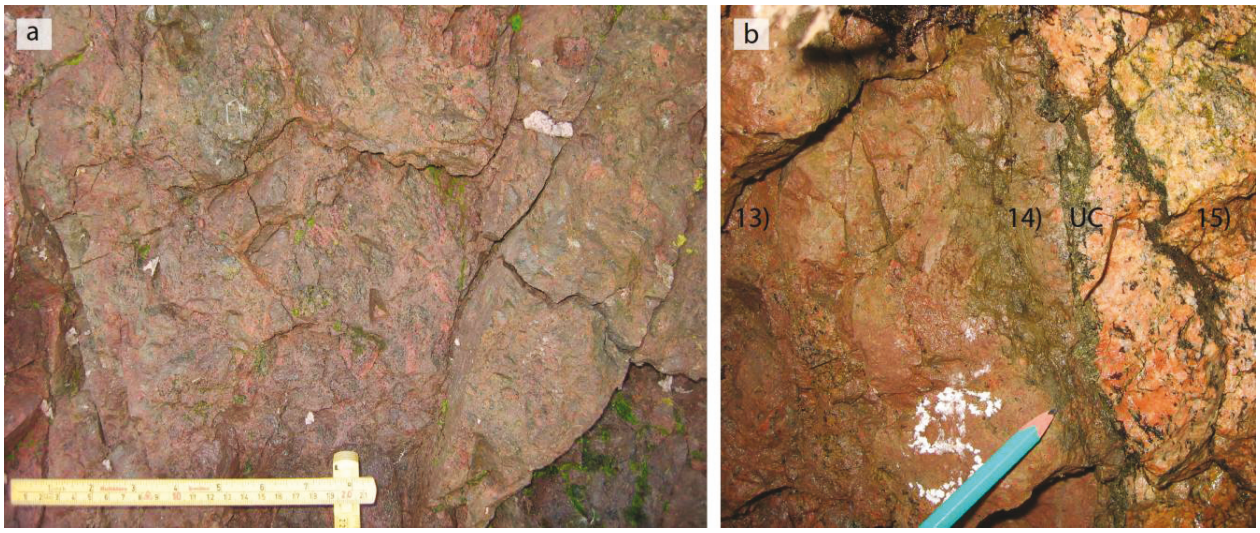

Figure 4-5: a) Photograph displays zone 13), a red, coarse cohesive breccia. b) Photograph displays zones 13), 14), UC – ultracataclasite, and zone 15). Pencil for scale.

Zones 14) to 19):

The next group of rocks consists of zones 14) to 19), is the most complex and deformed group of rocks in the Mulvik fault core. It is displayed in the detailed line-drawing of Figure 4-6. As seen on this figure, these zones are cut by at least two reverse faults, with the relative movement indicated by the arrows. Parts of the rocks in this group, zone 14) and zone 15) are displayed the photograph of Figure 4-5 b. It starts with zone 14), a red, medium-grained cohesive breccia. It grades into a narrow zone of ultra-cataclasite (described further in Chapter 4.1.3.). Zone 15) is seemingly less deformed, as it is a zone of altered plagioclase rich gneiss. But it is more fractured than the surrounding breccias, with mica minerals concentrated along foliation parallel fractures. Zones 17) and 19) consist of a chaotic, red, incohesive breccia. Zone 16) is similar to

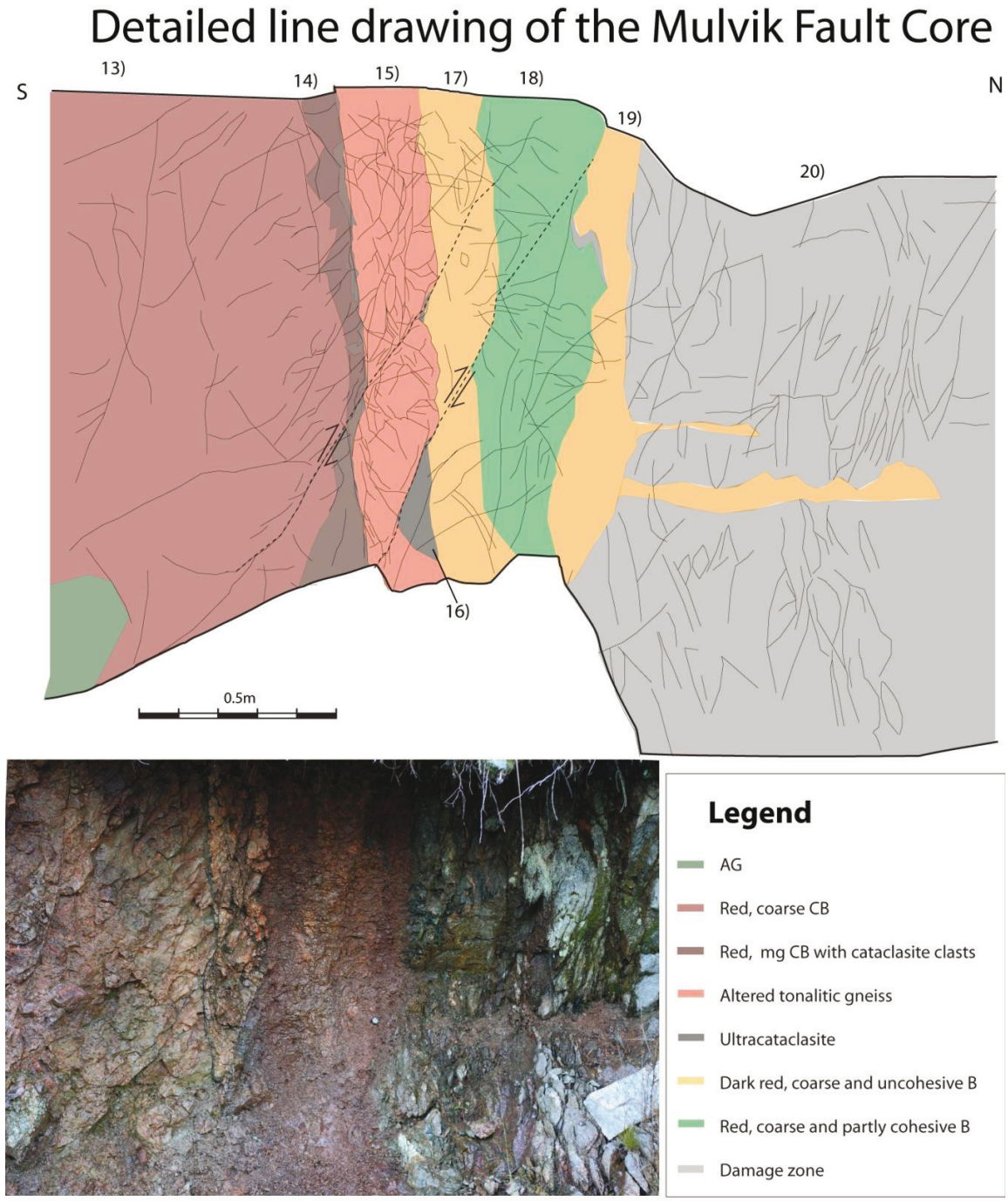

Figure 4-6: Detailed line drawing and appurtenant photograph of parts of Mulvik fault core see (Figure 4-4) for location. Abbreviations used are: CB – cohesive breccia, AG – altered gneiss, B – breccia and mg – medium-grained (1-5mm clasts).

these, but it has a black colour. It appears in boundaries towards other, cohesive fault rocks. Zone 18) is similar to zone 17), except it is slightly more coherent. The boundary between zone 18) and aligned rocks is appearing as a black gouge, marked black and grey on Figure 4-6.

Damage zone

Zone 20), the damage zone on the northern side of the fault core has a high frequency of fractures and zones 13) to 19) are cut by 'reverse' faults that might be Riedel shears. The fractures define elongated, flaky lenses of rock, defined by R- and P-shears, and are therefore Ls4 type lenses (Figure 2-7). The lenses are from 10 cm to 70 cm long, and often have opaque slickenlines on the margins. The fracture density (described further in Chapter 4.1.2) shows an abrupt decrease to a transition zone, where there are about 2 fractures per metre of host rock in zone 21) (see bottom of Figure 4-4 and the following chapter on fracture density, Chapter 4.1.2. Zone 19), the incohesive breccia, is interfering with the damage zone along sub-horizontal fractures. In these fractures it is can be classified to be a red gouge. As it is incohesive its exclusion is not clearly defined, and the line-drawing might appear strange here. Two other gouge zones are found in sub-horizontal fractures in the middle part of the fault core. They have a grey colour, and the sub-horizontal fractures probably represent a R_1 fracture set.

4.1.2 Fracture density

The fracture density from the section of Mulvik is shown in Figure 4-7. Due to superficial material, the measurements in the footwall stop after approximately 40 m. Preferably the measurements should continue further into the footwall to better compare the results of the footwall with the hanging wall.

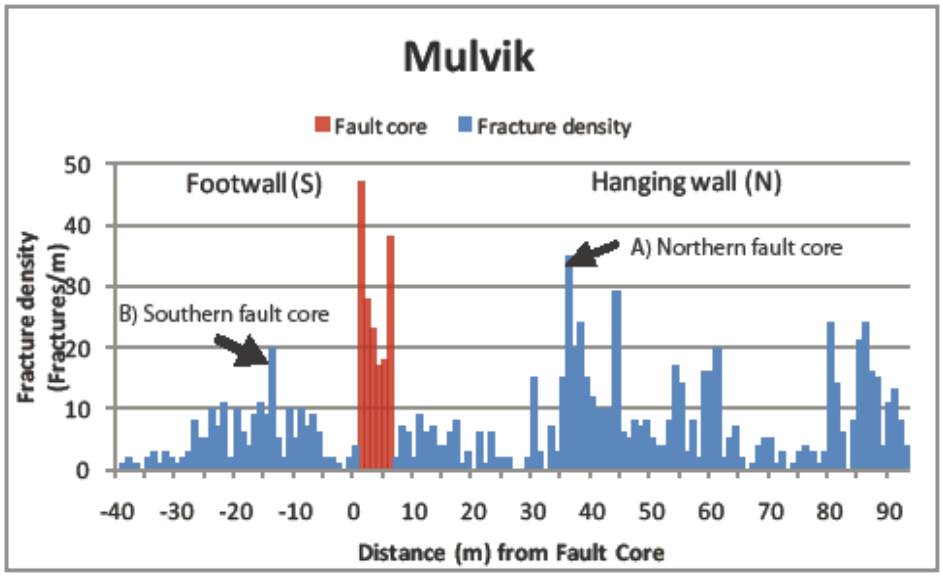

Figure 4-7: Fracture density at Mulvik. Note the increase in fracture density towards the fault core, and the peaks in northern and southern margin of the main fault core. C) The Mulvik fault core has a red colour in the histogram, and these 6 m of fracture density are displayed in lower part of Figure 4-4. The location of B) the southern fault core and A) the northern fault core are indicated by the arrows.

Fracture density across the section of Mulvik (Figure 4-7) indicates a more fractured hanging wall which is densely fractured zones represented by smaller fault cores as you get approximately 30 m away from the main fault core (displayed in red on Figure 4-7 and Figure 4-4). A peak of fracture density is found in the margins of the main fault core. The northern peak of the fracture density in the fault core represents the damage zone (zone 20) in Figure 4-4 and Figure 4-6). As there is several fault cores at Mulvik, there are several peaks of fracture density. These are however not marked red in the histogram of Figure 4-7. This is due to the variation in fault core widths. The fracture density also tends to increase where the gneiss is amphibolitic. The

foliation at Mulvik is steep. This will probably give an eminence in fracture density, as the fault is close to parallel to the foliation, and the anisotropy will give a general higher fracture density.

4.1.3 Fault-rocks

The 16 samples from the Mulvik fault core are described in detail in Appendix 1. The sampling locations are displayed in Figure 4-4. From modal analysis, the host rock sample MB 14 is granodioritic gneiss. It is holocrystalline, xenoblastic, medium-grained and crystalline, with steeply dipping foliation. The dominating paragenesis is qz + pl + hbl + ep + (bt), which is typical for epidote-amphibolite facies paragenesis. The sample is taken close to the damage zone, but seems relatively unaffected by the faulting in hand specimen. In thin section, saussuritization and spot-antiperthite are found in the plagioclase. Myrmekitization of the quartz, some sericitization and spot-perthite of microcline are evident

The following is a description of the rock with increasing deformation. Two of the samples (MB 04 and MB 06) are clasts of altered gneiss within breccias, and will not be described in further detail here.

The zeolite influenced protobreccias found in samples MB 01 and MB 02. These are highly saussuritized, and cut by zeolite growth in open fractures (indicated by arrows in Appendix 1) along the gneiss foliation. MB 09 is altered plagioclase-rich and coarse gneiss. It is strongly saussuritized, and in some parts a breccia has developed, where the matrix seems to be a product of the plagioclase alteration. Biotite crystals are concentrated along open fractures. MB 11 is a lens of granodioritic gneiss with striations. Towards the fault bounding surface there is an abrupt increase of fracturing and deformation. The peak of deformation is at the edge of this lens, towards the fault core, where thin layers of cataclasite have developed (Figure 4-12).

These are cut by reverse shear –bands, with the same trend as seen in outcrop scale on Figure 4-4 and Figure 4-6. MB 13 is a lens of altered and fractured dioritic gneiss. It shows epidotization, chloritization and feldspar alteration. It is found close to MB 11 in the damage zone in the right part of Figure 4-4.

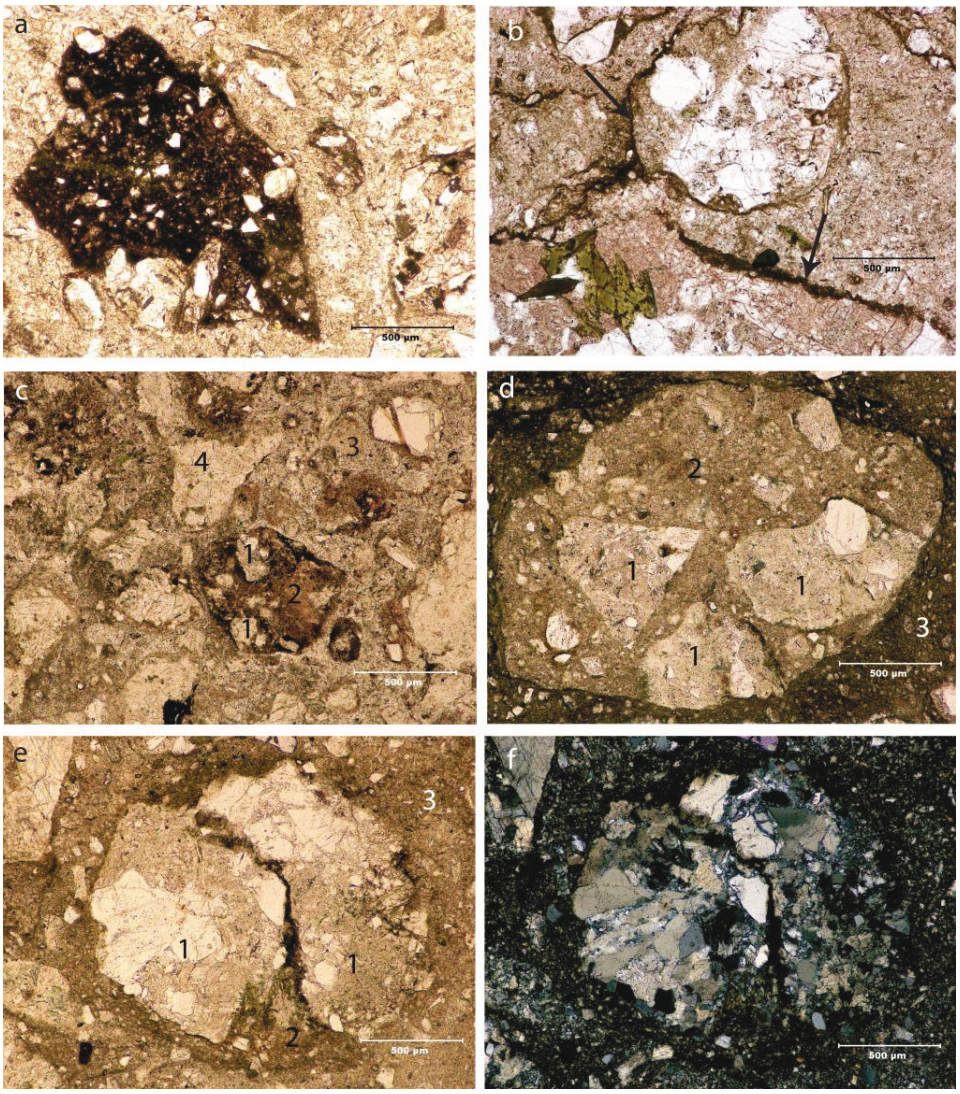

Figure 4-8: Micrographs of selected areas of some of the sampled fault rocks from locality 1) Mulvik. Scale bars represent 500 µm. a) Sample MB 05 displays a clast of opaque pseudotachylyte or ultracataclasite within a bright zeolite matrix. b) Sample MB 07: a breccia with opaque coating on the protobreccia clasts (arrows). c) Sample MB 08 displays possibly 4 generations of breccia: 1 being the eldest which is zeolite and host rock fragments, 2 which has an opaque matrix, 4 being a zeolite dominated clast (but the age relative to 1 and 2 is uncertain). 3 is the most recent matrix, being slightly opaque, zeolite breccia. d) Is from the green right part of MB 10, where the matrix is opaque, and the clast displayed includes 2 older generations of breccia, representing older events of deformation. Note that the opacity of the matrix increases with age (1 is the oldest, 3 is the most recent event. e) Sample MB 10 also displays 3 generations of breccia, but the most recent matrix is less opaque than that of the right (green) part of the sample. f) Is the same area, but with cross polarized light.

MB 16 is a dark green, coarse cohesive breccia. The clasts are sub-angular to sub-rounded remnants of gneiss, often as feldspar or quartz aggregates with an opaque coating. MB 05 is a medium-grained cohesive breccia with most clasts being protobreccias. One clast of pseudotachylyte/ ultracataclasite is found (see Figure 4-8 a). The matrix is dominated by zeolite, and the clasts are sub-angular to angular with random orientations. MB 07 is a coarse cohesive breccia with clasts of protobreccia, which is cut by zeolite veins (see Figure 4-9 c) and d)). At a later stage of deformation, the breccia has been cut by another set of zeolite-filled veins. The breccia clasts are coated with a more opaque matrix, marked with arrows on Figure 4-8 b). MB 08 is a chaotic zeolite and opaque dominated sample. In Figure 4-8 c) (and Figure 4-9 a) and b)) the different generations of breccia, cataclasite and pseudotachylyte/ ultracataclasite are displayed. (1) is opaque pseudotachylyte/ ultracataclasite within (2), zeolite dominated cataclasite. These are cut by a vein of zeolite (left arrow). This clast of cataclasite seems to be incorporated in a cohesive breccia (3), with a slightly opaque matrix. This again is a clast in the most recent breccia, which is more opaque (4). The clasts of this breccia are randomly oriented, and cut by a later zeolite-filled vein (right arrow).

MB 10 is grading from green to pale red medium-grained, indurated breccia. The left part of this sample is represented by Figure 4-8 e) and f), which has 3 generations of cataclasis. The last generation has a quite different matrix than the opaque matrix from the right part of the sample. The right part is presented in Figure 4-8 d) has at least one generation of cataclasite (1) captured in an indurated micro-breccia (2), which again is a clast in the cohesive breccia sampled. The matrix is impregnated by iron oxide. Note the opacity increases with age of the fault rock. Figure 4-10 b) displays a quartz grain which is surrounded by chemically zeolite dominated matrix (1), probably of zeolite. This is again a grain within another matrix, which is higher in iron (Fe) and magnesium (Mg). Along the edge of the sample, an ultracataclasite are found, displayed in Figure 4-10a), upper part and c) and d) to the right. The location of the ultracataclasite is shown on Figure 4-6, between 14) and 15). It consists of zeolite, alkali feldspar, biotite and opaque with grains of $< 5\mu m$.

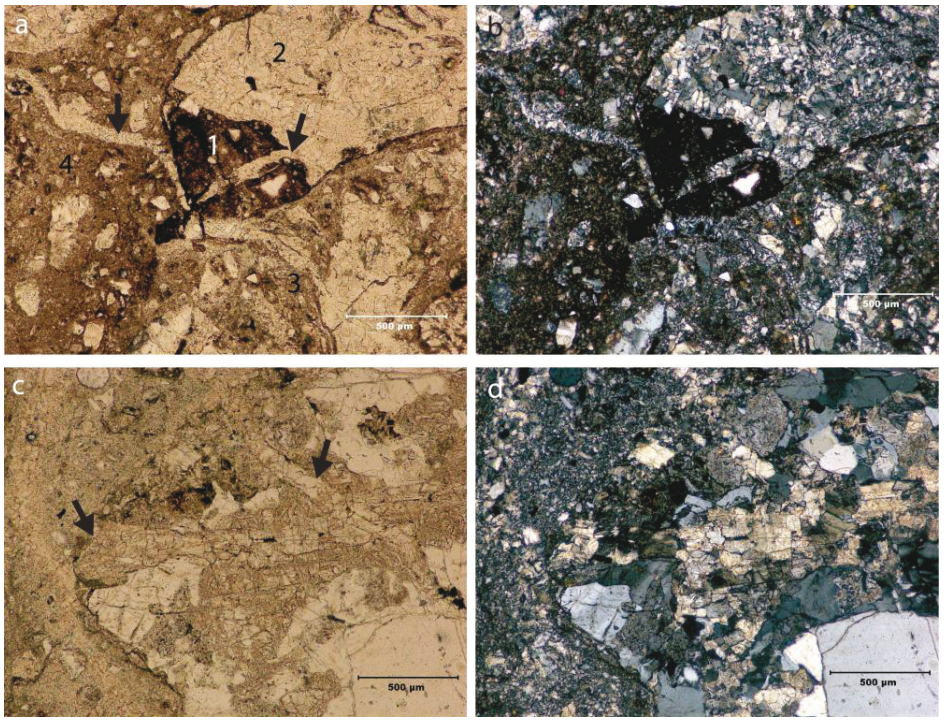

Figure 4-9: Micrographs of the different fault rocks from locality 1) Mulvik. Scale bars represent 500 µm. a) Sample MB 08 displays an opaque pseudotachylyte/ ultracataclasite within a zeolite breccia. Both are cut by zeolite veins (arrow to the right). They seem to be within a slightly opaque breccia (3) which again is within breccia 4. Breccias 3 and 4 are cut by a zeolite vein, marked with an arrow. b) Is the same area, but with cross-polarized light. c) Sample MB 07 displays a large host-rock and zeolite dominated breccia in a zeolite matrix. The clast is cut by 2 different generations of zeolite veins, where only one of them (the uppermost arrow) cuts through the surrounding matrix. d) Is the same area, but with cross polarized light.

MB 03 displays a transition from protobreccia to cohesive breccia with clasts of protobreccia. The breccia is a green, coarse cohesive breccia with sub-rounded to sub-angular clasts. It extends through the whole length of the fault core. MB 15 is a lens of cataclasite, cut by large fractures filled with zeolite. The matrix is of fine-grained zeolite. The sample is from the southern boundary between the protolith and the fault core.

MB 12 is the unconsolidated breccia shown in Figure 4-6. It is likely to represent the last breccia generation. The clasts consist of pseudotachylyte/ ultracataclasite, cataclasite, protobreccia and indurated breccia. The pseudotachylyte/ ultracataclasite is very opaque and floating in an opaque matrix. Due to its opacity, it is not possible to see it in optical microscope, but in Figure 4-10 f) it is displayed in a SEM backscatter image.

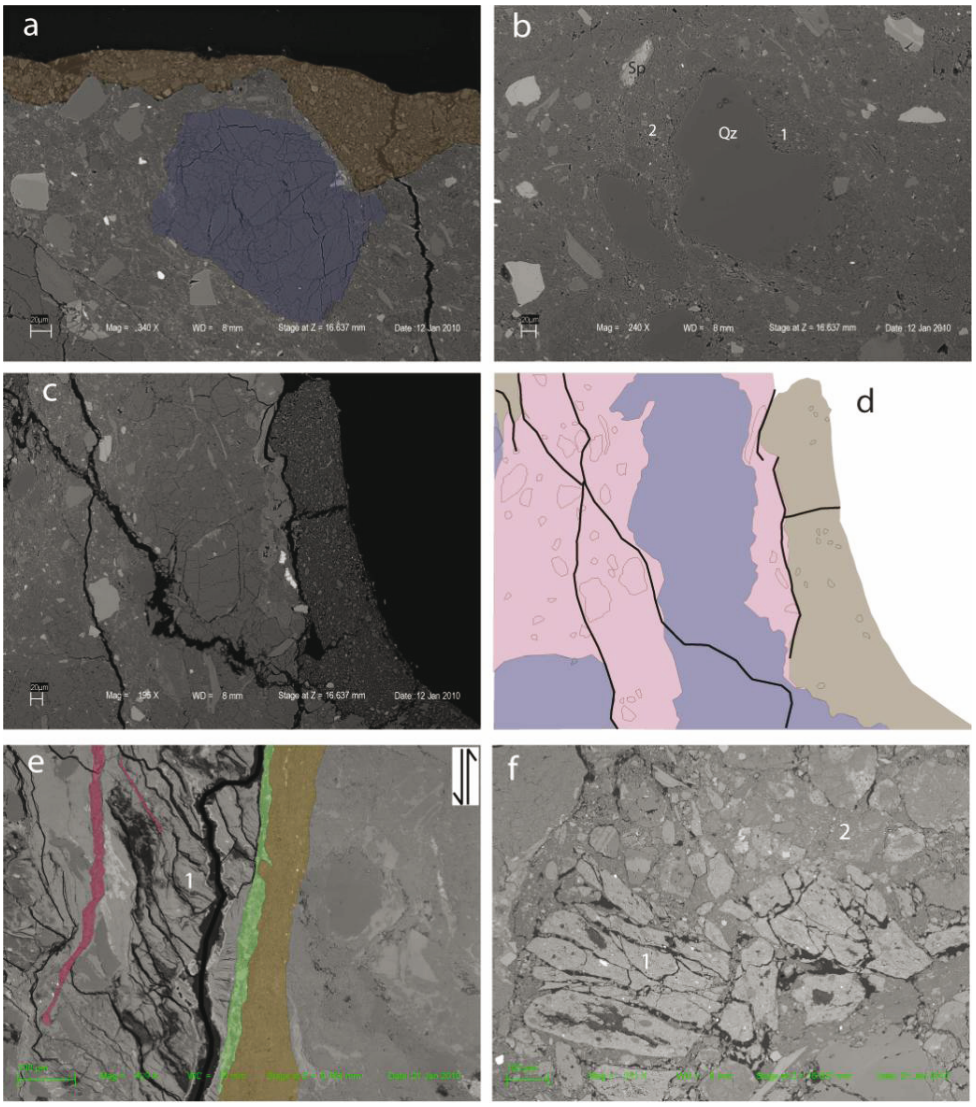

Figure 4-10: SEM backscatter images from Mulvik fault core. Scale bars lower left show 2 µm, except for e) and f), where it is 100 µm. a), b), c) and d) are from sample MB 10. a) Displays a 230 µm large grain of alkali feldspar (blue) within a breccia with a matrix of zeolite, quartz, biotite, sphene and opaques. On top of the image, and marked brown, is an ultracataclasite of zeolite, alkali feldspar, biotite and opaque. b) Displays a 200 µm large quartz grain with a close to pure zeolite matrix around it. This is again is within a breccia with matrix of quartz, alkali feldspar, biotite, sphene and opaque. c) and d) Show the different fault rock generations. The blue part is cataclasite clasts and elongated strings of cataclasite within opaque breccia (pink). The brown is ultracataclasite, also displayed in a). e) Is from MB 11, it displays elongated slivers of cataclasite and biotite accumulated in fractures. The biotite (1) is kinked and fractured. Some parts of the slivers are more opaque (marked with green). Relative movement of the fault are shown by the arrows. Zeolite veins are marked with pink. f) Is from MB 12, the incohesive breccia. It shows a faulted and cut by zeolite, opaque pseudotachylyte/ ultracataclasite clasts (1) within the gouge (2).

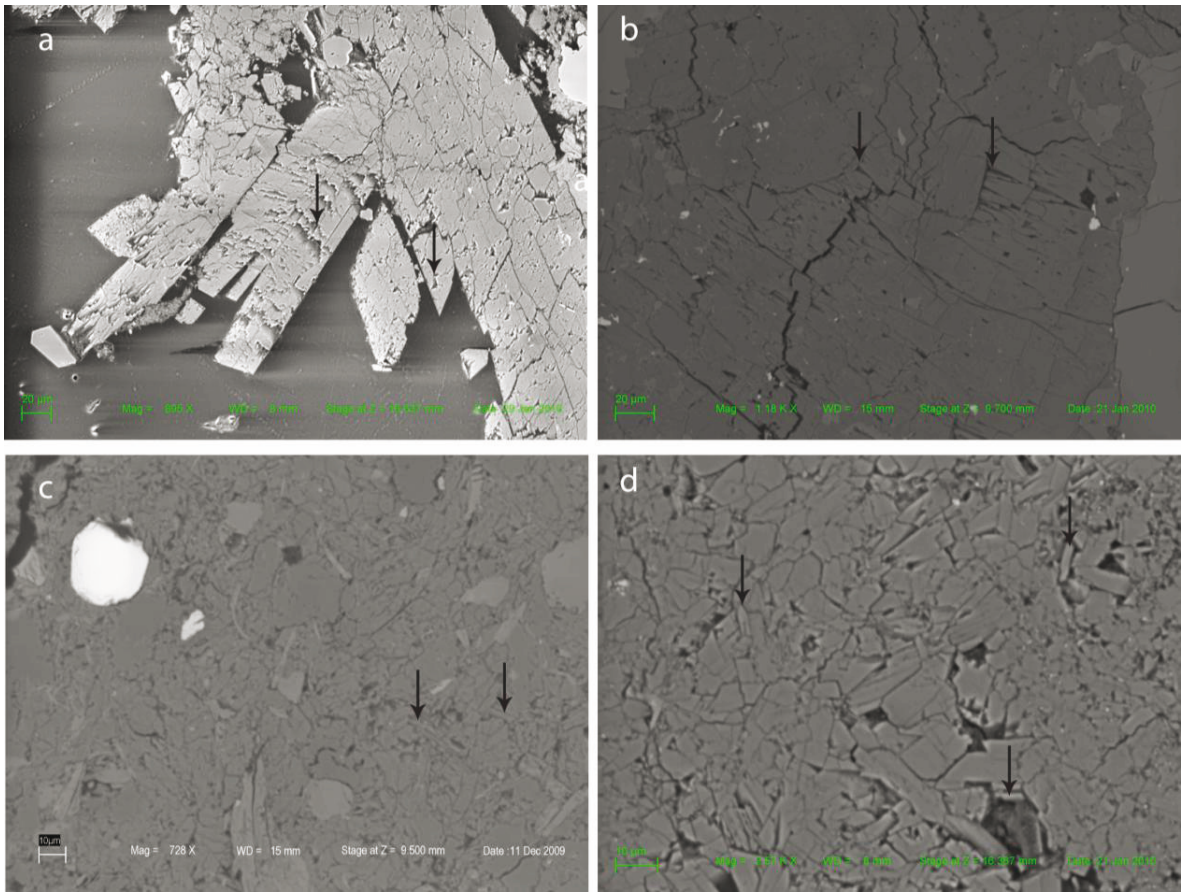

Figure 4-11: SEM backscatter images demonstrating how the zeolite crystals are brittly fractured and split into elongated laths. Scale bars down to the left represent 20 µm on a) and b), and 10µm on c) and d). a) Is from MB16, b) and d) are from MB15 and c) is from MB07. a) Zeolite growth in open fractures. Note the incised depressions marked with arrows. b) Large zeolite crystal aggregate with similar incised depressions as in a) marked with arrows. c) Displays a micro-breccia with zeolite laths matrix. d) Displays a pure zeolite micro-breccia.

Zeolite matrix evolution

In Figure 4-11, a series of backscatter images demonstrates how the zeolite vein mineral is brittly fractured and split into needles or lath-fragments. In Figure 4-11 a) zeolite growing in open fractures of sample MB 16 is displayed. From the probing these crystals have no Potassium (K),, and about 5 weight% of calcium (Ca).. The bright colour is artificial, to sharpen the image. On these crystals, and the large zeolite crystals found in sample MB 15, Figure 4-11 b), the crystallographic cleavage is clear. Fractures tend to develop along this cleavage as the crystals break down. This is indicated with black arrows on incised depressions on the figure. This is where,

what herein is called zeolite laths, originate from. In Figure 4-11 c), a matrix consisting of these zeolite laths are displayed. It is from MB 07, a red, coarse, cohesive breccia. Two laths are marked with arrows on the figure. Note the sub-microscopic size of these laths. In Figure 4-11 d) a breccia from MB15 is displayed. The matrix is zeolite dominated. The zeolite is analysed to have some K, and 6-7 weight% of Ca.

These zeolite laths appear to be a fundamental component in the matrix in breccias and cataclasites, from all the studied localities. It seems to be related to the vein minerals, and therefore both the vein minerals and the laths minerals of the matrix are probed and analysed in SEM.

4.1.4 Kinematics

The orientation of the faults described from Mulvik are A) the northern fault of 282/86, B) the southern fault of 252/82 and C) the Mulvik fault core of 250/80. They have a generally steep, but northerly dip, as indicated by the northern and southern faults and the near-vertical main fault core. In the slip-linear plot shown in the lower part of Figure 4-4, the fault measurements are shown. They show indications of a dip-slip movement of the fault. Geometries and plunge measurements indicate that this is a normal dip-slip fault, albeit the fault is so steep that 'north side down' may be a better way to describe it.

Two 'reverse' faults found in relation to the unconsolidated part of the Mulvik fault core, marked with split-arrows on Figure 4-4 and Figure 4-6. These are probably R-shears, related to 'northern side down' faulting. They are clearly cutting; zones 14), 15) and 16), but as it is going into the incohesive breccia it disappears. This is an indication of a probable establishment of these faults simultaneously with the establishment of the incohesive breccia.

These geometries are found in the thin section of sample MB 11, seen in Figure 4-12. These 'reverse' faults, are at an angle of 25˚ to 35˚ to the fault, and probably represent R-shears. They seem to be reverse, as the normal fault is very steep.

Kinematic at micro scale

The extensional fractures of the Mulvik fault core can be divided into two sets, where both are dominated by and filled with pink and white zeolite. One set is parallel to the fault, and is shown

in the southern part of the fault core, in zones 1) and 2). The other set is particularly prominent in zone 5), where the fractures are anastomosing, and at an angle of 30˚to 60˚to the fault.

The margin of sample MB 11 shows opaque, foliated cataclasite, sheared by several 'reverse' faults (see Figure 4-12). These faults have the same trend as seen in the outcrop line-drawings of Figure 4-4 and Figure 4-6. Within the foliated cataclasite, larger (< 0.1 mm) porphyroclasts of quartz, feldspar and epidote are found. Some of these are σ-types, like the porphyroclast shown on Figure 4-12. The tails of this porphyroclast contain Fluor and Phosphor, similar to the content of Fluor-apatite ($Ca_5(PO_4)_3F$).

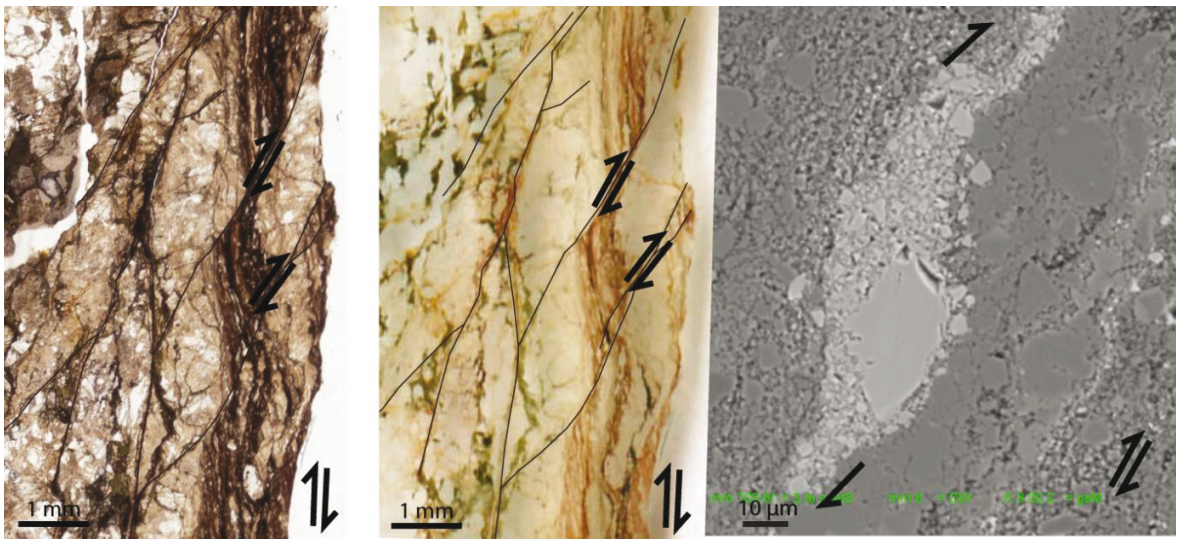

Figure 4-12: MB 11 in thin-section micrographs and one SEM backscatter image. Scale bar represents 1 mm on the micrographs, and 10 µm on the backscatter image. Foliated cataclasite cut by reverse shear-bands with same trend as 'reverse' faults seen in Figure 4-6. The backscatter image shows an σ-type porphyroclasts within the foliated cataclasite, showing a trend parallel to the Mulvik fault. North is to the right on all micrographs and the orientation of the Mulvik fault is shown in the lower right corner on all photographs.

4.2 Locality 2) Rød

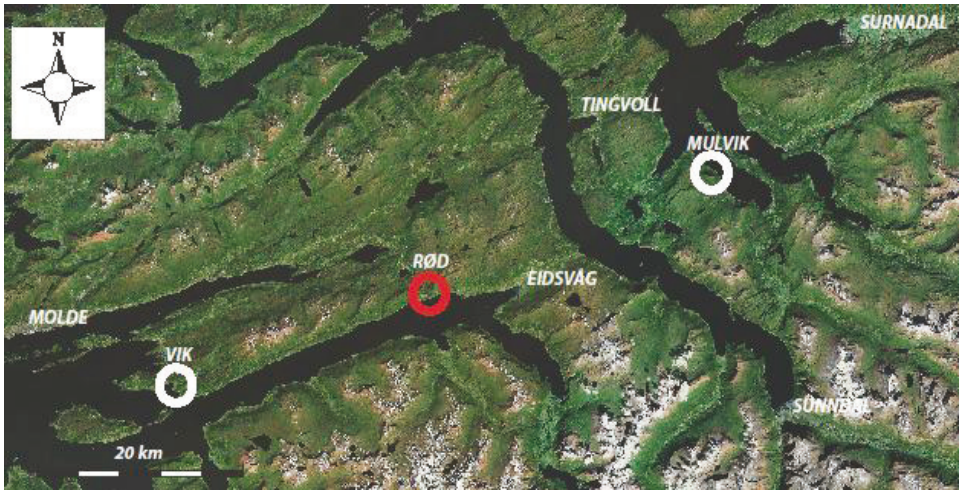

Figure 4-13: Red circle marks the location of locality 2) Rød (7˚53' 36'' E, 62˚46' 4''N). Satellite-photo from www.gulesider.no/kart

At Rød (Figure 4-13) a section of approximately 60 m exposes several smaller fault cores (on the cm scale), and one larger fault core with extensional duplexes. The extensional fractures display growth of zeolite. This mineral appears to have impregnated the fault core, resulting in a pink to brick colour of the deformed rock. The core was scanned with terrestrial LIDAR scanning, resulting in a model of the fault architecture (Figure 4-14). LIDAR model with photograph draped on top of the point cloud are found in Appendix 2.

4.2.1 Fault architecture

At Rød both hanging wall and footwall display well developed fault lenses. In the hanging wall of Figure 4-15 several fault lenses of gneiss have developed (right blue part on Figure 4-15). They can be seen as one 4 m long lens of the Ls6 type (Figure 2-7) with a dense network of shears within it, defining smaller secondary lenses. Large parts of the 1st order lens is not exposed, but the 2nd order lenses are defined by segment amalgamation (Figure 5-1 F).

On the top left part of the fault core (shown with darker brown colour in Figure 4-15), there is a zone of gouge and crush breccias. The zone is intensely fractured and has a chaotic appearance. The belonging fractures are interpreted to be Riedel shears.

Figure 4-14: LIDAR model of locality 2) Rød, here shown by the point cloud. Arrows indicate relative movement of the most recent event of faulting.

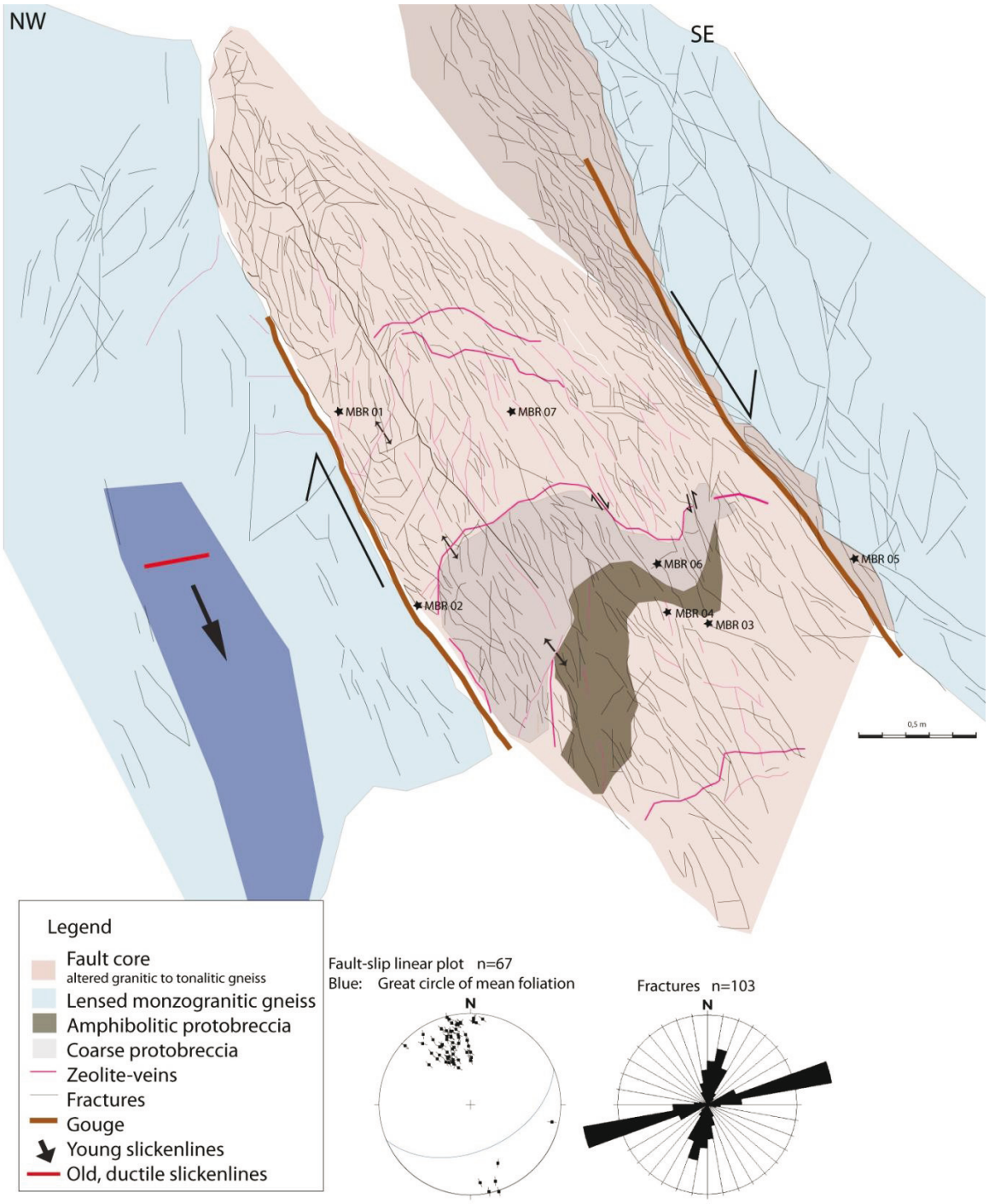

Figure 4-15: Fault core architecture at Rød. Large arrows indicate relative movement.

This zone is found along the fault core, marked as the upper gouge on Figure 4-15. This and the gouge zone below the fault core are the zones with concentrated deformation. These rocks are granulated and crushed to incohesive gouge and cohesive crush breccias.

The fault core at Rød is exposed in 3 dimensions, enabling its architecture to be studied in 3D detail. The fault core consists almost entirely of altered gneiss saturated by extensional zeolite veins (split arrows) in E-W direction. They have a sigmoidal form that might indicate that they pre-date a recent episode of activity. An N-S oriented and steeply dipping fracture set filled with zeolite cuts, and thus post-dates the extensional factures. Zeolite-filled fractures are marked with pink in Figure 4-15.

4.2.2 Fracture density

The outcrop at Rød exposes fault architectures about 5 m into the hanging wall, and 15 m of the footwall. The fracture density at Rød (Figure 4-16) has a slow decrease in the footwall, to 4 fractures/metre followed by a new fault core, with an increase in fracture density. The hanging wall has an abrupt decrease over 2 m away from the fault core. Only 5 metres of the hanging wall section is exposed.

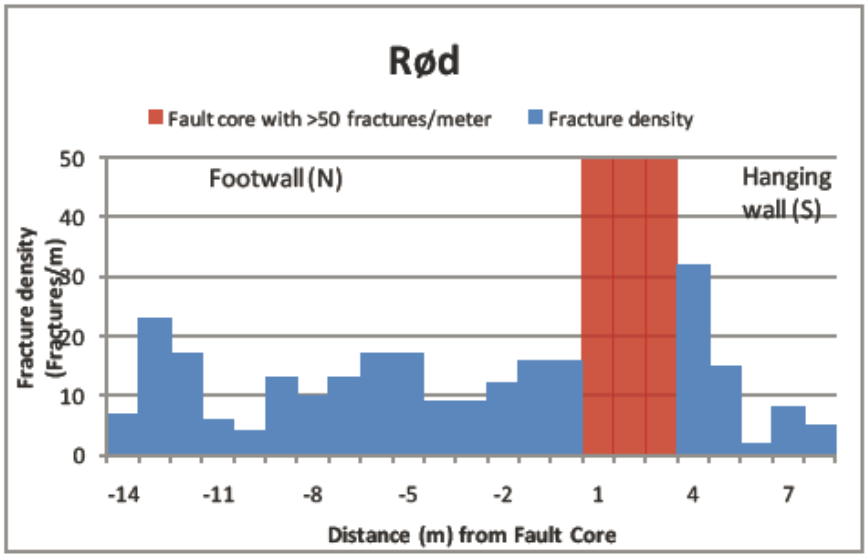

Figure 4-16: Fracture density across the Rød fault

4.2.3 Fault-rocks

The 7 samples from Rød are described in Appendix 1, and the sampling locations are displayed in Figure 4-15. The host rock sample MBR 07 is from modal analysis classified to be granitic gneiss. The following will be a description of the rocks with increasing deformation.

MBR 07, MBR 06 and MBR 05 are altered gneisses from the fault core, between the extensional duplexes. They are holocrystalline and xenoblastic with gneissic foliation. They are dominated by quartz and plagioclase, where the latter is highly saussuritized. MBR 06 is bisected with one part being amphibolitic gneiss, and the other being tonalitic gneiss. MBR 05 is coarse tonalitic gneiss, but towards the edge, where it borders the upper gouge zone on Figure 4-15, the rock is increasingly deformed. At some places the amphibole is crushed, and appear as a very local, green matrix (see lower parts of Figure 4-17). On the upper part of the photograph of Figure 4-17, an indurated gouge has developed. It has some quartz grains of 0.1mm, but the average particle size is 0.01mm.

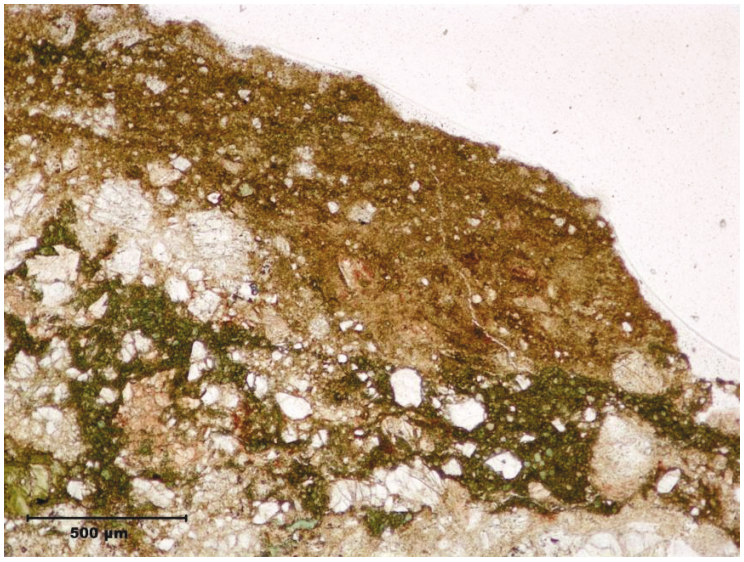

Figure 4-17: From sample MBR05. Scale bar is 500 µm. On top: consolidated gouge with quartz grains, marking the boundary to the gouge zone to the right on Figure 4-15. Below: indurated breccia, with very local amphibole-matrix (green).

MBR04 is a 7 mm wide vein of zeolite breccia, cutting through coarse granodioritic gneiss. The breccia has up to 3mm long zones of host-rock fragments floating in the matrix. Some veins are penetrating the host rock, cutting through large quartz and amphibole crystals as well as the ma-

trix. This is indicated in the micrograph in Appendix 1. MBR 03 has a network of zeolite veins that cut granodioritic gneiss. About 40% of the sample is zeolite. The vein mineral occurs in the N-S trending fractures. MBR 04 and MBR 03 are both analysed in SEM (Chapter 4.5.1).

MBR 02 is found in the gouge zone to the left on Figure 4-15. It is a pink, indurated micro-breccia with sub-round clasts, and a zeolite-saussurite matrix. The vein mineral seems to be the main component of the matrix, and some veins are cutting through the breccia.

MBR 01 represents the vein mineral growing in the open fractures in the extensional duplexes. The crystals are columnar with a perfect cleavage in {010}. It is colourless in thin section, but pink in hand specimen. The size of the crystals is between 0.1-0.2mm. The vein mineral of this sample is analysed in XRD, see results in Chapter 4.5.2.

Zeolite

At Rød, 2 samples are analysed in SEM, MBR 03 and MBR 04. MBR 04 represents the vein mineral in the extensional duplexes, which is cut by the N-S trending fractures, represented by MBR 03. The samples have a slight difference in chemistry, being: less aluminium (Al) and silicon (Si) in MBR 03 and more oxygen (O). This is probably due to a slight change in zeolite-chemistry, but it can be due to holes in the thin-section of MBR 03.

ELEMENT	MBR 04		MBR 03	
	From	To	From	To
Al	11.50	14.00	5.50	9.50
Si	29.00	31.00	14.00	20.00
Ca	7.50	9.00	2.50	5.50
O	49.00	49.00	56.00	62.00
Na				
K	0.00	0.80	0.20	0.80

Table 2: Results from SEM chemical probing at Rød.

4.2.4 Kinematics

The Rød fault plane is orientation is 086/66 +58, displayed as the red great circle of Figure 4-18. It is slightly steeper, but sub-parallel to the mean orientation of the foliation, which is 064/49. In the rose diagram two dominating fracture sets are evident. One is the trend of foliation and the fault (dark red), the other being approximately N-S (red). The N-S fractures cut and offset the extensional duplex-veins, and are frequently filled with zeolite (as described in Chapter 4.5).

The LIDAR data has been used as quality assurance of the field measurements. As seen on Figure 4-18, the field measurements and the LIDAR data give similar results. When comparing the rose diagrams, a dominating fracture set of ENE-WSW is clear in both datasets. The N-S fractures have a slightly different orientation in the LIDAR-based dataset.

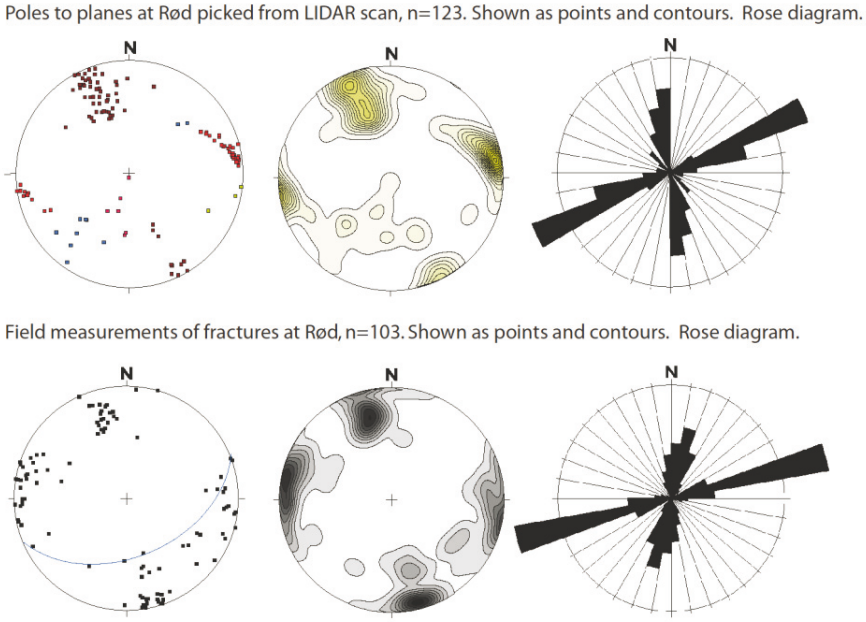

Figure 4-18: LIDAR fractures compared with fractures measured in field.

4.3 Locality 3) Vik

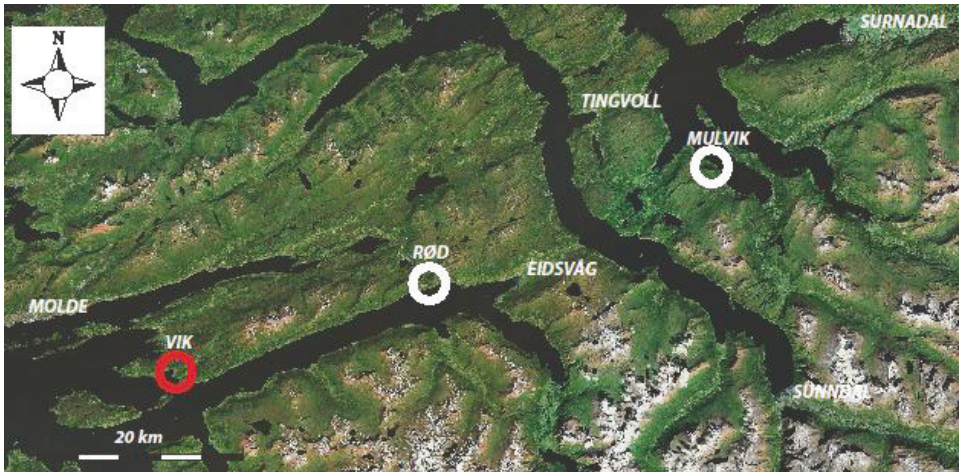

Figure 4-19: Red circle marks the location of locality 3) Vik (7˚27' 15''E, 62˚41' 26''). Satellite-photo from www.gulesider.no/kart

The outcrop at Vik is found in the western end of Langfjorden (Figure 4-19). It displays a 3-dimensional exposure of a fault system that consists of numerous faults, synthetic as well as antithetic to the main fault plane in the north-western part of the outcrop. Some of the fault cores are chaotic systems of fractured fault products. They are wet, and seem to host well-developed transportation systems for fluids. This also results in parts being overgrown with moss, and complicates the detailed descriptions, but several good cores are well exposed and herein described.

4.3.1 Fault architecture

The LIDAR model of Vik is shown in Figure 4-21 and in Appendix 2. In Appendix 2, the model is displayed as 1) the point cloud, and 2) the point cloud with the photograph draped on top of the point cloud.

Model 2), with the photograph draped on the point-cloud are used to interpret the surfaces of the main fault planes. These are coloured after orientation. Red colour represent the main fault plane (to the left) and planes parallel to this. Blue and green represent antithetic fault planes, where the green planes define the fault core shown in Figure 4-25. As the LIDAR models indicate, the outcrop has a quite complex architecture. To systemize it, successively numbers, from W to E in the outcrop, are assigned for the faults, (see Figure 4-21). Fault 1) is the main fault plane, with faults

3), 6) and 7), being sub-parallel to it. The best developed fault core is defined by faults 9), 10) and 11). This is an antithetic fault to the main fault plane, and is therefore not referred to as the main fault. Faults 3) and 4) are sub-parallel to these, and are therefore also antithetic faults.

Figure 4-20: Photograph looking to the west in the outcrop of Vik. To the left is the main fault plane, fault 1 in Figure 4-21.

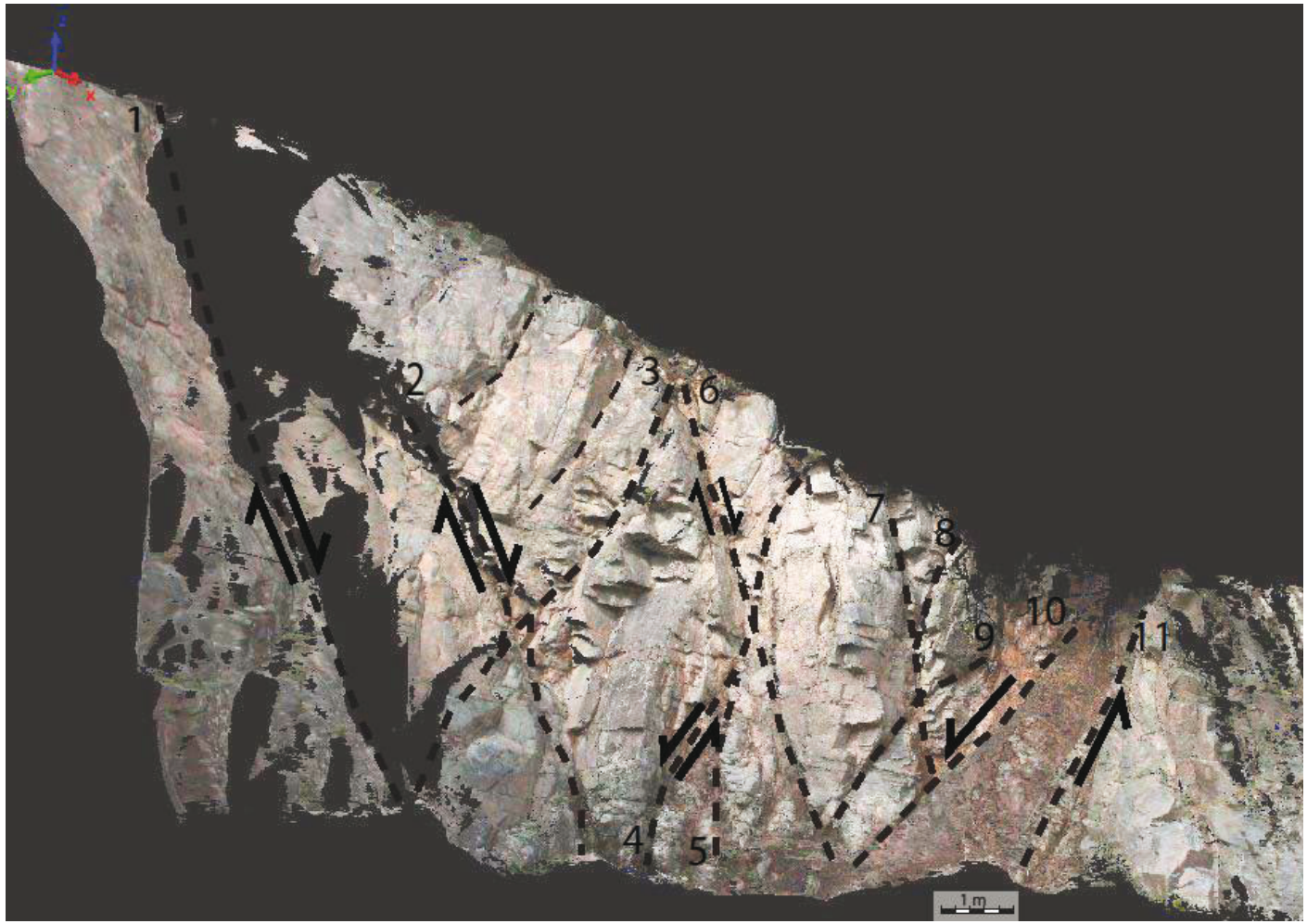

Figure 4-21: Here the picture is draped on the point cloud. The main fault planes are stippled, and numbered. The dominant movement is indicated by arrows. The master fault is shown to the left, marked as nr 1).

Fault 1

Fault 1, the main fault plane, has developed a small fault core displayed in picture and line drawing on Figure 4-22. It has some elongated slivers of green cataclasite, with clasts of protobreccia, and zeolite mineralization along it. The fracture density increases in the fault core, and many fractures have concentrations of black material in it. The foliation has a generally fluctuating orientation, but the change across the fault is marked.

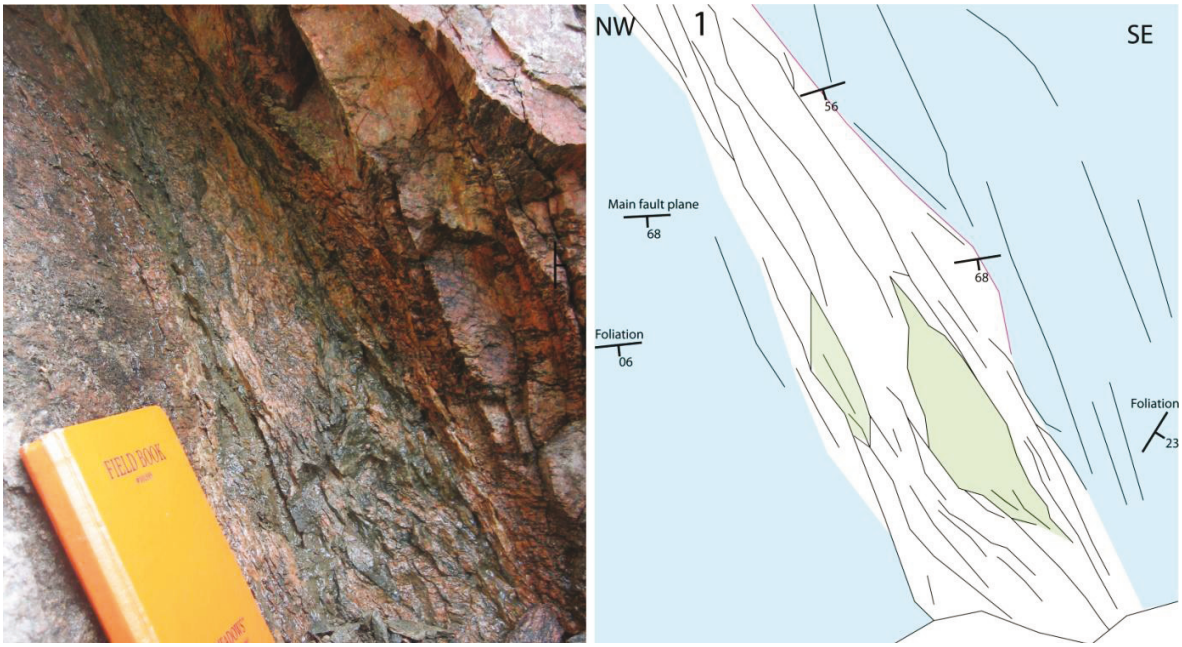

Figure 4-22: Small fault core at the main fault plane, 1 at Vik. Note the dark green cataclasite (marked green) that has developed in lenses found along and within the fault core and the change in foliation across the fault. Some zeolite mineralization occurs along the fault plane.

Fault 2

Fault 2 splays out from and amalgamates into fault 1. This can be seen to the left in the photograph of Figure 4-20. Together these faults define a fault lens made by segment splaying and segment amalgamation.

Fault 3

The bottom part of fault 3 displays a fault lens of the Ls4 type (Figure 2-7 from Braathen, et al., 2009), with a swarm of fractures. It has a chaotic zone of highly fractured rock on each side. The fault bounding surface to the left has an orientation of 090/85, and to the right of 068/83-55.

Faults 4, 5 and 6

Faults 4, 5 and 6 are displayed in the photograph and line drawing in Figure 4-23. In fault 4 a elongated sliver of green cataclasite is found. Fault 5 seems to be a branch of fault 4, where a lens is formed between them. One, approximately 2 m long Ls3 type (relative to fault 5) fault lens is found between faults 5 and 6. It has a dense network of shears. Some zeolite mineralizations are found. The fault cores are pink, and it is likely that they contain zeolite veins. However these are microscopic, and cannot be seen in outcrop. Fault 6 might predate faults 4 and 5 because it seems to be cut by these. Several fault lenses are shown in Figure 4-23. These are discussed further in the discussion. The one to the right in the figure is an approximately 4 m long lens of gneiss. It is an Ls4 type lens with open to dense network of shears.

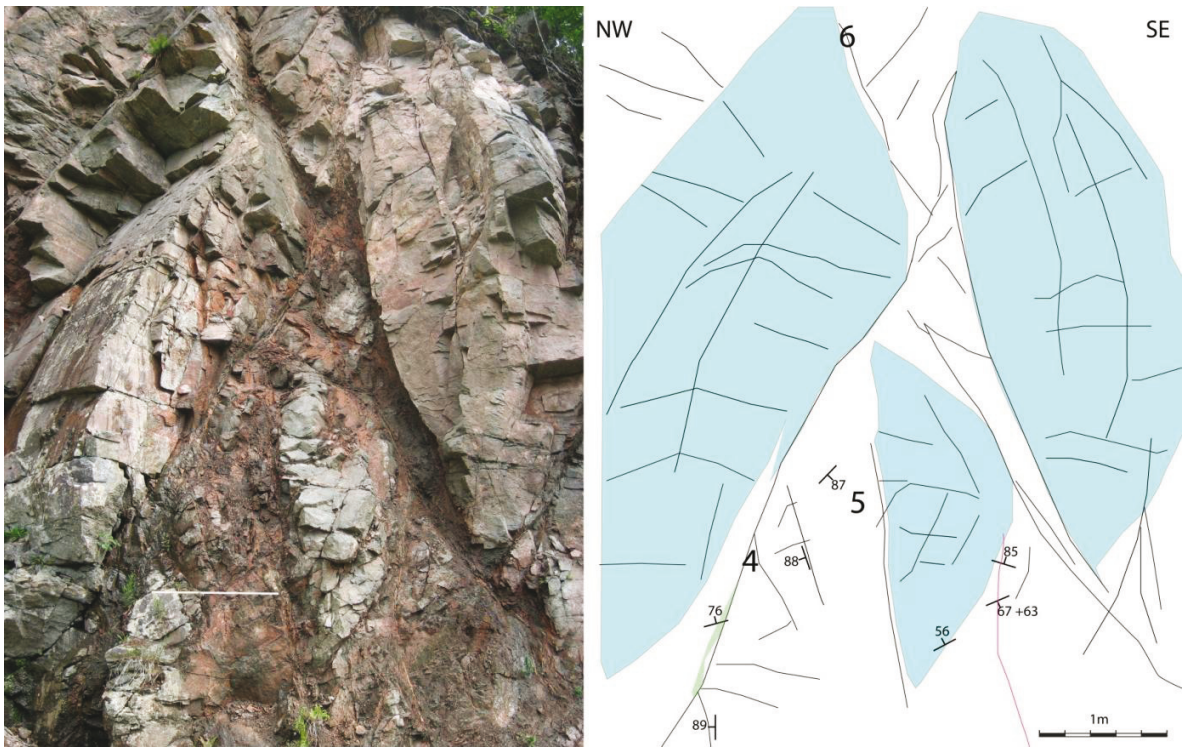

Figure 4-23: Detailed photograph and appurtenant line drawing of fault 4, 5 and 6. Several fault lenses are displayed.

Eastern fault

A few metres away from the scanned part of the outcrop another fault is found, shown in the photograph and line drawing in Figure 4-24. It is N-S trending and dips steeply to the west with a fault core of cohesive protobreccia and breccia. As marked on the figure, extensional fractures with zeolite growth, as well as P-shears and Riedel shears indicate a dip-slip normal movement along the fault. Two zones have developed elongated, green cataclasite. One zone in the top of the fault core might be a pegmatitic vein from the gneiss, similar to the ones described in the next paragraph. This zone seems to be brecciated along the fault, resulting in a pink breccia. As this is in an inaccessible part of the outcrop, this is somewhat speculative. The green cataclasite found here display black slickenside lineations, whilst the pegmatite-breccia has yellow and green lineated slickenlines, probably by epidote.

In a fracture parallel to the extensional fractures, a thin zone of pink cataclasite is found. This can be seen in Figure 4-28 b).

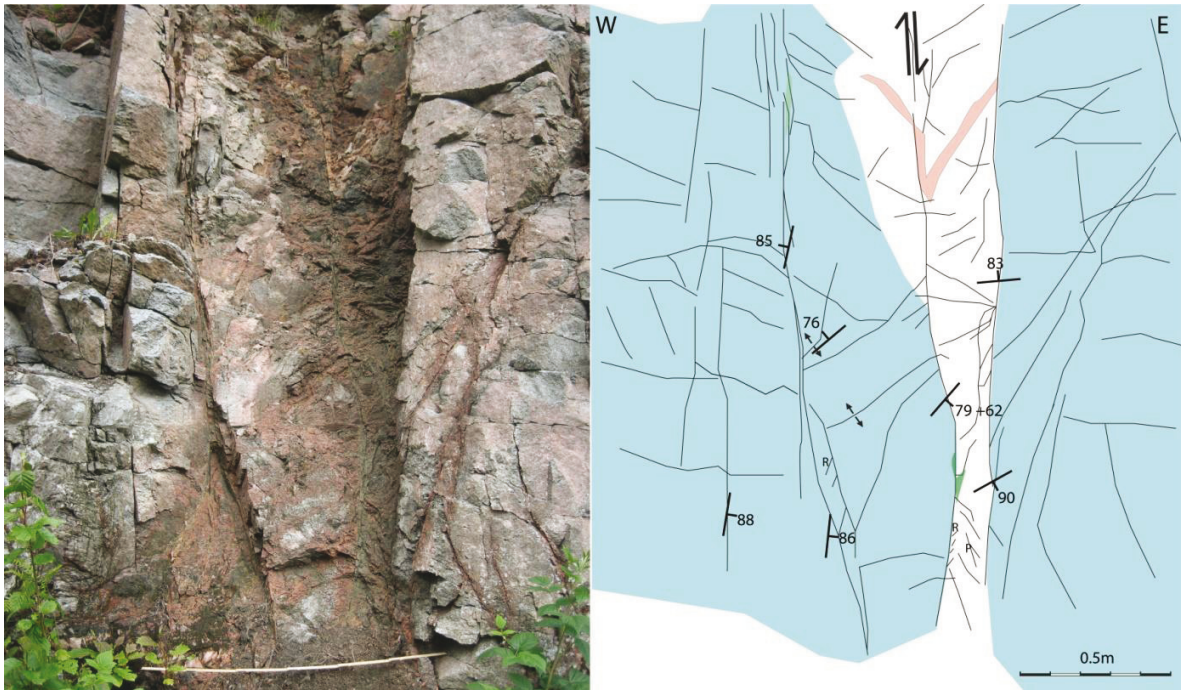

Figure 4-24: Photograph and appurtenant line-drawing of N-S trending fault core, ~10 m to the east of fault 11.

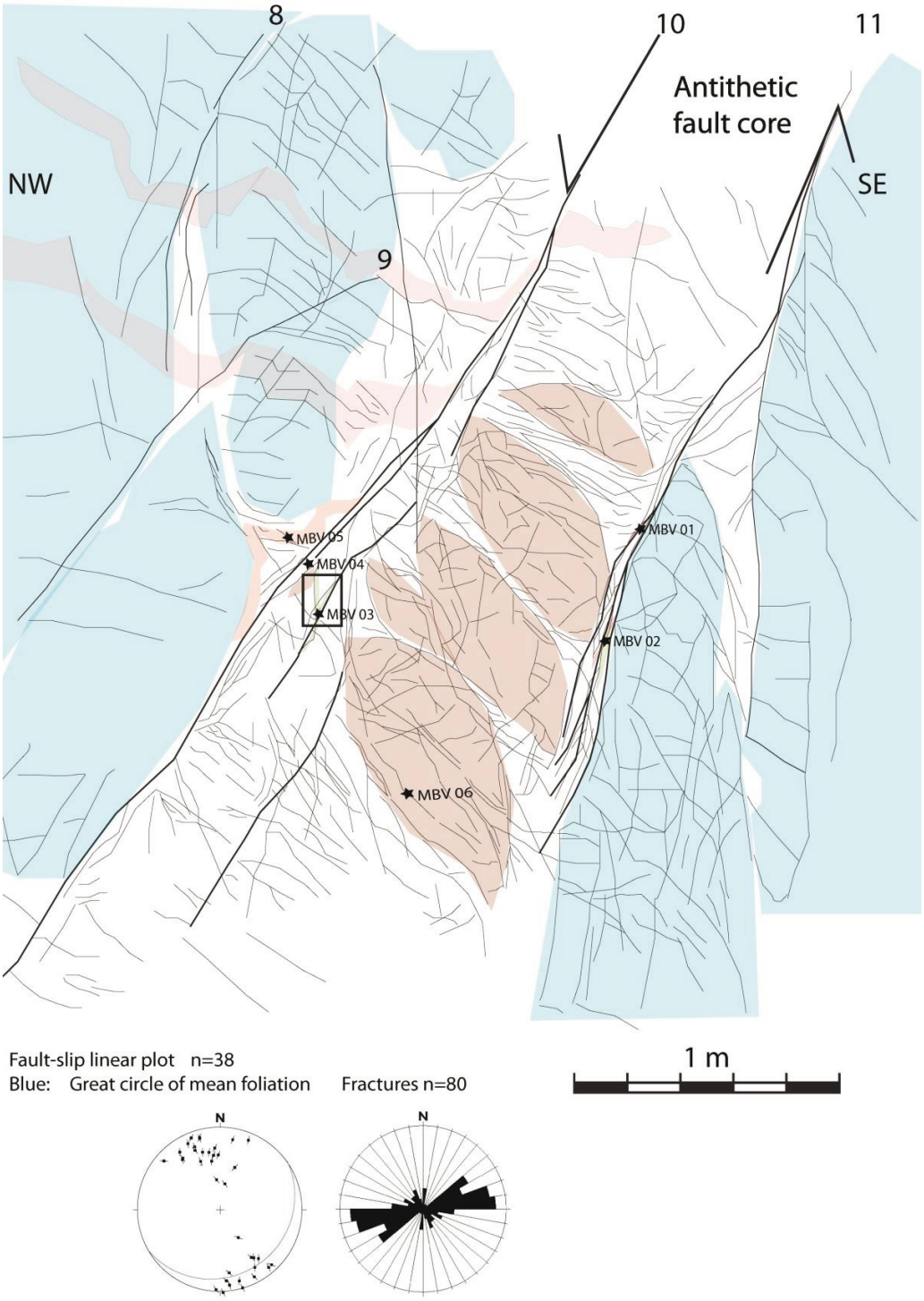

Figure 4-25: Antithetic fault core at Vik bounded by faults 9, 10 and 11. Note the synthetic rotated fault lenses within the fault core.

The antithetic fault core

In Figure 4-25, the antithetic fault core is shown as a line drawing. Faults 8, 9, 10 and 11 on Figure 4-21 are displayed, where 10 and 11 define the fault core. The damage zone is marked with blue. It consists of highly fractured host rock, but it is less deformed than the rocks of the fault core. The foliation of the gneiss shows some layers of pegmatitic gneiss, marked with bright brown colour. These are faulted, and can be traced into the fault core.

The fault core is defined by 2 zones of intense deformation. They have long, anastomosing strings of black fault rock material stretching along the whole core. They are marked on Figure 4-25 by thicker black lines. On both sides green cataclasites (marked green on the figure) are found in connection to these. On the right side there are also some light pink cataclasite found (marked pink on the figure).

Within the fault core, a set of lenses of gneiss and protobreccia have formed. They are bounded by high strain zones surrounding them. This makes the lenses highly fractured, as indicated by the Figure 4-26. The boundary between lenses has a high susceptibility of fractures. Each lens has surfaces with green and red lineations, and zeolite strings following the top and bottom surfaces. The relative movement of the fault blocks is indicated by the pegmatitic layers, and one particularly evident set of Riedel shears are observed on the right side of the fault core. The relative movement of the fault lenses within the fault core is counter clockwise, being synthetic to the fault. This is consistent with steep, extensional fractures (in MBR 06) and the bounding surfaces of the lenses being X- and R_1-shears.

The fault lenses found in this locality are probably formed by segment splaying and tip-line coalescence for the 1st order lenses, while the 2nd order lenses are made by segment amalgamation, segment linkage and segment splay. This is discussed further in the Chapter 5.1

4.3.2 Fracture density

The Vik outcrop displays the hanging wall of a normal fault dipping to the south. The fracture density is therefore measured only in the hanging wall (Figure 4-26). The master fault is further north in the figure. The fault core marked red in Figure 4-26 is seen between faults 10 and 11 on

Figure 4-21. Its fracture density is estimated to be >50 fractures/m, as the fragments between each fracture are less than 2 cm wide.

The fracture density is increasing in intensity from the master fault to the antithetic fault core, where it reaches its maximum. Further away from the master fault, towards the south-east, the fracture density is then decreasing. Despite the antithetic fault core and the increase in fracture density towards it, the general trend of the fracture density at Vik is that the height of the peaks decreases from north to south. The peaks represent the fault cores.

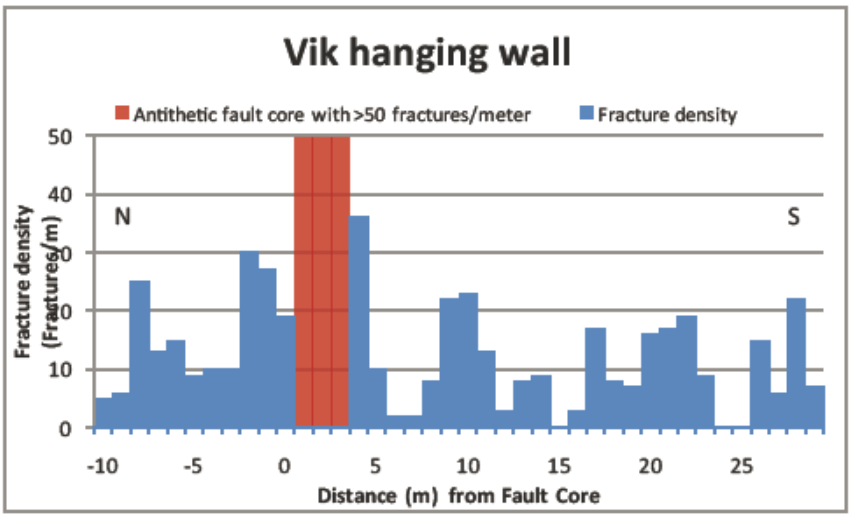

Figure 4-26: Fracture density Vik

4.3.3 Fault-rocks

The 7 samples from the Vik are described in Appendix 1, and the sampling locations are displayed in Figure 4-25. The host rock sample MBV 07 is from modal analysis classified as granitic gneiss. It is holocrystalline with xenoblastic, medium-grained crystals. It has a well-defined foliation with accumulations of dark minerals (amphibole and biotite). The following will be a description of the fault rocks, sampled at Vik, with increasing deformation.

A general observation from the fault rocks in the outcrop scale is that the darker the fault rock is, the more fine grained the matrix. The matrix at Vik is often green to black, consistent with very fine grain-series.

MBV 06 is an altered quartz-monzonite with one dominant vein of pink zeolite, cutting through the gneiss foliation at a high angle. MBV 05 is proto-brecciated pegmatitic gneiss. It has developed a saussurite-zeolite matrix between large (up to 2 cm) microcline grains. MBV 04 is a light pink, indurated micro-breccia, with a matrix of saussurite and zeolite. MBV 03 is from the left part of the antithetic fault core, displayed in the picture to the left of Figure 4-27. It is a green cataclasite, with clasts of an older cohesive breccia and protobreccia (indicated on the figure). Other clasts are single minerals, like amphibole, quartz, apatite, microcline and zircon.

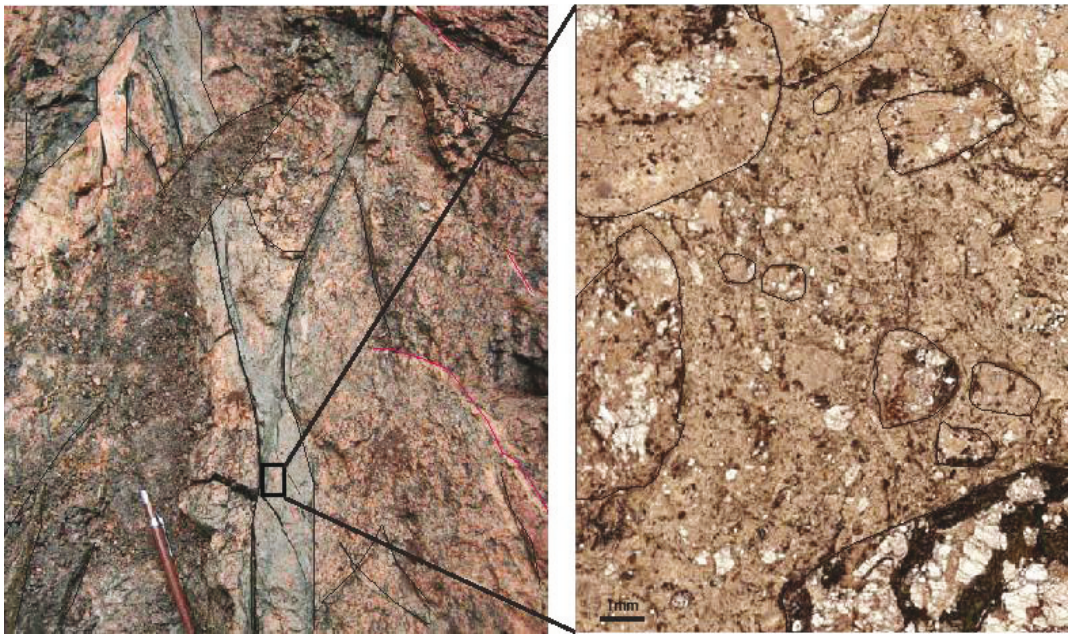

Figure 4-27: Photograph (shown as a square in Figure 4-25) of the sampling point of MBV 03. It is a green cataclasite, with larger clasts of protobreccia as shown on the micrograph to the right.

The samples MBV 02 and MBV 01 are taken from the right boundary of the antithetic fault core. They are both ultracataclasites, consisting almost entirely of zeolite-matrix. Both have sub-rounded clasts up to 0.2mm, whilst the matrix is less than 0.01mm. The fault rocks are cut by younger white zeolite veins. MBV 02 is a green cataclasite, whilst MBV 01 represents a gradational transition from green to red cataclasite. On the edge of MBV 01 an opaque pseudo-tachylyte/ ultracataclasite has developed. It seems to have injected and brecciated the ultracataclasite, thus producing a micro-breccia with clasts of opaque-coated ultracataclasites (see Figure 4-28 a).

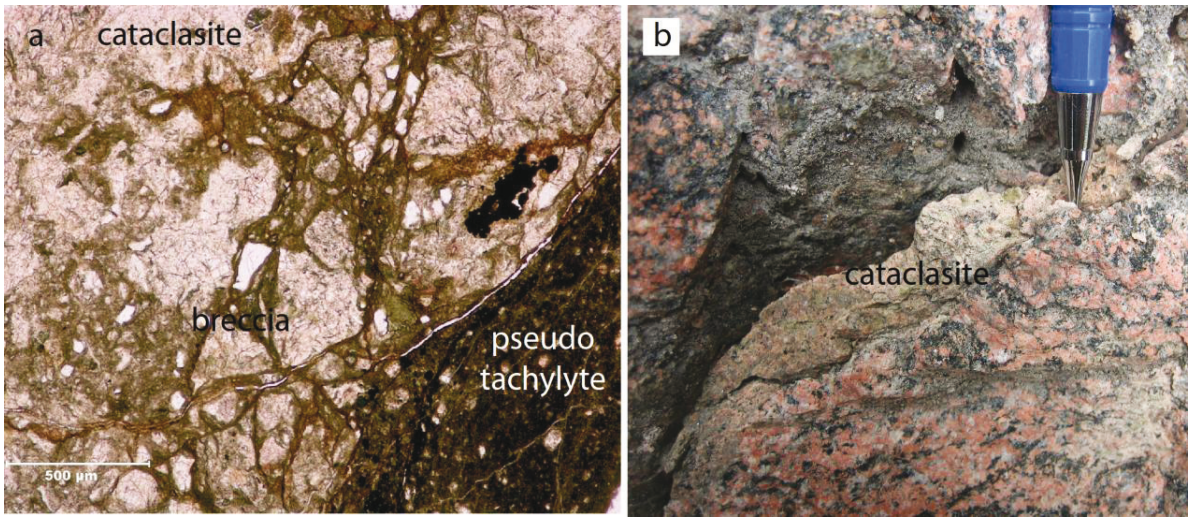

Figure 4-28: a) Micrograph of MBV 01, displaying ultracataclasite (upper left) grading into a breccia with clasts of ultracataclasite. They are within a matrix, coating the clasts, and seemingly associated with the pseudotachylyte/ ultracataclasite in lower right. Scale bar is 500 µm. b) From Eastern fault: A light pink, zeolite bearing cataclasite with green clasts found in a fracture of altered gneiss.

Zeolites

The ultracataclasites of MBV 01, MBV 02 and MBV 03 have a zeolite lath-dominated matrix. MBV 01 and MBV 02 are also cut by two sets of zeolite veins, making a total of at least 3 events of zeolite mineralization at Vik.

ELEMENT	MBV 03		MBV 02
	From	To	
Al	11.00	14.00	12.00
Si	25.00	30.00	26.00
Ca	6.50	8.50	7.50
O	49.00	52.00	51.00
Na	0.00	1.50	
K			0.60

Table 3: Results from SEM chemical probing at Vik.

The laths of the matrix in the samples MBV 03 and MBV 02 were analysed. The samples represent cataclasites from the left and the right side of the antithetic fault core respectively. Their chemistry is consistent, except for the negligible amounts of Na and K. The chemistry of the zeo-

lite laths in sample MBV 02, from the right side of the fault core are similar to the zeolites found in the extensional duplexes at Rød (MBR 04). They have K replacements, but lack Na replacements of Ca.

4.3.4 Kinematics

LIDAR data and field measurements of the fractures at Vik are displayed in Figure 4-29, as poles to the planes, contoured poles to planes and at last a bidirectional rose-diagram of the fractures. Three well-defined populations of orientations are clear from the LIDAR-data. These are marked with red, dark red and pink. Similar populations are found in the field-measurements, but not well defined. The red population represents the NNW-SSE fractures, whereas dark red are fault parallel fractures, close to E-W. The foliation at Vik is sub-horizontal, generally with a southerly dip. One fracture population is sub-parallel to this, but dipping to the north, represented by the pink poles in the figure. The last population is not that well defined. It is marked blue and represents the WNW-ESE fractures.

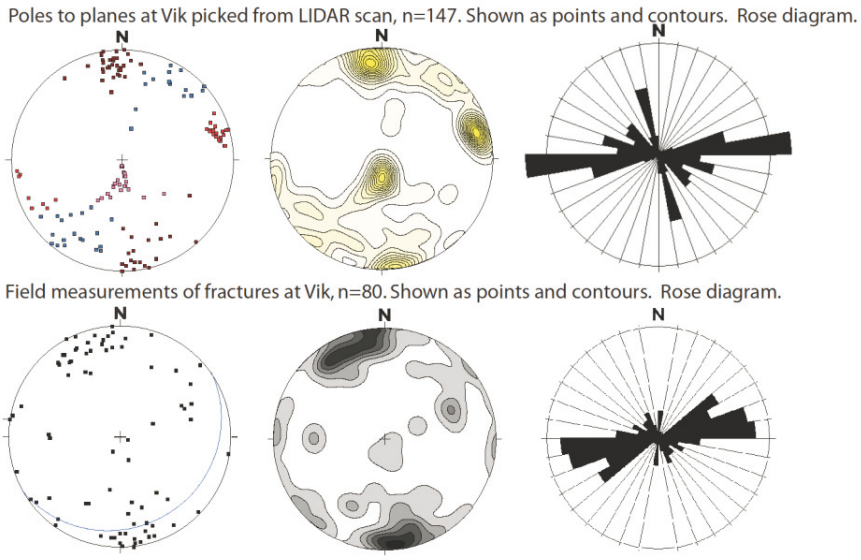

Figure 4-29: LIDAR fractures compared with fractures measured in field.

The master fault plane at Vik is oriented 087/80. From the LIDAR data the main fault plane has an orientation of 083/80, which is probably more correct representation of it, as the LIDAR value is an average orientation of a larger part of the fault plane. The antithetic fault plane at Mulvik has an orientation of 239/70. Both faults are strike-parallel to the foliation, but unlike the Mulvik, Rød and Tjelle localities, they are cutting the foliation at a high angle. Only few measurements were made of the foliation, and the average of two measurements from fault 1 is represented by the blue great circle in Figure 4-29, being 058/14. In general the foliation is E-W oriented with a shallow dip towards the south.

4.4 Tjelle Fault

Not far away from the Rød fault we find Tjelle rockslide, with the Tjelle back-scarp. Its location can be seen in the terrain in relation to Rød fault and Langfjorden on Figure 4-30. Close to the backscarp, fault core outcrops are found. One of which will be briefly described here. This outcrop is not the focus of this study, but as it has similar structures as described in the other localities. Tjelle fault probably played an important role in the release of the rockslide in 1756.

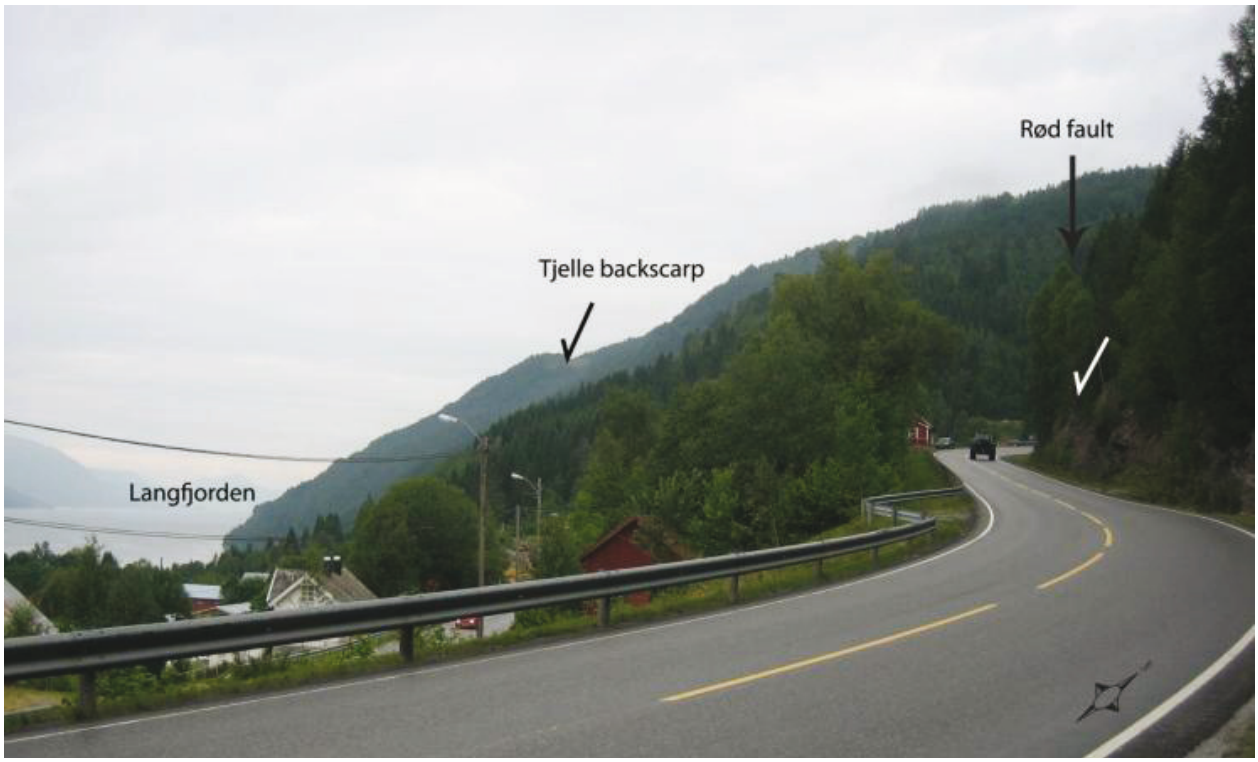

Figure 4-30: View from Rød towards Tjelle and Langfjorden

4.4.1 Architecture

Both at Rød and Tjelle the main fault plane is close to parallel to the regional foliation. At Tjelle the fault seems to be cutting down with a slightly steeper dip than the foliation, and then following the foliation in the lower part of Figure 4-31, where it is less steep. The upper part can be classified to be an R fracture, although it is a part of the main fault. As seen in Figure 4-31 this

locality has a well developed lens of bedrock pierced with zeolite veins and captured in the fault core. From the classification on Figure 2-7 this is an Ls4 lens with 4 dense network shears.

4.4.2 Kinematics

This is another south-dipping fault, sub-parallel to the foliation. The old ductile lineation can be seen in the picture (to the right of my head), but the youngest event seems to be normal dip slip with a strike/dip of 063/80. Only one measured lineation: (244/88 -74) is possibly the most recent.

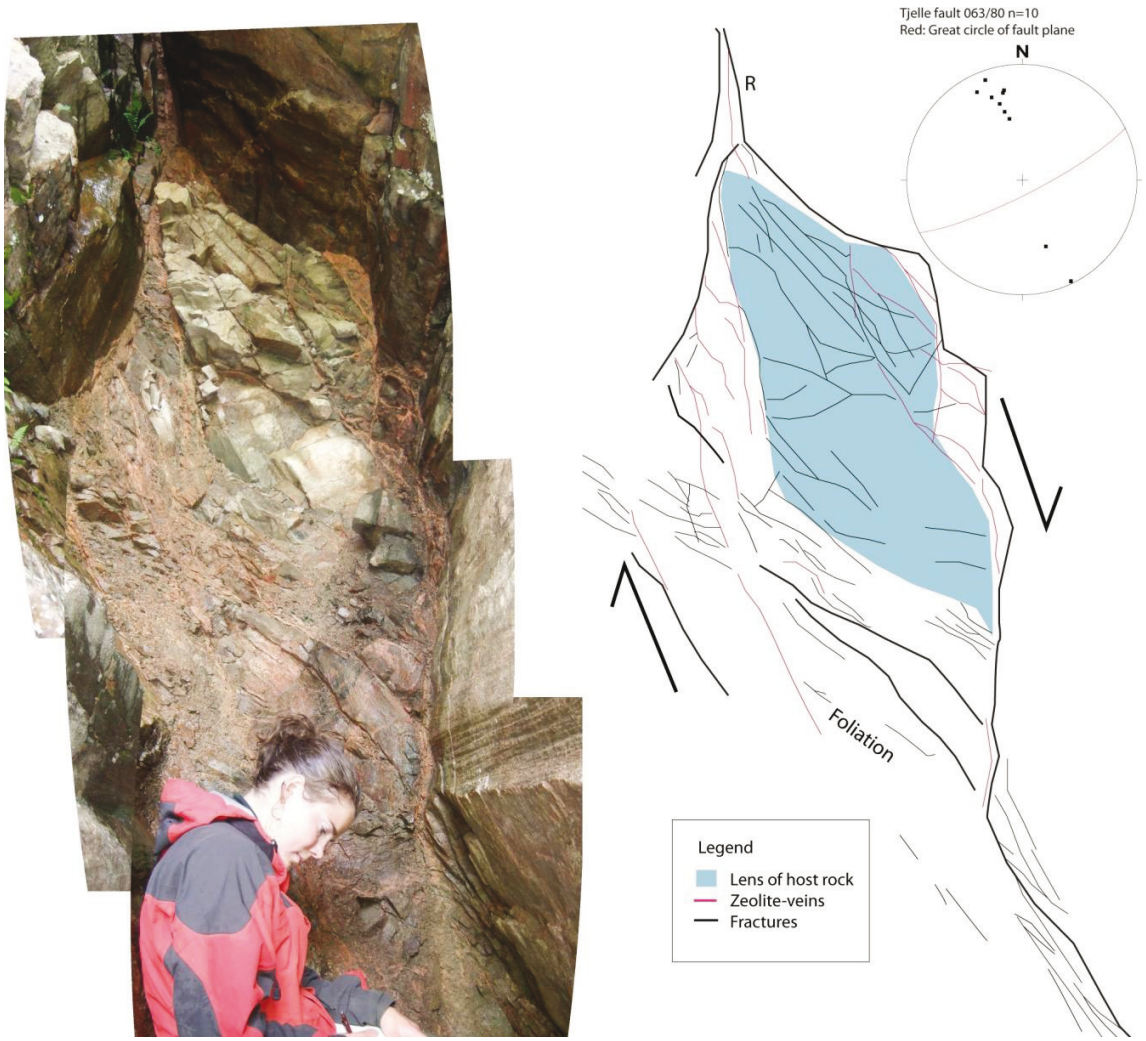

Figure 4-31: Fault core at Tjelle backscarp. Note the pink material and the well developed fault lens.

4.5 Zeolite

As described from the outcrops and the sampled fault rocks. Zeolites are repeatedly occurring in the outcrops of this study. It is occurring as white or pink vein growing material both in outcrop-scale, and microscopic scale. In some thin sections it is found to be a major component in breccia and cataclasite matrix. Older breccia and cataclasite clasts are cut by zeolite, and young breccias are cut by newer zeolite veins.

4.5.1 SEM

The chemistry of the minerals is summarized in the right part of Table 4, where the compositions of the minerals are relatively consistent, being a Ca-rich alumino-silicate. In SEM one cannot decide whether it contains hydrogen (H) or not, but as the mineral probably is a zeolite, an assumption of some presence of hydrogen is made.

To have a hint of what the analysed mineral this is, this homepage: www.mindat.org is used. Here an initial mineral search by chemistry displays an unrealistic list of minerals. The suggested minerals have too much Ca compared to the mineral studied. When searching for minerals containing Ca, Al, silicon (Si) and oxygen (O) and include H; a more realistic result is suggested. Most of the minerals are framework-silicates and zeolites. In Table 4, three possible zeolites and their chemical compositions are listed. One additional suggestion is could be prehnite, but it has probably has too much Ca and has too little O, compared to the results of this study. However stilbite, laumontite and scolecite are qualified candidates. For better knowing what this mineral is XRD analyses of three samples have been performed.

ELEMENT	ZEOLITE WEIGHT % BASED ON DATA FROM TABLE 42 IN (DEER, ET AL., 1967)			SEM	
	Scolecite $Ca[Al_2Si_3O_{10}]•3H_2O$	Stilbite $(Ca, Na_2K_2)[Al_2Si_7O_{18}]•7H_2O$	Laumontite $Ca[Al_2Si_4O_{12}]•4H_2O$	From	To
Si	21.53	26.26	23.68	15.00	35.00
Al	13.25	9.08	11.92	3.00	14.00
Fe	0.38	-	0.03		
Mg	0.19	0.24	-		
Ca	10.13	6.12	8.25	1.00	9.00
Na	-	-	0.30	1.00	2.00
K	0.02	0.26	0.25	0.00	1.00
O	52.93	56.04	53.97	48.00	68.00

Table 4: Weight percent of elements in 3 hydrated alumino-zeolites compared to SEM measurements of analyzed mineral.

4.5.2 XRD analysis

Three samples, MBR 01 (black), MBV 06 (blue) and MB 02 (red), were analysed in the XRD. Figure 4-32 displays the results. From the analysis it is clear that the vein mineral found at all three localities is laumontite. Each sample was analysed and compared with known minerals in a database. This gave a consistent result, where only laumontite were matching the peaks on the 2 θ scale of the graph of the analysed mineral. At Figure 4-32 the three results are aligned. The peaks appear at similar places on the 2 θ scale, although they are not equally intense at all times. Individual graphs from each sample with the compared laumontite dataset can be found in Appendix 3.

Micrographs of the analysed mineral in the respective samples are seen in Appendix 1. From MB 02, crystals of up to 3 mm are analysed, see optical photographs in Figure 4-33. These are white with a faint pink appearance. The mineral analysed from MBR 01 do not show any crystal growth. It is just a powdery and friable mass of light pink material. MBV 06 is a 2 mm wide vein of faint pink mineral growing in an open fracture in the gneiss.

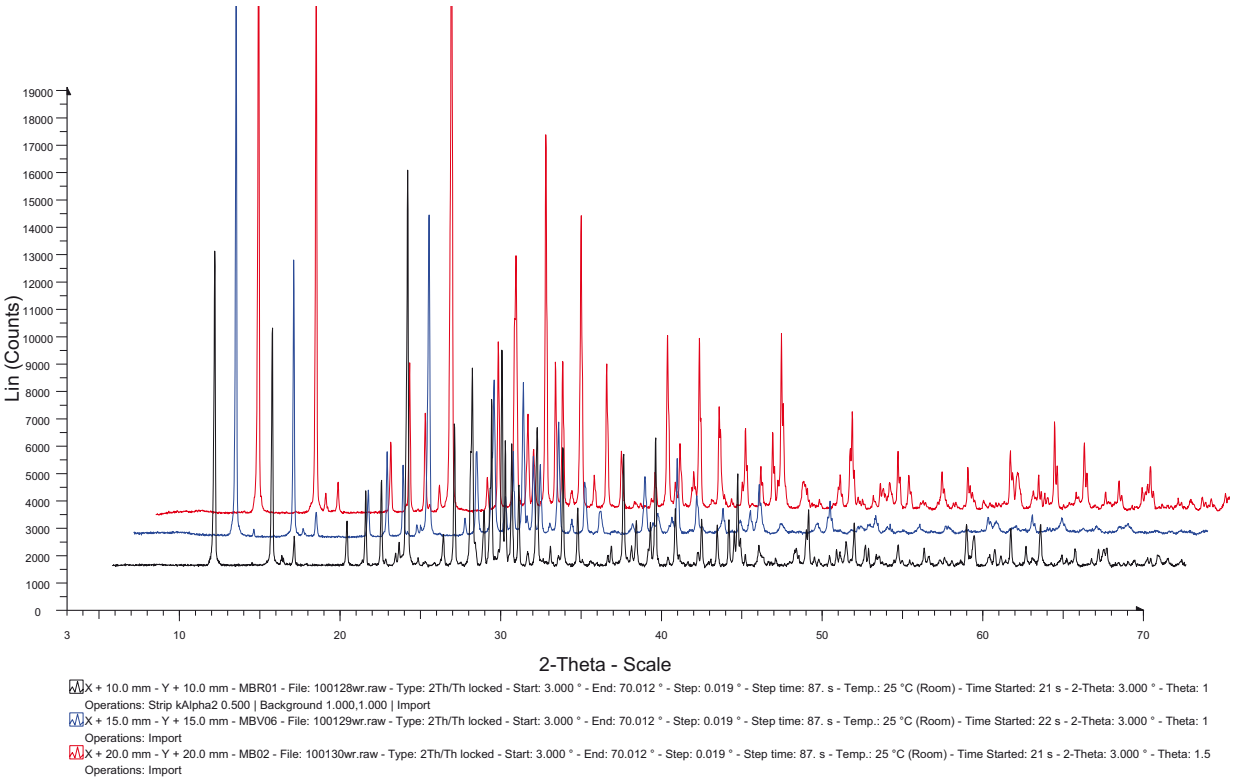

Figure 4-32: XRD results indicating that the vein material is a zeolite called laumontite. The results are very similar at all localities with peaks at the same angles of θ.

Laumontite and faults

Laumontite ($Ca\,[Al_2Si_4O_{12}]\cdot 4H_2O$) is a very friable mineral. It is monoclinic with perfect cleavages in {010} and {110}. It is a Ca-rich, hydrated zeolite, but can have some Na and K replacements. The colour is usually white, but when impure the colour can be pink, as found at the localities of this study. When exposed to dry air the mineral dehydrates, and becomes powdery friable (Bishop, et al., 2005). This is observed from the samples at Rød and Mulvik.

Laumontite has been described from fault zones before. In the San Andreas Fault zone, at Cajon Pass, Southern California, it had been described by James et al. (1988) and Vincent et al. (1988). Here replacements of plagioclase by laumontite and stilbite in granodiorite are described. Albite-rich plagioclase tends to be replaced by this mineral and, in addition, it occurs in micro fractures and it fills open fractures.

In Figure 4-33 laumontite from MB 02 (also tested in XRD) is shown in optical microscope, both in crossed polarised light and in planar light. The sample from Mulvik is the most pure sample, as it has well developed crystals.

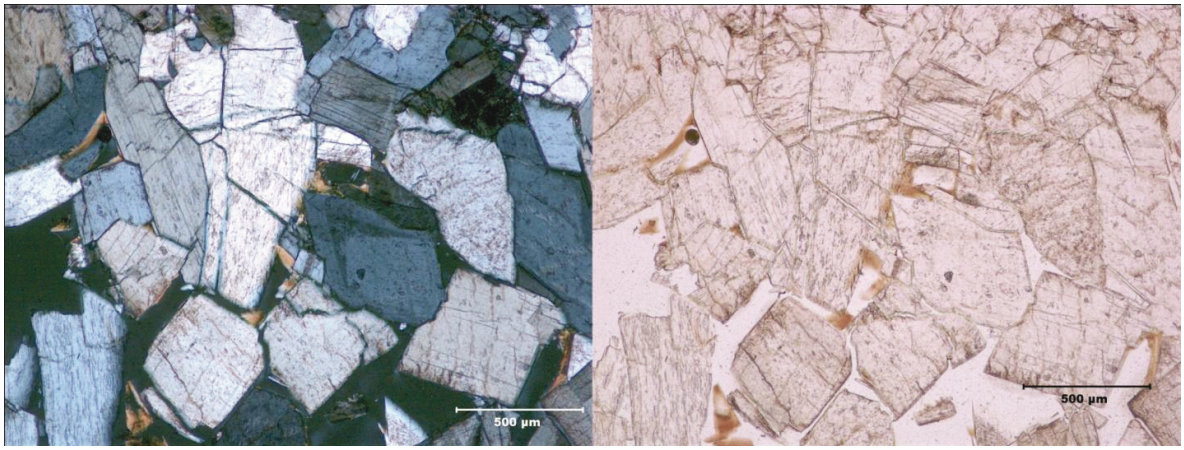

Figure 4-33: Micrographs of laumontite vein in protobreccia in MB 02 from locality 1) Mulvik in cross polarized light (left) and planar light (right). Note very good cleavage. Scale bars represent 500 µm.

5 Discussion

The outcrops of this study are somewhat different concerning type of fault architecture and fault rocks found in the fault cores. In the following, fracture density of fault zones, and the types and evolution of fault lenses will be discussed.

The documented fault rocks are summarized and their similarities are discussed, followed by a suggested development sequence of the different generations. Specific samples from Mulvik show a range of fault rock generations. These have been the basis for establishing a fault rock development sequence for the Tjellefonna Fault. As a summary, this is discussed with regards to previously dated and published faulting sequences along the MTFC.

5.1 Fault architecture

5.1.1 Summary of the outcrops

The three main outcrops represent different aspects of fault outcrops.

1) At Mulvik a sub-vertical fault zone with several, slightly north dipping, normal faults, is displayed. One particularly well developed fault core displays a rich ensemble of fault rocks. These give a good foundation for interpretation of fault rock generation and faulting history, as well as mechanisms related to the different events of faulting.
2) At Rød two gouge zones confine an extensional duplex. The duplex has large amounts of zeolite growth in open extensional fractures. Within the core, N-S trending fractures are faulting and cutting, and therefore post-dates, E-W trending extensional fractures related to dip-slip faulting. Both above and below the fault core, fine-grained incohesive gouge to crush breccias have developed. These have a matrix consisting of zeolite and saussurite.
3) At Vik a 3-dimensional fault architecture is exposed. In contrast to the other localities, the faults at Vik are cutting the foliation at a high angle. This has resulted in the formation of well developed fault lenses in a complex pattern, bounded by anastomosing faults. Fault rocks developed here are mainly protobreccia and ultra-cataclasites, saturated with

several sets of micro-zeolite veins. These might be related, but they have different orientation, and are therefore though to represent more than one generation of mineral precipitation.

5.1.2 Fracture density

Fracture densities from the three main localities are somewhat variable. As the outcrops differ in size and dimensions, care should be taken when comparing the results. The measurements from locality 1) Mulvik are from the most ideal outcrop, concerning the length of the scan, and the good representation of both hanging wall and footwall. The histogram in Figure 4-7 displays a more deformed hanging wall than footwall, which after Braathen and Gabrielsen (2000) is common for normal faults. The other outcrops studied here expose only parts of the faulted section.

At Rød the hanging wall is only exposed for a few metres, whilst at Vik, only the hanging wall is exposed. The fracture density at Rød (Figure 4-16) is fairly even, with between 4 and 22 fractures per metre, through most of the section. Similarly the fracture density at Vik (Figure 4-26) is at most between 5 and 25 fractures per metre, where some parts have less and some more. The fault cores show an increase in fracture density; this is particularly clear in the antithetic fault core at Vik. All outcrops contain smaller fault cores, some in the footwall and some in the hanging wall. If the fault cores are > 1 m, they are often the cause of the peaks in the histograms.

In the fault zones studied, both the fault rocks and fractures are wet. They are therefore thought to be important concerning transport of fluids. This particularly evident at Vik, where the different zones also are in contact with each other, and therefore make communication between the faults and their fluids. When the rock is wet, pore-pressure increases, and this will weaken the fault rock (discussed further in Chapter 5.3.1)

5.1.3 Fault lenses

A theory on how fault lenses form is presented in Gabrielsen and Clausen, (2001) and in Figure 5-1. It suggests that fault lenses are formed by either: A) tip-line coalescence, B) segment linkage, C) tip-line bifurcation, D) asperity bifurcation, E) segment splaying or F) segment amalgamation (Figure 5-1).

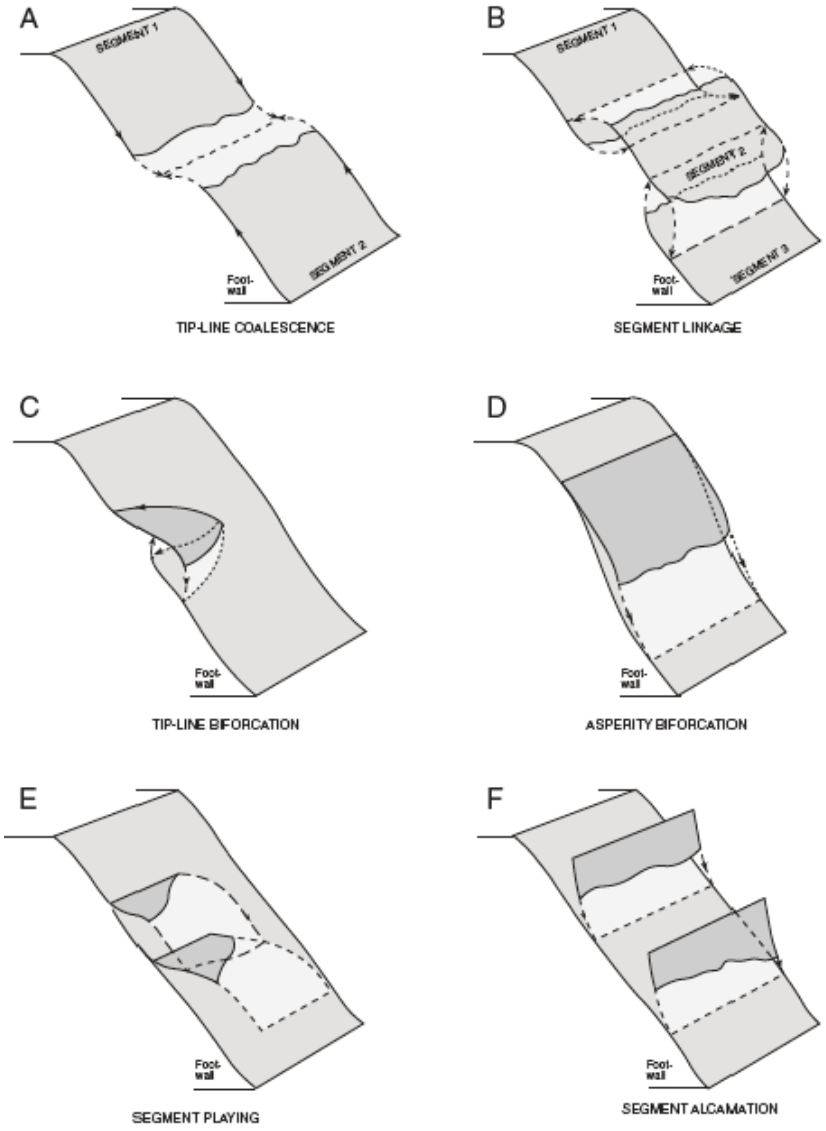

Figure 5-1: Theory on how fault lenses may form in extensional faults, from Lindanger et al. (2007) who modified it from Gabrielsen and Clausen (2001).

When new fault planes are established under strain-softening deformation, asperity bifurcation is believed to be the main mechanism resulting in fault lenses (Gabrielsen and Clausen, 2001). From Lindanger et al. (2007), primary or 1st order fault lenses form mainly by C) tip-line bifurcation, A) tip-line coalescence or E) segment splaying. Secondary lenses (2nd order or higher) form by B) segment linkage, F) segment amalgamation or D) asperity bifurcation. In the fault core, asperity faulting are thought to be the dominating fault mechanism, whilst in the damage zone,

fault splaying and amalgamation will dominate (Gabrielsen and Clausen, 2001). Riedel shears are thought to control the angle of F) segment amalgamation and E) segment splaying.

In normal faults developed in crystalline rock, like in this study, the fault lenses are usually bounded by fault segments that splay or amalgamate from the main fault.

In the northern and southern faults of locality 1) Mulvik, splaying and amalgamation of faults are particularly evident. This outcrop however lacks exposures of complete and large fault lenses. The localities Rød, Tjelle and Vik however, do show sets of lenses.

From the classification of fault lens formation given on Figure 5-1, the lenses seen in the hanging wall of locality 2) Rød are made by segment amalgamation (Figure 5-1 F), whilst at the additional locality of Tjelle, tip-line bifurcation seems to be the main mechanism resulting in one fault lens within the fault core. This lens is again divided into smaller 2nd order lenses. The architecture of the Rød fault is related to segment amalgamation. At Rød the fault lenses are systematic and parallel, and are resulting in a duplex of fault lenses.

Fault lens evolution at Vik

The faults at Vik are cutting the foliation at a high angle, resulting in complex fault architecture with several faults. An evolution scenario and classification of selected examples lenses are suggested in Figure 5-2, according to the classification of Gabrielsen and Clausen (2001) and Lindanger et al. (2007).

In Figure 5-2 a) a fault lens from the hanging wall of fault 1 is displayed. It can be seen in the overview photograph of Figure 4-20. The proximate hanging wall displays a large 1st order lens formed by segment splaying (Figure 5-1 E). This lens is further divided into several 2nd and 3rd order lenses by segment amalgamation (Figure 5-1 F).

In Figure 5-2 b) three 1st order lenses, associated with faults 4), 5) and 6) are displayed. The 1st order lenses have formed by segment splaying and tip-line coalescence. All 1st order lenses have developed 2nd order lenses, and some 3rd order lenses are seen. 2nd and 3rd order lenses appear to

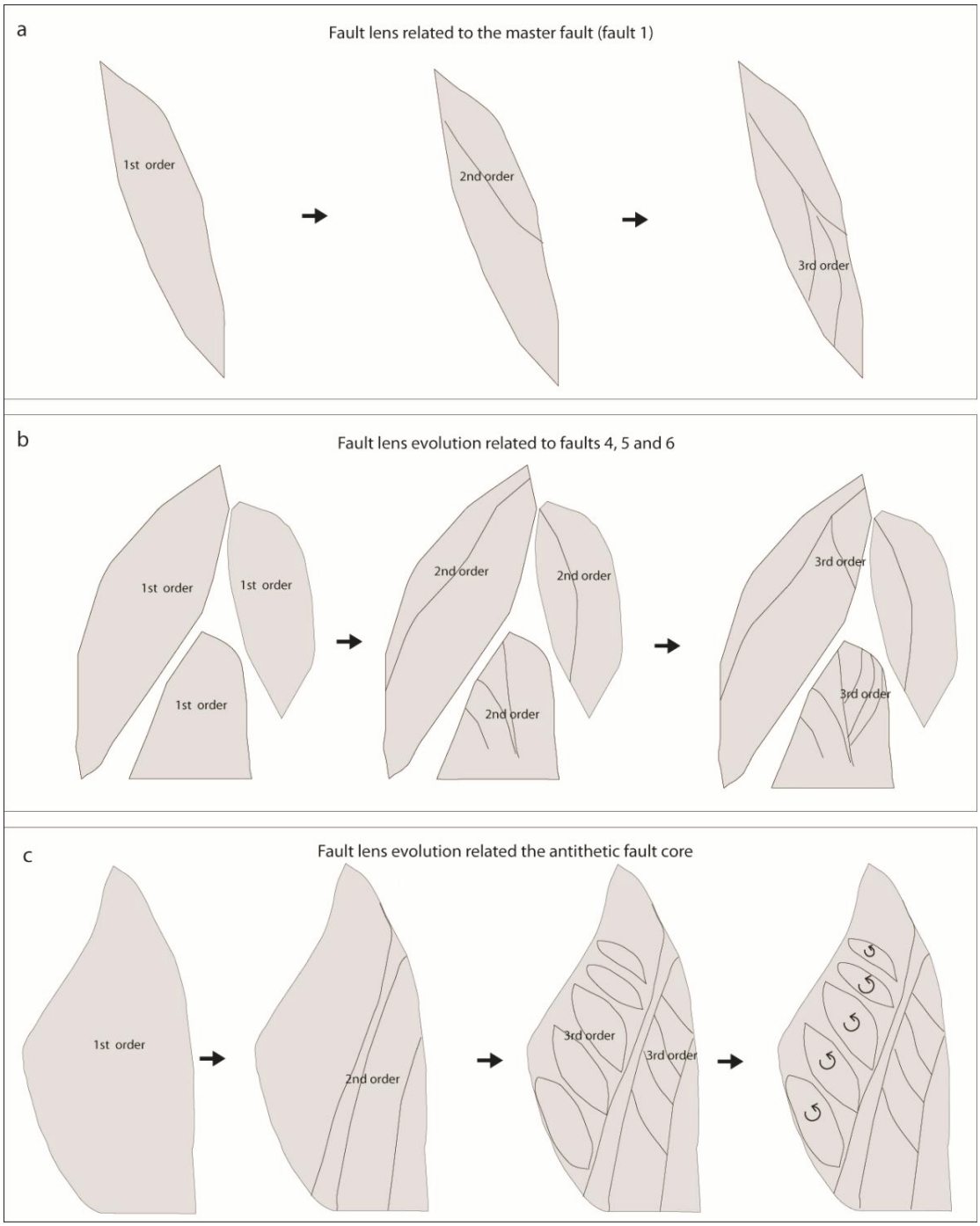

Figure 5-2: Fault lenses from locality 1) Vik, showing probable successions of lens evolution, from a) 1st, 2nd and 3rd order lenses in the hanging wall of the master fault, fault 1. The 1st order lens is ~5 m long b) 1st, 2nd and 3rd order lenses related to faults 4, 5 and 6. The 1st order lens is to the left is ~6-7 m long. c) A suggested evolution of the antithetic fault core. The 1st order lens is ~5 - 6 m long.

have formed by segment amalgamation and segment linkage. The line-drawings are based on the photograph of Figure 4-23.

Figure 5-2 c) shows a possible interpretation of the lenses of the antithetic fault core, based on the same photograph as the line-drawing of Figure 4-25. Initially, a large fault lens developed. The shape of this is unknown as it is higher than the height of the fault. This lens has a similar orientation as the 1st order lens of fault 1. Further, a set of 2nd order lenses form within it, and what later becomes the antithetic fault core is now defined. These are formed by segment splay and segment amalgamation. At a later stage, the prominent lenses within the antithetic fault core developed. These are then 3rd order lenses made by coalescence of Riedel shears and other secondary shears. This has resulted in thick lenses with anastomosing network of shears. At a later stage these are synthetically rotated as indicated in the last step of Figure 5-2 c).

However, the theory presented above is based on how fault lenses may form in an extensional environment. As described in Chapter 2.1.3, the MTFC has experienced both sinistral and dextral strike slip movement, in addition to repeated periods of extensional normal faulting. Therefore the mechanisms suggested here may have been accompanied also by other mechanisms that are common in for example strike-slip faults. However the kinematics shows that the faults associated with the lens formation are related to normal faulting.

5.2 Fault rocks

The fault rocks found in this study are mostly cohesive cataclasites and breccias. From all localities the main mineral of the different fault rocks' matrix seem to be of zeolite. These are laths, originating from vein-growing zeolite crystals. Three main events of brittle faulting are observed, resulting in formation of cataclasites, cohesive breccias and incohesive breccias. Events of zeolite mineralizations seem to have occurred repeatedly, in relation to these events of brittle faulting. The last event of zeolite mineralization found is laumontite.

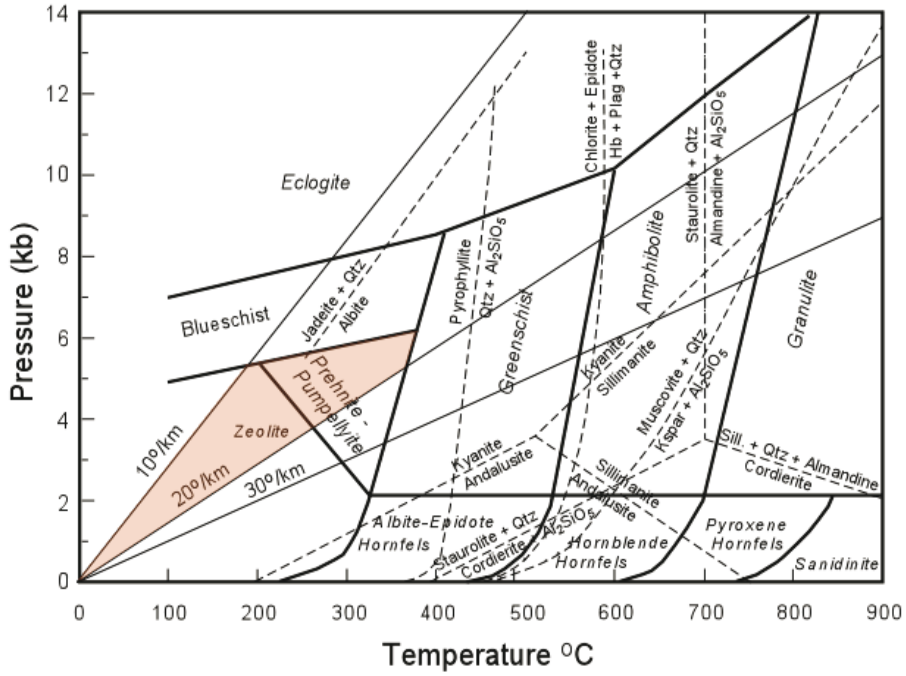

Figure 5-3: Pressure-Temperature plot of different facies. At a geothermal gradient of 20 ˚ C/km zeolites form at temperatures up to 250˚ C and pressure of 5kb. The zeolite and prehnite-pumpellyite facies is coloured. From www.tulane.edu/~sanelson/

Zeolites form at shallow crustal depths. As indicated on Figure 5-3, the zeolite facies, in an area with a geothermal gradient of 20˚C/km, is at temperatures below 250˚C and pressures below 5 kb. However a major fault zone has higher heat flow than the surrounding protolith, 35˚C/km is suggested for the Verran Fault of the MTFC (Grønlie, et al., 1991). The zeolites in such a fault zone may form at temperatures up to 300˚C and pressures up to 3.5 kb, giving a crustal depth of up to 9 km. Grønlie, et al. (1991) suggested the sequence of zeolite mineralization in the Verran Fault to be as follows. The early prehnite formed at 7.5-8 km (250 -300˚C), laumontite at < 6 km (< 230˚C) and the latest was stilbite that formed at 3-4 km (< 170˚C).

5.2.1 Fault rocks from the localities along the Tjellefonna Fault

Remnants of average fine-grained and opaque fault rock, most likely a pseudotachylyte or ultra-cataclasite, are found as fragments in MB 05 and MB 08 and MB 12 from Mulvik. It is not possible to tell if they are pseudotachylytes or ultracataclasites, only that they are very opaque and has more than 90% of matrix. They represent an earlier phase of faulting than the host breccia.

At locality 1) Mulvik in the Mulvik fault core, thin zones of opaque ultracataclasite are found in the boundaries between the different fault rocks, particularly towards the incohesive breccia. In addition, one elongated lens of cataclasite is found in the boundary between southern part of the fault core and the host rock. Similarly in the southern part of the antithetic fault core of locality 3) Vik, zeolite-bearing cataclasites are found. These two cataclasite zones occur in the boundary between fault core and damage zone, and both have large clasts of proto-breccia within it.

The cataclasites of MBV 01 and MBV 02 are similar to MBV 03 (Figure 4-27), but these not have large clasts of protobreccia within them. These are micro-ultracataclasites with a few clasts of single crystals. The rock has a green and pink colour. Two sets of zeolite mineralization, cutting the cataclasites are found.

The black elongated strings found in the antithetic fault core at Vik are thought to be a younger pseudotachylyte/ ultracataclasite. It is sampled in MBV 01, and can be seen in Figure 4-28 and in the lower right part of the thin section micrograph of Appendix 1. This opaque pseudotachylyte/ ultracataclasite has brecciated the zeolite bearing cataclasite (Figure 4-28), and therefore has to post-date this.

At Rød two samples can be classified as crush breccias; MBR 02 and MBR 05. They are found proximate to the lower and upper fault gouge zones, respectively. They are crushed down by granulation, as these zones experience the most movement and therefore concentration of deformation. Similar rocks are found in the north-western part of the antithetic fault core at Vik, in sample MBV 04 and MBV 05, found proximate to the fault core/damage zone boundary.

Cohesive breccias are mainly found at locality 1) Mulvik. One generation with zeolite-dominated matrix and one later more opaque with elements of biotite, sphene and other minerals. They are both cut by a set of zeolite mineralization (Figure 4-9 a) and b)). In one sample, MB 08, an ultracataclasite is cutting through these breccias.

Many of the breccias and cataclasites from locality 1) Mulvik and cataclasites from locality 3) Vik show opaque coating between the clasts and the matrix. This indicates that the matrix has been mobile during deformation.

The incohesive part of the Mulvik fault is very dark red, and dominated by opaques. Compared to the cohesive breccias it is far more opaque, and is therefore not easily studied in the microscope. The SEM backscatter image in Figure 4-10 f) shows a faulted clast of pseudotachylyte/ ultracataclasite within the incohesive gouge. The interpretation of this sample is not extended any further, due to possible sources of errors made under the preparation of the thin-section.

5.2.2 Grain size reduction

The samples collected and analysed during this study are generally formed under fluid associated, brittle faulting. When comparing the mechanisms of mechanical breakage of particles from Henderson et al. (2010), the mechanism dominating in this study would be by abrasion. These authors describe abrasion as round grains being reduced in size by particle margin fracturing. This is a process leading to a bimodal grain-size distribution, with rounding of the larger grains, that are floating in a matrix of elongated grains. The longer the rock is under deformation by faulting, the rounder will the clasts be.

In this study however, laths of zeolite are found to be the dominating component in the matrix. The laths originate from friable zeolite crystals with perfect crystallographic cleavages. These crystals have another geometric basis than the clasts described by Henderson et al. (2010), being monoclinic crystals. They are reduced in size by small elongated fragments being torn off by particle marginal fracturing along the crystallographic cleavage.

5.2.3 Fault-rock generations/mineralizations

Two samples of cohesive breccia from Mulvik show a large spectre of brittle fault rocks. The fault zone is repeatedly cut by sets of zeolite. With focus on the relative age of the different generations, the faulting events are discussed below. Later, in Chapter 5.4 a comparison of these and previously published history of the MTFC is given.

Development sequence at Mulvik

Cohesive and uncohesive breccias are mainly found in locality 1) Mulvik. Several samples show breccias, with clasts of protobreccia and gneiss. Other breccias have clasts of other breccias, cataclasites and pseudotachylyte/ ultracataclasite. In Table 5 a development sequence is suggested, where the lowest number represents the oldest fault rock.

AGE OF EVENT	FAULT PRODUCT DE-VEOLOPMENT SE-QUENCE	MB08	MB10
1?	Zeolite		
2	Pseudotachylyte/ Ultracataclasite	x	
3	Cataclasite	x	x
4	Zeolite	x	x
5	Cohesive Breccia	x	x
6	Cohesive Breccia	x	x
7	Zeolite	x	x
7? 8?	Injected ultracataclasite		x
8	Incohesive breccia (MB 12)		

Table 5: Displays the relative fault product development in MB 08 and MB 10 from pseudotachylyte/ ultracataclasite to injected ultracataclasite. Event 8, the incohesive breccia is found in sample MB 12.

In MB 08, opaque pseudotachylyte/ ultracataclasite (event 2 in Table 5) is found within, and predates a zeolite-dominated cataclasite (event 3). These are the oldest fault rocks-clasts found in this study. As this cataclasite (event 3) is zeolite dominated, there has probably been a period of hydrothermal fracturing before the cataclasites were formed. This will then represent an early event of zeolite mineralization, referred to as event 1 in Table 5. However it may have formed after event 2, but this remains unclear. A new generation of zeolite veins (event 4), cuts rocks 1 to 3, but not the surrounding cohesive breccias (event 5 and 6). The matrix of the first cohesive breccia (event 5) is zeolite dominated, and the second cohesive breccia (event 6) has contributions of other minerals, like biotite, sphene and opaques. The whole section is cut by a new generation of zeolite mineralization (event 7), seen in Figure 4-9 a).

A young ultracataclasite is also found in MB 10. It has probably been mobile during formation, and was therefore injected into the cohesive breccia of event 6. The relative age of this ultracataclasite is uncertain, and may be related to event 7, the last zeolite mineralization or the formation of the incohesive breccia (event 8) found in MB 12.

The incohesive breccia represents the most recent event of faulting at Mulvik.

MB10 show similar fault products and relative ages, as sample MB 08, plotted in Table 5. Thin section micrographs of this sample and its generations are shown in Figure 4-8 d) and e).

Zeolite generations

Zeolites are often associated with hydrothermal faulting activity. They can appear in open extensional fractures or as alteration products from, for example, feldspars. Magnetic data of the MTFC is very complex. This can be indicative of hydrothermal alteration during one or several events of faulting (Gabrielsen, et al., 2002). Zeolites often occur under such conditions, and Grønlie et al. (1991) have previously described zeolites found in the MTFC. Based on apatite fission track dating, the main phase of hydrothermal activity and zeolite mineralization was probably in post-Mid Jurassic (Grønlie, et al., 1991).

As described in the fault rocks at Mulvik and Vik, at least three events of zeolite mineralization are evident. As the cataclasites consist of reworked zeolite, the first zeolite event was before the cataclasites evolved. At Mulvik, another zeolite-event post-dates the cataclasites, but pre-dates the consolidated breccias, whilst the third event post-dates most fault rocks found in this locality (Table 5).

Three samples of vein minerals were studied in XRD. The analyses of the samples are all showing laumontite. This analysis however only done on recent vein minerals, and does not mean that all zeolites described in this study are laumontite.

SEM analysis indicates that the material growing in veins comprises a substantial part of the cataclasitic and breccia matrix. From SEM, chemical composition of the matrix minerals indicates that the matrix mineral is probably scolecite, stilbite or laumontite.

These zeolites have similar chemical composition and optical characteristics. As the laths found in the matrix are around 10μm in size a more detailed characterization of these are complicated. XRD analysis on the matrix would probably give more detailed answers to this.

5.3 Relationship between faults and rock slope failure mechanisms

The fault rocks found on the outcrops of this study have mostly developed from deformation of gneiss at depths corresponding to the Elastico-Frictional regime (Figure 2-9), i.e. at less than 15 km crustal depths. They are cataclasites, cohesive breccias and incohesive breccias. The main component in the matrix of these fault rocks are of zeolites, which is generally weak minerals. This makes the fault cores particularly weak compared to the surrounding gneisses. The concentration of fracture density in damage zones and fault cores, the zeolite mineralization and the occurrence of semi-consolidated and unconsolidated fault products, make the fault zone in general highly weakened.

The faults seem to hold water, both within the fault rock, and in the open fractures. Fluids increase the pore-pressure of a rock. In Figure 5-4 the effect increased pore-pressure has on a rocks' shear strength is shown. It will decrease considerably. The black curve in the figure indicates the strength of the rock, and when σ_3 become negative, tensional fractures form.

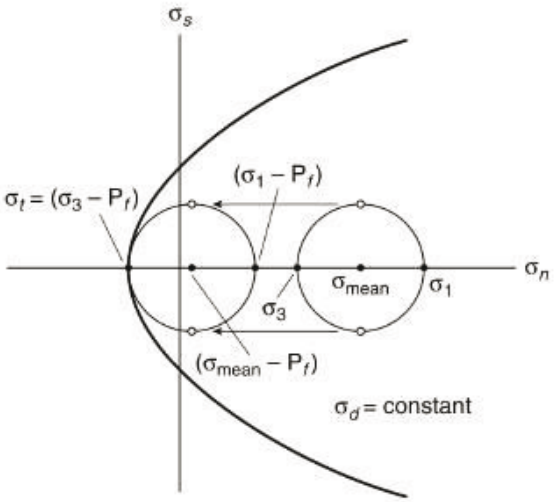

Figure 5-4: Mohr-diagram showing the effect of increased pore-pressure in a rock. The Mohr circle is moved towards the right and the σ_{mean} decreases. The large black curve indicates the strength of the rock, and when σ_3 is negative (like in this figure) tensional fractures form.

5.3.1 Role of inheritance

The faults at Mulvik, Rød and Tjelle are sub-parallel to the Caledonian foliation. Redfield and Osmundsen (2009) suggested that these faults partly reactivate the foliation. Together with the

topography of the northern side of Langfjorden, these structures are dipping towards the fjord. The combination of these factors makes the hills at Tjelle and Rød vulnerable for rockslides. The weak rocks of the fault cores may fail under for example an earthquake. The faults are steep, and the failure may stop unless it can slide further along a weak plane, like the foliation.

5.4 History of the MTFC

The fault rock assemblage found at Mulvik, shows a range of fault rocks from different periods of activity (shown in Table 5). In Table 6, these fault rocks are compared with the previously registered faulting events and fault rocks of the MTFC (Chapter 2.1.3).

AGE OF EVENT	MULVIK FAULT ROCK	REACTIVATION AGE OF THE MTFC	SENSE OF FAULTING	REFERENCE	DATING METHOD
		Late Silurian to Early Devonian	Ductile, sinistral strike-slip	Grønlie and Roberts, 1989	Ar-Ar
1	Zeolite?	Late Devonian/ Early Carboniferous	Sinistral strike-slip	Grønlie et al., 1991	
2	Pseudotachylyte/ Ultracataclasite	Permo - Carboniferous	Sinistral transtension	Watts 2001	Argon isotope
3	Cataclasite	Permo - Carboniferous	Sinistral transtension	"	"
4	Zeolite	post-Mid Jurassic	Associated with dip-slip and dextral strike-slip movement	Grønlie et al., 1991, Watts 2001	Apatite fission track
5	Cohesive Breccia	Late Jurassic - Early Cretaceous	Normal faulting	Grønlie and Roberts, 1989	Fluorite fission track
6	Cohesive Breccia	Late Jurassic - Early Cretaceous	Normal faulting	"	"
7	Zeolite				
8	Incohesive breccia	Late Cretaceous - Cenozoic	Fault block uplift	Redfield et al., 2004	Apatite fission track

Table 6: Showing the fault rocks found in MB 08 and MB 10, with the previously registered ages and related sense of shearing. In parentheses the extensional direction is indicated.

The MTFC was established in the Late Devonian to Early Devonian (Grønlie and Roberts 1989) as a ductile sinistral strike-slip system. A sub-horizontal ductile lineation is found both at locality 2) Rød and at the Tjelle fault.

In Permo-Carboniferous sinistral transtensional movement resulted in pseudotachylytes and cataclasites (Watts, 2001). The pseudotachylytes were dated by Argon isotope dating, with an age of 291±14 Ma. The earliest developed fault rocks found at Mulvik are opaque pseudotachylyte/ ultracataclasite and cataclasite. These could have developed during faulting in Permo-Carboniferous times. This would indicate that the generations of zeolites that pre-date the pseudotachylyte/ ultracataclasite were also Palaeozoic in age.

Watts (2001) documents dip-slip faulting followed by dextral strike-slip in post-Mid Jurassic, along the Verran Fault of the MTFC. This is consistent with the studies of Grønlie et al. (1991), who reported a main generation of zeolite mineralization in relation to these events. In the samples found at Mulvik, zeolite mineralizations are found, post-dating pseudotachylyte/ ultracataclasite and cataclasite, whilst cohesive breccias pre-date a later event of zeolite mineralization. These zeolite veins are therefore suggested to post-date Mid Jurassic. As the cohesive breccias post-date this event, they are probably from Late Jurassic and later.

There are at least two dominant faulting events, resulting in cohesive breccias. They are suggested to represent extensional faulting in Late Jurassic to Early Cretaceous. The incohesive breccia of sample MB 12 probably represents the latest event of activity. This is indicated by AFT age patterns from the Møre og Romsdal, published by Redfield et al. (2004), to be younger than 100 Ma. The faulting was probably in Late Cretaceous and/or in Cenozoic. The matrix of MB 12 is incohesive and has therefore deformed at a shallow crustal depth of 1-4 km (Sibson, (1977), Figure 2-9).

As the ultracataclasites found at Vik are cut by two sets of zeolite, the formation of these was probably related to the early cataclasites found at Mulvik, i.e. in the Permo-Carboniferous. Whether the fault at Vik was established before this remains unknown, as no ductile lineations are found at this locality.

6 Conclusions

1st order fault lenses at Vik were probably established by segment splaying and tip-line coalescence, while higher order lenses formed under segment amalgamation, segment linkage and segment splaying. The architecture of the lenses and their internal 2nd and 3rd order lenses suggest that there have been at least three periods of normal faulting. This was then followed by a later period of normal faulting, where the fault lenses of the antithetic fault core were rotated counter clockwise.

The dominant matrix component found in cataclasites and breccias from localities 1) Mulvik and 3) Vik, is zeolite laths. These were formed by brittle fracturing along the cleavage of monoclinic zeolite crystals. Elongated laths are torn off, resulting in a matrix dominated by zeolite laths. The early cataclasites have a more homogeneous matrix, whereas later breccias are more opaque. The later the fault rock has deformed the more opaque the matrix is.

Early cataclasites from Vik and Mulvik are thought to have formed during Permo-Carboniferous transtensional activity. These are found to post-date an event of zeolite-mineralization. This means that the brittle faulting along the Tjellefonna Fault from Permo-Carboniferous has probably been at crustal depths of 9 km and shallower (if the geothermal gradient of the fault zone was 35˚C/km).

The fault at Mulvik is the one that provides evidence for the most generations of fault rocks, indication multiple phases of reactivation. The first two are event 2) pseudotachylyte / ultracataclasite and event 3) cataclasite, possibly representing sinistral transtension from Permo-Carboniferous activity. The next event 4) is a set of zeolite mineralization, thought to be from the post-Mid Jurassic. Events 5) and 6) are cohesive breccias, which may relate to phases of Late Jurassic to Early Cretaceous rifting. The cohesive breccias are cut by event 7) another period of zeolite mineralization. One zone consists of event 8) unconsolidated breccia. This is thought to be from activity after Late Cretaceous and possibly in the Cenozoic.

The incohesive breccia at Mulvik is the most deformed part of this fault core. Its last activity was simultaneous with seemingly ‘reverse’ faults, cutting most fault rocks, but dying out in the inco-

hesive part of the fault. These faults are interpreted as R-shears, and indicate an overall "north-west side down" sense of movement on the sub-vertical fault.

XRD analysis shows that both the white zeolite from Mulvik and the pink zeolite from Vik, found in close-to vertical extensional fractures are laumontite. This mineral was also found in veins in the extensional-duplex at Rød.

The fault cores of this study are more porous than the surrounding protolith. They seem to conduct fluids, and their faulting activity has repeatedly been hydrothermal. An increase of pore pressure in the fault cores compared to the surrounding protolith is therefore probable, and these fault cores has therefore decreased shear strength. This makes them more likely to fail again.

Bibliography

Allaby, M. 2008. *Oxford Dictionary of Earth Sciences.* Third edition. s.l. : Oxford University Press, 2008.

Berg, S. S. 2004. The architecture of normal fault zones in sedimentary rs. ocks: Analysis of fault compostion, damage zone asymmetri, and multi-phase flow properti. [ed.] University of Bergen. *Ph.D-thesis.* s.l. : University of Bergen, 2004. p. 118 pp.

Bering, D. 1992. The orientation of minor fault plane striae and the associated deviatoric stress tensor as a key to the fault geometry in part of the More-Trondelag fault zone, on-shore central Norway. [book auth.] R.M. Larsen, et al. *Structural and tectonic modelling and its application to petroleum geology.* 1. Special Publications. s.l. : Norwegian Petroleum Society, 1992, pp. 83-90.

Bishop, A.C., Woolley, A.R. and Hamilton, W.R. 2005. *Guide to Minerals, Rocks & Fossils.* London : Philip's in association with the Natural History Museum, 2005.

Blenkinsop, T.G. 1991. Cataclasis and Processes of Particle Size Reduction. *Pure and Applied Geophysics.* 1991, 136.

Boggs, S.,Jr. 2006. *Principles of Sedimentology and Stratigraphy.* 4th Edition. 2006.

Braathen, A. and Gabrielsen, R.H. 2000. *Bruddsoner i fjell - oppbygning og definisjoner.* s.l. : Geological survey of Norway, 2000.

—. 1998. Lineament architecture and fracture distribution in metamorphic and sedimentary rocks, with application to Norway. *Geological survey of Norway, Report.* 1998, 98.043, p. 78p.

Braathen, A., et al. 2009. Fault facies and its application to sandstone reservoirs. *AAPG Bulletin.* 2009, 93, pp. 891-917.

Braathen, A., Osmundsen, P.T. and Gabrielsen, R. 2004. Dynamic development of fault rocks in a crustal-scale detachment: an example from western Norway. *Tectonics.* 2004, 23, pp. 1-21.

Brattli, B. 1992. *Mikroteksturer i magmatiske og metamorfe bergarter.* Trondheim : NTH, 1992.

Bibliography

Bryhni, I., et al. 1991. Tingvoll. Berggrunnskart; Tingvoll; 13201; 1:50 000; sort/hvit. s.l. : Geological Survey of Norway, 1991.

Caine, J.S., Evans, J.P. and Forster, C.B. 1996. Fault architecture and permeability structure. *Geology.* November 1996, 24, pp. 1025-1028.

Chester, F.M., et al. 2004. Structure of large-displacement, strike-slip fault zones in the brittle continental crust. [book auth.] G.D., Taylor, D.B., Driscoll, N. W. & Kohlstedt, D.L. Karner. *Rheology and Deformation in the Lithosphere at Continental Margins.* New York : Colombia University Press, 2004, pp. 223-260.

Deer, M. A., Howie, R. A. and Zussman, J. 1967. *An Introduction to the Rock Forming Minerals.* 2nd. London : Longmans, 1967.

Faulkner, D.R., et al. 2008. On structure and mechanical properties of large strike-slip faults. [book auth.] C.A.J. Wibberley, et al. *The Internal Structure of Fault Zones: Implication for Mechanical and Fluid-Flow Properties.* 299. s.l. : The Geological Society of London, 2008, pp. 139-150.

Fossen, H. and Gabrielsen, R.H. 2005. *Strukturgeologi.* Bergen : Fagbokforlaget Vigmostad & Bjørke AS, 2005.

Fossen, H., et al. 2007. Deformation bands in sandstone: a review. *Journal of the Geological Society, London.* 2007, 164, pp. 755-769.

Gabrielsen, R.H. and Clausen, J.A. 2001. *Horses and duplexes in extensional regimes: A scale modeling contribution.* 193. Boulder : The Geological Society of America, Inc., 2001. pp. 207-220.

Gabrielsen, R.H., et al. 2002. Tectonic lineaments of Norway. *Norwegian Journal of Geology.* 2002, 82, pp. 153-174.

Gabrielsen, R.H., Odinsen, T. and Grunnaleite, I. 1999. Structuring of the Northern Viking Graben and the Møre Basin; the influence of basement structural grain, and the particular role of the Møre-Trøndelag Fault Complex. *Marine and Petroleum Geology.* 1999, 16, pp. 443-465.

Grønlie, A and Roberts, D. 1989. Resurgent strike-slip duplex development along the Hitra-Snåsa and Verran faults, Møre-Trøndelag Faul Zone, Central Norway. *Journal of Structural Geology.* 1989, 11, pp. 295-305.

Grønlie, A., Nilsen, B. and Roberts, D. 1991. Brittle deformation history of fault rocks on the Fosen Peninsula, Trøndelag, Central Norway. [book auth.] A. Grønlie. *Joint, fault and breccia systems in outer parts of Trøndelag, Central Norway.* Trondheim : Norges Tekniske Høgskole, 1991.

Healy, D., Jones, R.R. and Holdsworth, R.E. 2006. Three-dimensional brittle shear fracturing by tensile crack interaction. *Nature.* 2006, 439, pp. 64-67.

Henderson, I.H.C., Ganerød, G.V. and Braathen, A. 2010. The relationship between particle characteristics and frictional strength in basal fault breccias: Implications for fault-rock evolution and rockslide susceptibility. *Tectonophysics.* 2010, 486, pp. 132-149.

Heynekamp, M.R., et al. 1999. Controls on Fault-Zone Architecture in Poorly Lithified Sediments, Rio Grande Rift, New Mexicon: Implications for Fault-Zone Permeability and Fluid Flow. *Faults and Subsurface Fluid Flow in the Shallow Crust.* 113. Geophysical Monograph : American Geophysical union, 1999, pp. 27-49.

Hine, R., et al. 1978. Contrasts between I- and S-type granitoids of the Kosciusko Batholith . *Australian Journal of Earth Sciences.* 1978, 25, pp. 219-234.

James, E.W. and Silver, L.T. 1988. Implications of zeolites and their zonation in the Cajon Pass Deep Drillhole. *Geopgysical Research Letters.* 1988, 15, pp. 973-976.

Jones, P.J. 1987. *Applied Mineralogy: Aquantitative approach.* London : Graham & Trotman, 1987.

Bibliography

Koenemann, F.H. 1993. Tectonics of the Scandian Orogeny and the Western Gneiss Region. *Geologische Rundschau.* 1993, 82, pp. 696-717.

Krill, A.G. 1987. Stangvik. Berggrunnskart; Stangvik; 14204; 1:50 000; sort/hvit. s.l., Møre og Romsdal : Geological Survey of Norway, 1987. 14204.

Lapworth, C. 1885. The highland controversy in British geology: its causes, course and consequences. *Nature.* 1885, 32, pp. 558-559.

Lindanger, M., Gabrielsen, R.H. and Braathen, A. 2007. Analysis of fault rock lenses in extensional faults. *Norwegian journal of geology.* 2007, 87, pp. 361-372.

Marrett, R. and Allmendinger, R.W. 1990. Kinematic analysis of fault-slip data. *Journal of structural geology.* 1990, 12, pp. 973-986.

Oppikofer, T., et al. 2009. Characterization and monitoring of the Åknes rockslide using. *Natural Hazards and Earth System Sciences.* 2009, 9, pp. 1003-1019.

Osmundsen, P.T., et al. 2006. Exhumation and 'old red' basin formation in central Norway: kinematics of the Høybakken detachment zone and the Møre Trøndelag Fault Complex. 163, 2006, pp. 303-318.

Osmundsen, P.T., et al. 2010. Fault-controlled alpine topography in Norway. *Journal of the Geological Society.* 2010, 167.

Redfield, T.F. and Osmundsen, P.T. 2009. The Tjellefonna Fault system of Western Norway: Linking late-Caledonian extension, post-Caledonian normal faulting, and Tertiary rock column uplift with the landslide-generated tsunami event of 1756. *Tectonophysics.* 2009, 474, pp. 106-123.

Redfield, T.F., et al. 2004. Mesozoic and Cenozoic tectonics of the Møre Trøndelag Fault Complex, central Norway: constraints from new apatite fission track data. s.l. : Physics and Chemistry of the Earth, 2004. 29, pp. 673-682.

Redfield, T.F., Osmundsen, P.T and Hendriks, B.W.H. 2005. The role of fault reactivation and growth in the uplift of western Fennoscandia . *Geological Survey of Norway.* 2005, 162.

Riedel. 1929. Zur Mechanik geologischer Bruncherscheinungen. Ein Beitrag zur Problem der "Fiederspalten". 1929, B, pp. 354-368.

Seranne, M. 1992. Late Paleozoic kinematics of the Møre Trøndelag Fault Zone and adjacent areas, central Norway. 1992, 72, pp. 141–158.

Sibson, R.H. 1977. Fault rocks and fault mechanisms. *Journal of the Geological Society.* 1977, 133, pp. 191-213.

Vincent, M.W. and Ehlig, P.L. 1988. Laumonite minerlization in rocks exposed north of San Andreas Fault at Cajon Pass, Southern California. *geophysical Research Letters.* 1988, 15, pp. 977-980.

Waters, A.C. and Campbell, C.D. 1935. Mylonites from the San Andreas fault zone. *American Journal of Science.* 1935, 29, pp. 473-503.

Watts, L.M. 2001. *The Walls Boundary Fault Zone and the Møre-Trøndelag Fault Complex: a Case Study of Two Reactivated Fault Zones.* Durham : University of Durham, 2001.

Wibberley, C.A.J., Yielding, G. and Toro, G.D. 2008. Recent advances in the understanding of fault zone internal structure: a review. [book auth.] C.A.J. Wibberley, et al. *The Internal Structure of Fault Zones: Implication for Mechanical and Fluid-Flow Properties.* London : The Geological Society of London, 2008, pp. 5-33.

www.ngu.no/no/hm/Kart-og-data/

www.gulesider.no/kart

www.norgeibilder.no

www.mindat.org

www.tulane.edu/~sanelson/

Appendix 1 – Thin section descriptions

MULVIK – Thin sections

Host rock: Granodioritic gneiss

Appendix 1 - Thin section descriptions, Mulvik

Sample: MB01, Mulvik 2008	
Macroscopic description:	
Colour:	Weathered surface dark brown/brick red with black and green stripes
Minerals:	Quartz, feldspar, biotite, epidote, zeolite
Grain size:	1-5mm
Structure:	Foliated
Other:	Pink mineral grown in veins with two different orientations
Microscopic description:	
Mineral content:	pl (40%), qz (25%), bt (10%), kfs (5-10%), ze (5-10%), cl (3%), sp (3%), ap (3%), ep (1%), opaque
Texture:	Holocrystalline, xenoblastic, medium grained, crystalline rock. Feldspar is well altered, and there is some development of matrix. The rock is foliated and gneissic Mineral veins penetrate the gneiss, probably zeolite. Saturated by zeolite neomineralization
Mineral description:	
Plagioclase:	Grain size: 0.2-1mm. Strongly saussuritized, resulting in a matrix of Saussurite is common and spot-antiperthite is evident. Anhedral crystal habit.
Quartz:	Grain size: 0.1-1.5mm. Sub grain divisions of undulating extinction. Amobidal with caries margins.
Biotite:	Grain size: 0.2-1mm. Lamellar crystals with straight grain boundaries. 3rd to 4th order interference colours.
Microcline:	Grain size: 0.2-0.3mm. Anhedral crystal habit. Spot-perthite is evident.
Zeolite:	Grain size: 0.2-0.5mm. Perfect cleavage. Euhedral
Chlorite:	Grain size: 0.2mm. Prismatic/lamellar with straight/caries margins
Sphene:	Grain size: 0.5-1mm. 4th order interference colours. Euhedral or subhedral crystals with high relief.
Apatite:	Grain size: 0.2-1mm. High relief, 1st order grey interference colours. Small grains are round.
Epidote:	Grain size: 0.1-0.2mm. Round and anhedral crystals with no colour or faint green.
Matrix:	Saussurite-laumontite
Classification:	Proto-breccia of granodioritic gneiss

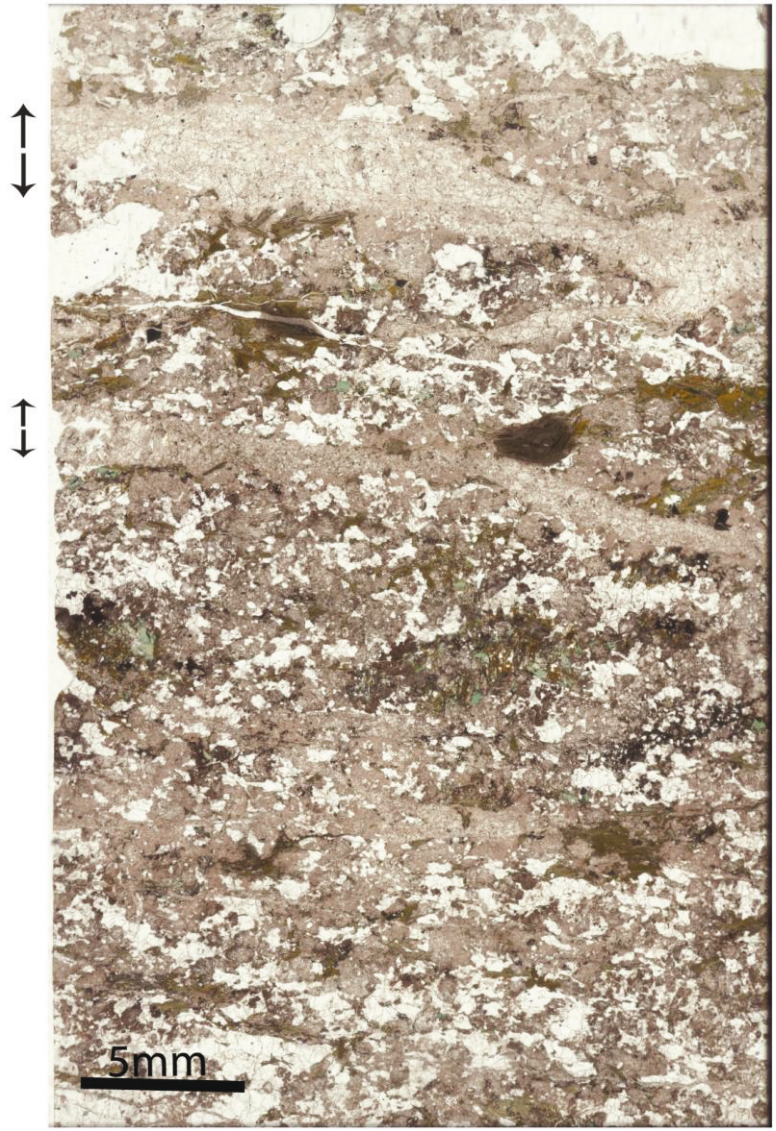

Mulvik 1

Sample: MB02, Mulvik 2008	
Macroscopic description:	
Colour:	Light pink with black stripes and white mineral veins
Minerals:	Quartz, feldspar, biotite, amphibole, zeolite
Grain size:	1-3mm
Structure:	Foliation
Microscopic description:	
Mineral content:	qz (50%), pl (20-30%), la (10-20%), bt (5%), kfs (5%), sp (3%), cl (1%), ep (<1%), opaque
Texture:	Holocrystalline, xenoblastic, medium grained, crystalline rock. Feldspar is well altered, and there is some development of matrix. The rock is foliated and gneissic. White mineral-veins have penetrated the gneiss, probably zeolite. Saturated by zeolite neomineralization
Mineral description:	
Quartz:	Grain size: 0.2-3mm. Sub grain divisions of undulating extinction. Amobidal with caries margins.
Plagioclase:	Grain size: 0.4-1mm. Strongly saussuritized, resulting in a matrix of Saussurite. Grains are not distinguishable. Hard to separate from fine-grained zeolite. At one place remnants from albite twins are seen.
Laumontite:	Grain size. 0.1-1mm. Euhedral. Perfect cleavage in {010}. Grow in veins, and appear in saussurite aggregates.
Biotite:	Grain size: 0.2-0.4mm. Lamellar crystals with straight grain boundaries. 3rd to 4th order interference colours.
Microcline:	Grain size: 0.5-1mm. Anhedral crystal habit. Appear with quartz in non-altered areas.
Sphene:	Grain size: 0.1-0.3mm Euhedral to subhedral crystals with high relief.
Chlorite:	Grain size: 0.2-0.4mm. Pseudomorf from biotite.
Matrix:	Saussurite
Classification:	Proto-breccia of granodioritic gneiss

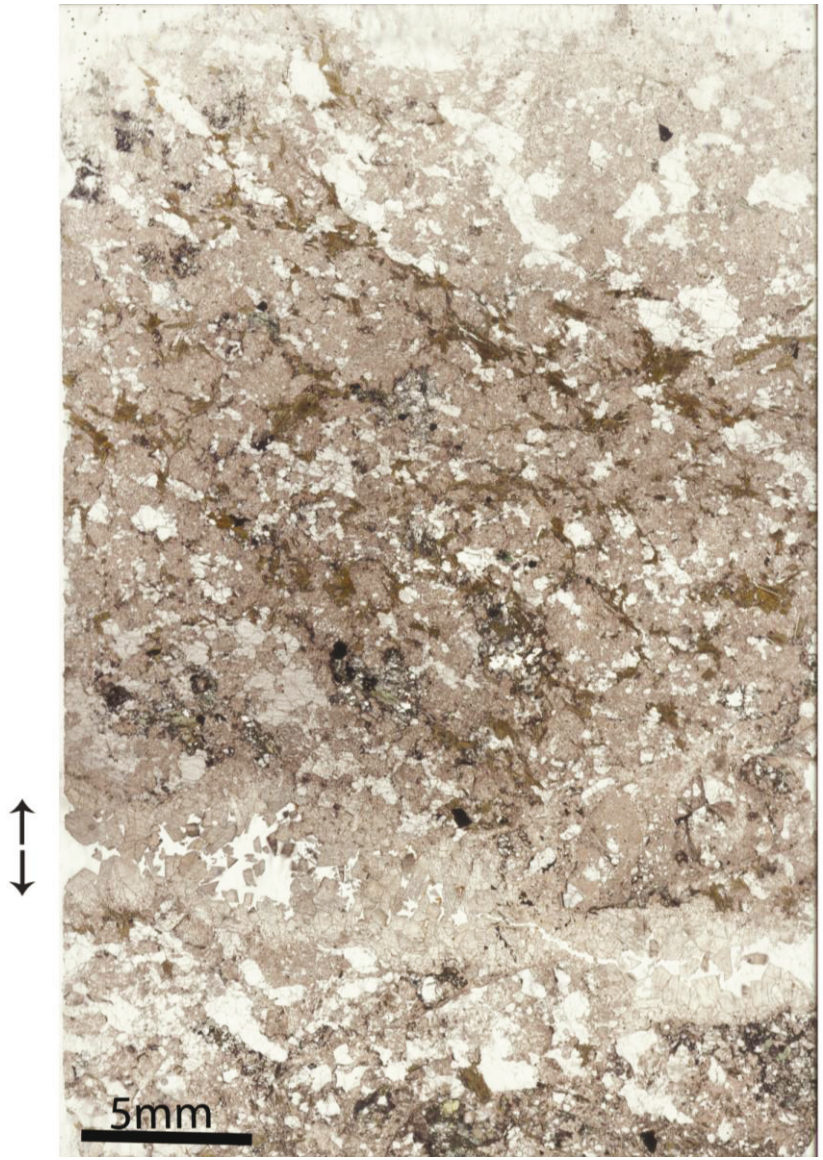

Sample: MB03, Mulvik 2008	
Macroscopic description:	
Colour:	Proto-breccia is pink with white and black stripes. Breccia is grey/green with pink clasts of proto-breccia
Minerals:	Feldspar, quartz, epidote, biotite, zeolite
Grain size:	1-22 mm breccia clasts. Minerals: 1-4mm
Structure:	Sub-angular to angular clasts in a green matrix
Microscopic description:	
Mineral content:	qz (10%), kfs (5%), pl (7%), ze (5%), sp (2%), bt (3%), ep (1%), ap (4%), opaque (3%), matrix (60%)
Texture:	Breccia consists of 60% matrix and clasts of proto-breccia Clasts are sub-angular to sub-rounded
Mineral description:	
Plagioclase:	Grain size: 0.1-1mm Saussuritization Antiperthite
Microcline:	Grain size: 0.5-1mm Perthite
Quartz:	Grain size: 0.2-2mm
Epidote:	Grain size: 0.05-0.1mm 3rd order interference colours
Sphene:	Grain size: -1mm Extreme interference colours. Twinning
Biotite:	Grain size: 0.1-0.2 mm
Apatite:	Grain size: 0.2-0.5mm High relief
Zeolite:	Grain size: 0.01.
Matrix:	Zeolite, opaque
Classification:	Coarse, cohesive breccia

Sample: MB04, Mulvik 2008	
Macroscopic description:	
Colour:	Weathered surface: dark red. Fresh surface: grey/pink
Minerals:	Quartz, feldspar, biotite
Grain size:	1-3mm
Structure:	Foliated, altered
Microscopic description:	
Mineral content:	qz (40-50%), kfs (20-30%), bt (10%), ap (5%), sp (3%), ep (1%), cl (1%), zr (1%), opaque, matrix (9%)
Texture:	The few mica-minerals present are oriented along a foliation, making it gneissic. Holocrystalline, xenoblastic, medium-grained and crystalline with some secondary minerals and alterated minerals
Mineral description:	
Quartz:	Grain size: 0.05-1.5mm Undulating extinction – strained. Amobidal with caries grain boundaries
Microcline:	Grain size: 0.5-2mm. Twins Prismatic with straight to lobate margins
Biotite:	Grain size: 0.1-0.4mm. Light green/brown Lamellar with straight margins. 4th order interference colours
Apatite:	Grain size: 0.2mm. High relief. Not altered. Hexagonal or round
Epidote:	Grain size: 0.1mm. Colourless, round. Assciated with biotite
Chlorite:	Grain size: 0.1-0.2mm Green. Lamellar with straight grain boundaries.
Sphene:	Grain size: 0.1-3mm. Diamond form. High relief. 4th order interference colours.
Zircon:	Hexagonal, elongated. High relief, 2nd to 3rd order interference colours.
Matrix:	Brown, rough mass with grey/white 1st order interference colours. Zeolite
Classification:	Proto-breccia of granitic gneiss

Sample: MB05, Mulvik 2008	
Macroscopic description:	
Colour:	Pale pink/green with pink veins and pink proto-breccia clasts
Minerals:	Feldspar, biotite, zeolite
Grain size:	1-6mm
Structure:	Sub-angular to sub rounded clasts in a fine grained matrix
Microscopic description:	
Mineral content:	qz, kfs, cl, ep, ze, sp, bt, pl, matrix (60-70%)
Texture:	Breccia with clasts of ▪ Proto-breccia (with epidotization) ▪ pseudotachylyte/ ultracataclasite Clasts are angular to sub-angular
Mineral description:	
Quartz:	Grain size: 0.2-1.5 mm
Plagioclase:	Grain size: 0.3-1.5 mm Spot and string antiperthite and saussurite Sericitization and myrmekite
Microcline:	Grain size: 0.2-0.5 mm Perthite and twins are common
Biotite:	Grain size: 0.1-0.3 mm Lamellar with straight margins. Often replaced by epidote and chlorite Kinked chlorite
Sphane:	Grain size: 0.1-0.8 mm. Twinning is common. Euhedral crystals. Extreme interference colours
Zeolite:	Grain size: <0.01 Columnar crystals with perfect cleavage in {010}. Sometimes growing in open fractures
Apatite:	Grain size: 0.2-1mm. High relief
Epidote:	Grain size: 0.2-1mm. Zonated growth
Matrix:	Matrix is bright zeolite and opaque matrix
Classification:	Medium grained cohesive breccia.

Sample: MB06, Mulvik 2008	
Macroscopic description:	
Colour:	Weathered surface: dark red. Fresh surface: grey/red/pink
Minerals:	Quartz, feldspar, biotite, epidote, opaques
Grain size:	1-10mm
Structure:	Foliated, altered
Microscopic description:	
Mineral content:	qz (40-50%), kfs (20-25%), pl (10%), bt (10%), ap (5%), ep (3%), cl (3%), sp (3%), abl (<1%), opaque
Texture:	The few mica-minerals present are oriented along a foliation, making it gneissic. Holocrystalline, xenoblastic, medium-grained and crystalline with some secondary minerals and alterated minerals
Mineral description:	
Quartz:	Grain size: 0.2-0.5mm. Undulating extinction Some of the quartz are recrystallized in aggregates Amobidal with caries margins
Microcline:	Grain size: 0.5-2mm Sericite is present between big microcline grains Spot perthite. Prismatic with straight to lobate margins
Plagioclase:	Grain size: 0.5mm. Spot perthite. Saussuritization
Biotite:	Grain size: 0.1-0.4mm Light green, sometimes kinked. Lamellar with straight grain boundaries 4th order interference colours
Apatite:	Grain size: 0.2mm. High relief. Not altered
Epidote:	Grain size: 0.1mm. Colourless, round
Chlorite:	Grain size: 0.1-0.2mm Green
Sphene:	Grain size: 0.1-1mm. High relief Appear together with Biotite. 4th order interference colours. Light brown colour
Amphibole:	Grain size: 0.1 mm Dark green
Classification:	Granitic gneiss

Sample: MB07, Mulvik 2008	
Macroscopic description:	
Colour:	Fresh surface: faint green with pink veins and pale pink clasts
Minerals:	Feldspar, quartz, biotite, amphibole
Grain size:	Clasts: 1-20 mm
Structure:	Angular to sub angular clasts in a fine grained matrix. No structure.
Microscopic description:	
Mineral content:	qz (12%), pl (8%), kfs (8%), sp (1%), bt (3%), ap (3%), ze (5%), matrix (60%)
Texture:	Clasts of ▪ Proto-breccia ▪ Single crystals Most clasts have opaque mineral coating. Sub-angular to sub-rounded, in the size of 1-10mm
Mineral description:	
Zeolite:	Grain size: <0.2mm. Perfect cleavage in {010}
Quartz:	Grain size: 0.1-1mm. Amobidal with lobate grain boundaries
Microcline:	Grain size: 0.2-1mm Spot perthite
Plagioclase:	Grain size: 0.2-1mm Twinning and saussuritization is common Some spot-antiperthite
Apatite:	Grain size: 0.4-1.5mm High relief. White colour and grey interference colours
Sphene:	Grain size: 0.1-0.5mm High relief. Twinning with extreme interference colours
Biotite:	Grain size: 0.2-0.3mm Brown to beige colour and 3rd order interference colours
Matrix:	Matrix of zeolite laths
Classification:	Coarse cohesive breccia with zeolite veins and clasts of: • Proto-breccia

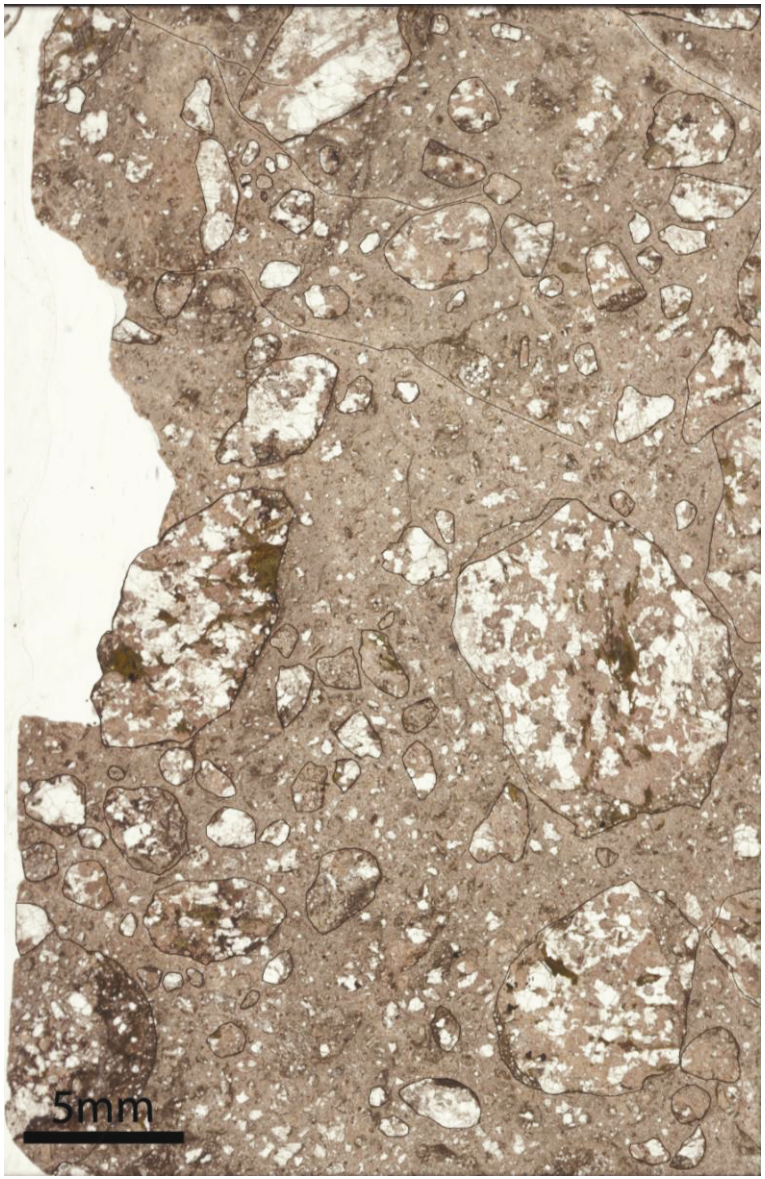

Sample: MB08, Mulvik 2008	
Macroscopic description:	
Colour:	Opaque, red matrix with pale pink clasts and veins. One big clast is green breccia with pink clasts – similar to MB07. Most clasts seem to be of the same orign. On edge: fine grained opaque/green breccia.
Minerals:	Feldspar, quartz, biotite, zeolite
Grain size:	1-15mm
Structure:	Sub angular clasts in a fine grained matrix
Microscopic description:	
Mineral content:	ze, qz, kfs, ep, ap, bt, sp, matrix (50-60%)
Texture:	Clasts are often coated by opaque matrix. The breccia fragments are micro cataclasite dominated by light pink zeolite matrix. The clasts are penetrated by old mineral veins, similar to younger veins, cutting the most recent breccia generation. Clasts are sub-angular to angular and consist of: • Pseudotachylyte/ ultracataclasite • Micro-breccia • Zeolite dominated cataclasite
Mineral description:	
Zeolite:	Grain size: 0.01-0.5mm Columnar crystals with perfect cleavage in {010}
Quartz:	Grain size: 0.2-1mm. Crushed and fractured
Matrix:	Dominated by opaque and zeolite, and seems to be injected
Classification:	Medium-grained, cohesive breccia with zeolite veins

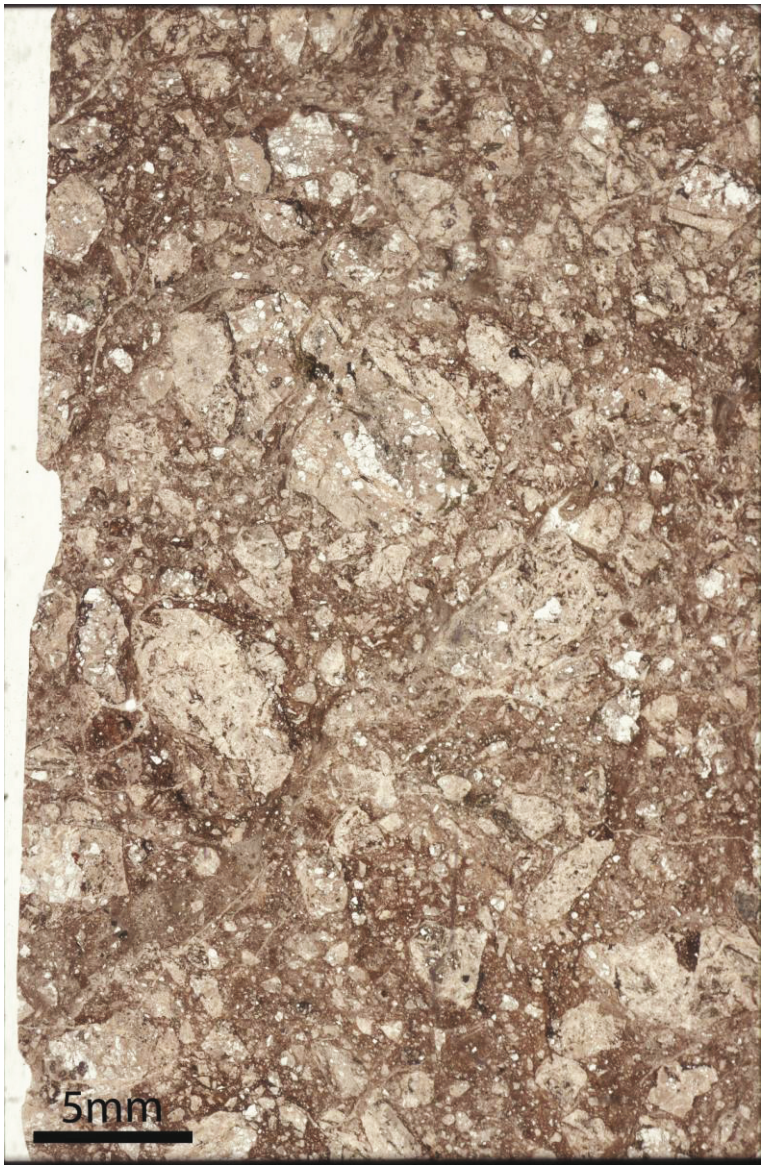

Sample: MB09, Mulvik 2008	
Macroscopic description:	
Colour:	Light pink with white and black stripes
Minerals:	Quartz, feldspar, biotite
Grain size:	1-4mm
Structure:	Foliation – gneissic
Microscopic description:	
Mineral content:	pl (50%), qz (20-30%), bt (5-10%), ap (10-15%), ep (1%)
Texture:	Holocrystalline, xenoblastic, medium grained, crystalline rock. Gneissic with a weak foliation.
Mineral description:	
Quartz:	Grain size: 0.2-3mm Undulating extinction Myrmekite Amobidal with caries margins
Plagioclase:	Grain size: 0.2-4mm Spot antiperthite. Saussuritization. Albite twins. Margins are diffuse due to saussuritization.
Biotite:	Grain size: 0.1-0.4mm Parallel extinction Sometimes kinked. Lamellar with straight margins 4th order interference colours
Apatite:	Grain size: 0.4-2mm High relief. Not altered, but fractured. Some are round and are found in a saussurite-'matrix'
Epidote:	Grain size: 0.1mm. Colourless, with yellow 2nd order interference colour.
Matrix:	It is possible to see a beginning of a fine-grained matrix. Some places it seems like the saussuritization of plagioclase becomes a fine-grained matrix. This is in parts or zones of the rock where the grain size decreases toward a 'centre' of comminution. Biotite is concentrated along such zones/fractures
Classification:	Tonalitic gneiss

Sample: MB10, Mulvik 2008	
Macroscopic description:	
Colour:	Green to pale red with various breccia clasts and pink clasts
Minerals:	Feldspar, quartz, biotite
Grain size:	1-5mm
Structure:	Sub-angular to sub-rounded clasts in a fine grained matrix. Gradation from red to green breccia
Microscopic description:	
Mineral content:	qz (10%), pl (8%), bt (2%), kfs (4%), sp (1%), ep (1%), spi (<1%), ze (5%), matrix (60-70 %)
Texture:	To the left the sample is similar to MB08, medium-grained, cohesive breccia with clasts of medium-grained cataclasite. Towards the right part it grades into a green, medium-grained cohesive breccia, with darker matrix, and clasts of: • cataclasite • micro-breccia
Mineral description:	
Microcline:	Grain size:0.2-1 mm Spot to network perthite is very common
Quartz:	Grain size: 0.2-1 mm
Plagioclase:	Grain size: 0.2-0.5 mm. Saussuritization
Epidote:	Grain size: 0.1-0.2 mm
Sphane:	Grain size: 0.2-0.3 mm. Euhedral crystals with twins, extreme interference colours and high relief
Spinel:	Grain size: 1mm. Within a breccia fragment with quartz and microcline
Biotite:	Grain size: 0.2-0.3 mm. Lamellar with straight margins 3rd order interference colours
Breccia:	Pure zeolite-breccia: the zeolites are columnar, in the size of 0.01-0.2 mm. Perfect cleavage in {010} Gneiss remnants: dominated by quartz, but with biotite, saussuritized plagioclase and microcline. Epidote, sphene, myrmekite
Matrix:	Matrix is dominated by opaque to the left. Darker matrix to the right Some flow structures.At least 3 generations of cataclasis
Classification:	Medium-grained, cohesive breccia

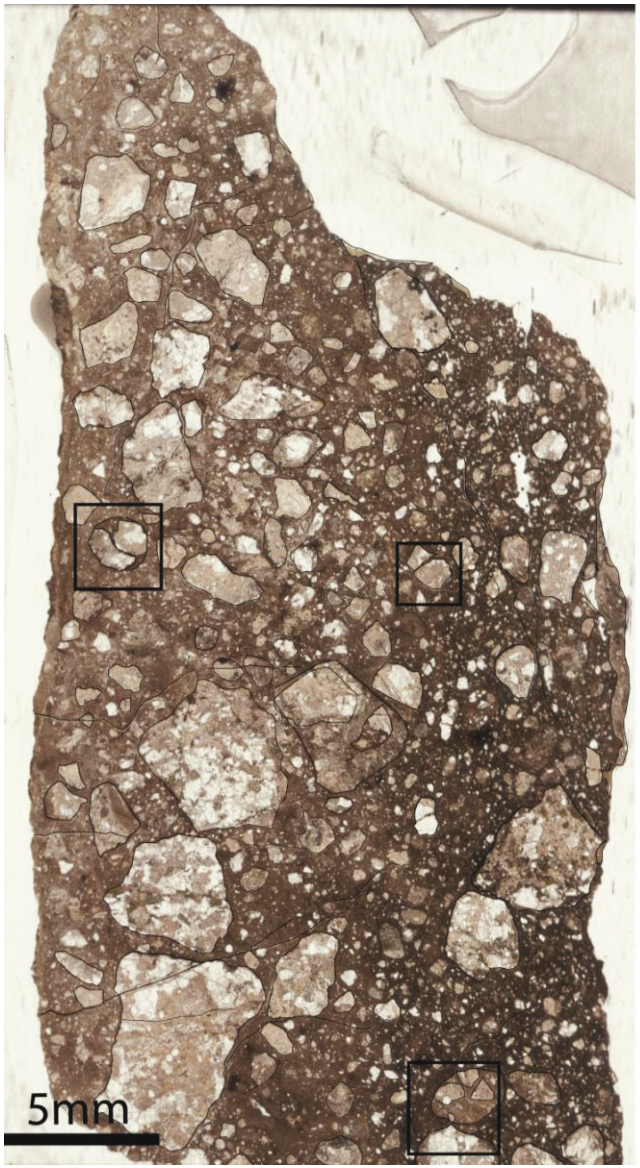

Sample: MB11, Mulvik 2008	
Macroscopic description:	
Colour:	Fresh fracture: Grey with black stripes. In weathered fracture it is
more	clay-grey to red and pale pink. This is the mineral-lineation.
Minerals:	Quartz, feldspar, amphibole, biotite, opaque lineations
Grain size:	1-5mm
Microscopic description:	
Mineral content:	qz (30-40%), pl (20-30%), bt (10%), kfs (10%), ap (5%), ep (5%), sp (3%), abl (3%), zr(3%), cl(1%)
Texture:	Holocrystalline, xenoblastic, medium grained, crystalline rock. Gneissic with a weak foliation. On edge a very fine-grained, opaque cataclasite has developed.
Mineral description:	
Quartz:	Grain size: 0.1-1mm Amobidal with caries margins and undulating extinction. Appear in aggregates with saussuritized plagioclase.
Plagioclase:	Grain size: 0.2-2mm. String antiperthite. Myrmekite and opaque m myrmekite. Saussuritization. Some remnants of albite twins.
Biotite:	Grain size: 0.2-0.4mm. Parallel extinction Sometimes kinked. Lamellar with straight margins 4th order interference colours
Microcline:	Grain size: 0.4-1mm Prismatic crystal habit with lobate margins. Anhedral
Apatite:	Grain size: 0.1mm. High relief. Not altered, but fractured. Some grains are round.
Epidote:	Grain size: 0.1-0.2mm. Round, anhedral crystal habit. Colourless, with yellow 2nd order interference colour.
Sphene:	Grain size: 0.2-0.3mm
Amphibole	Grain size: 0.2-1mm Altered to a yellow/green colour. Seem opaque in edges. Appear near chlorite.
Zircon:	Grain size: 1mm. Zoned. High relief and subhedral crystal habit.
Chlorite:	Grain size: 0.2mm. Pseudomorf from Biotite.
Matrix:	Cataclasite along the edge of the lens. Looks 'old' due to saussuritization. It is very fine-grained. The recognizable grains are 0.01-0.05 mm, and seem to be quartz, feldspar and epidote grains. They are rounded and follow a stringed, opaque matrix. In some areas the matrix is yellow/green, in other areas it is dark red, opaque.
Classification:	Granodioritic gneiss with foliated cataclasite, cut by shear bands

Sample: MB12, Mulvik 2008	
Macroscopic description:	
Colour:	Dark red with bright red clasts
Minerals:	Feldspar and opaque gouge/matrix
Grain size:	0.1-20mm
Structure:	No structure – unconsolidated breccia
Microscopic description:	
Mineral content:	pl, qz, bt, ze, sp , cl, gouge (20%)
Texture:	Incohesive breccia with clasts of: • Pseudotachylyte/ ultracataclasite (15%) • Cataclasite (35%) • Proto-breccia (20%) • Cohesive breccia (10%)
Mineral description:	
Plagioclase:	Grain size: 0.2-2 mm Saussuritized
Quartz:	Grain size: 0.5-2 mm Fractured and penetrated by micro-zeolite veins
Zeolite:	Grain size: <0.02 mm
Biotite:	Grain size: 0.2-2 mm Lamellar with straight margins
Matrix:	Clasts are floating in an opaque gouge, where the green parts in top left of the thin section is rich in mica
Classification:	Incohesive breccia

Sample: MB13, Mulvik 2008	
Macroscopic description:	
Colour:	Light pink with black stripes
Minerals:	Feldspar
Grain size:	1-3mm
Structure:	Highly fractured with dark material in most fractures.
Microscopic description:	
Mineral content:	pl (60%), cl (15-20%), ep (15-20%), sp (5%), opaque
Texture:	Holocrystalline, heterogranular, medium-grained crystalline rock with foliation and gneissic appearance. The rock is an altered gneiss with evidence of saussuritization, chloritization and epidotization.
Mineral description:	
Plagioclase:	Grain size: 1-3mm Highly saussuritizated Yellow interference colours Evident albite-twins
Chlorite:	Grain size: 0.3-1mm Secondary mineral from chloritization of biotite Lamellar with straight margins
Epidote:	Grain size: 0.5-1mm Secondary mineral Often in aggregates and/or together with chlorite along the foliation. At some places in veins. 3rd order interference colours. One major aggregate is in the order of 7mm
Sphene:	Grain size: (enclosed in chlorite) Prismatic with straight margins
Alteration:	Epidotization and feldspar alteration
Classification:	Altered dioritic gneiss.

Sample: MB14, Mulvik 2008 Host rock	
Macroscopic description:	
Colour:	Light grey with dark stripes in fresh fracture. Some pink fractures. Some fractures have yellow/green mineralization
Minerals:	Quartz, feldspar, amphibole biotite, epidote
Grain size:	2-3 mm
Structure:	Foliation
Microscopic description: Modal analysis (400 points)	
Mineral content:	qz (50%), pl (24.7%), kfs (10%), abl (6.5%), bt (5.2%), cl (1.5%), ap (1%), ep (0.2%), sp (0.7%), opaque
Texture:	Holocrystalline, xenoblastic, medium-grained, crystalline rock with weak foliation and gneissic appearance
Mineral description:	
Quartz.	Grain size: 0.1-1mm Amobidal with lobate margins. Undulating extinction Myrmekite in kfs edges (coalesced of quartz and plagioclase)
Plagioclase:	Grain size: 0.5-2mm Saussuritization. Albite twins are rare. Spot-antiperthite
Microcline:	Grain size: 0.3-3mm. Sericitized and spot-perthite are found. Prismatic crystals with straight, but irregular margins
Biotite:	Grain size: 0.1-0.8mm. Brown/beige, lamellar grains with straight margins.
Amphibole:	Grain size: 0,2-4mm. Often found near bt and ap Prismatic grains with straight margins
Epidote:	Grain size: 0.1mm Round to irregular with caries/lobate margins
Sphene:	Grain size: 0.1-0.2mm Lamellar with straight margins
Chlorite:	Grain size: 0.2-0.4mm Lamellar with straight margins. Appear with amphibole
Apatite:	Grain size: 1mm. High relief
Classification:	Granodioritic gneiss Domination paragenesis is qz + pl + hbl + ep + (bt), which is typical for epidote-amphibolite facies paragenesis.

Sample: MB15, Mulvik 2008	
Macroscopic description:	
Colour:	Pink with opaque veins and white zeolites
Minerals:	Feldspar, biotite, zeolite
Grain size:	0.1-1mm
Structure:	Elongated lens, but no recognisable gneiss structures. Friable
Microscopic description:	
Mineral content:	ze (20%), qz (15%), pl (10%), kfs (6%), sp (2%), cl (2%), ep (2%), bt (3%), matrix (40%)
Texture:	Elongated clasts (up to 2cm) of gneiss in an cohesive breccia together with sub-rounded clasts of zeolite aggregates It has open fractures with zeolite Opaque strings of pseudotachylyte/ ultracataclasite?
Mineral description:	
Plagioclase:	Grain size: 0.1-1 mm Saussuritized. Twinning
Quartz:	Grain size: -2mm. Fractured, with zeolite growth in the fractures.
Microcline:	Grain size: 0.4-1.5 mm Saussuritized spot perthite
Sphene:	Grain size: -2.5 mm. Extreme interference colours. Fractured
Epidote:	Grain size: 0.1-0.2 mm 3rd order interference colours
Zeolite:	Grain size: 0.1-1 mm
Biotite:	Grain size: 0.2-0.4 mm Lamellar with straight margins
Chlorite:	Grain size: 0.3 mm
Matrix:	Matrix of fine grained zeolite
Classification:	Cataclasite lens saturated with zeolite growing in open fractures

Sample: MB16, Mulvik 2008	
Macroscopic description:	
Colour:	Grey to green with various clasts: pink and white
Minerals:	Quartz, feldspar, amphibole, zeolite
Grain size:	0.1-12mm
Structure:	Opaque mineral coating on clasts
Microscopic description:	
Mineral content:	qz (15%), ze (2%), kfs (6%), bt (5%), pl (7%), cl (2%), ep (2%), opaque (1%), matrix (60-70%)
Texture:	Breccia with clasts of gneiss and single crystals Clasts are sub-rounded to sub –angular and coated by opaque matrix
Mineral description:	
Quartz:	Grain size:0.2-2 mm In aggregates
Zeolite:	Grain size: 0.01 mm Columnar with perfect cleavage in {010}
Microcline:	Grain size: 0.3-1.5 mm Spot perthite
Plagioclase:	Grain size:0.2-1 mm Antiperthite and saussuritization are common on subhedral crystals Myrmekite is at one place replaced by opaques
Biotite:	Grain size: 0.1-0.2 mm Often replaced by epidote or chlorite Lamellar with straight margins
Matrix:	Matrix is of gneiss fragments and zeolite
Classification:	Dark green, coarse, cohesive breccia

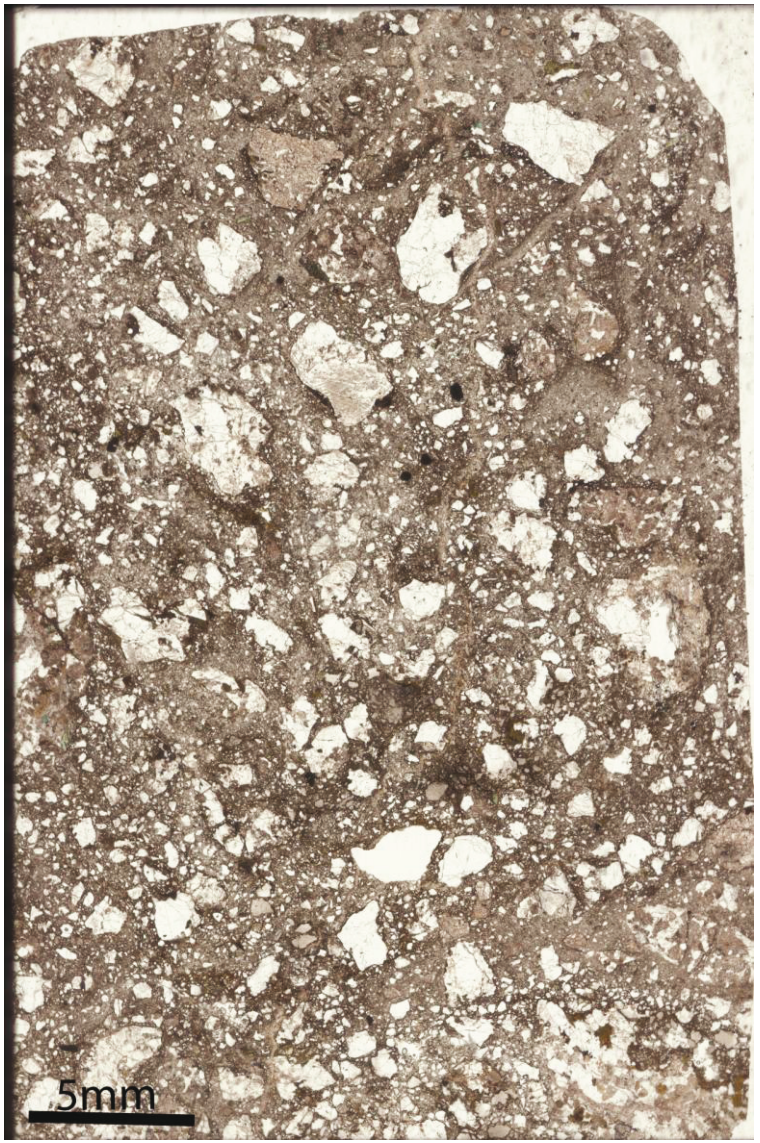

RØD – Thin sections

Host rock: Granitic gneiss

Sample: MBR01 Rød 2009	
Macroscopic description:	
Colour:	Pink with green/black lineation
Minerals:	Feldspar, epidote, quartz, amphibole, zeolite (pink and white)
Grain size:	1-2mm in gneiss
Structure:	Very loose, powdery and friable
Microscopic description:	
Mineral content:	la (30%), qz (20%), pl (20%), kfs (15%), ap (5%), bt (5%), cl (3%), sp (2%)
Texture:	Holocrystalline, xenoblastic, medium-grained and crystalline rock with very fine grained zeolite vein.
Mineral description:	
Laumontite:	Grain size: <0.05mm. Length/width 3:1. Perfect cleavage {010}. Colourless to faint brown. Grow in open fractures. Some are up to 0.1-0.2mm
Quartz:	Grain size: 0.2-0.4mm. Occur in aggregates where grains have undulating extinction Amobidal with caries margins
Plagioclase:	Grain size: 0.2-2mm. Spot antiperthite Saussuritization. Some of the grains still have clear Albite twins
Microcline:	Grain size: 1mm. Twinning
Apatite:	Grain size: 0.2-1.2 mm. High relief
Biotite:	Grain size: 0.1mm. Colour is brown. Some are kinked. Lamellar appearance with straight grain boundaries.
Sphene:	Grain size: 0.1-0.2mm. Subhedral crystals with high relief.
Chlorite:	Grain size: 0.1-0.2mm. Pseudomorph from biotite
Classification:	Proto-breccia from granodioritic gneiss

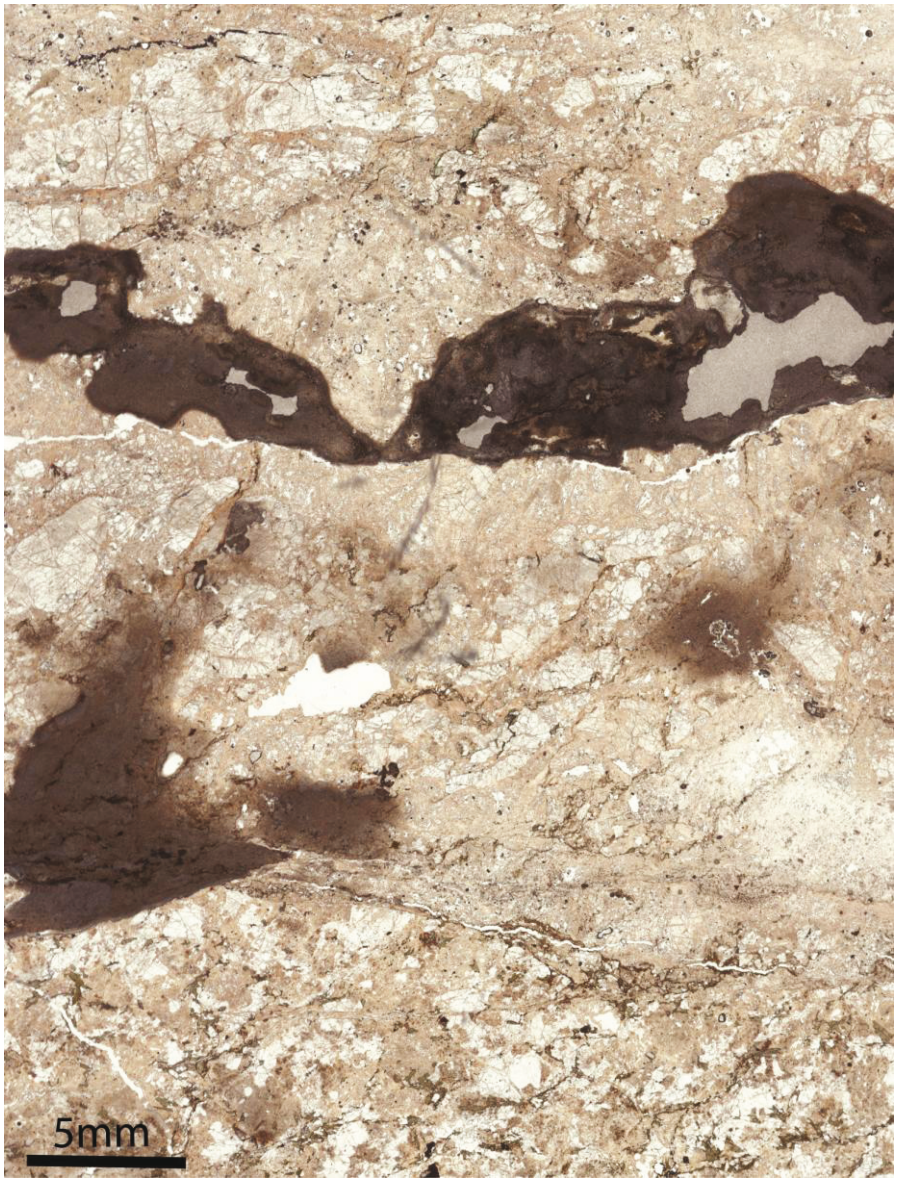

Sample: MBR02 Rød 2009	
Macroscopic description:	
Colour:	Pink with black/green and white stripes. Pink Zeolite veins
Minerals:	Feldspar, quartz, amphibole, epidote, biotite, sphene, zeolite
Grain size:	0.5-1mm with some host rock clasts of 5mm
Structure:	Brecciated/crushed. Pink Zeolite growth in veins
Microscopic description:	
Mineral content:	Matrix: ze (30%), qz (30%), kfs (25%), ap (10%), bt (3%), cl (2%), ep (1%), sp, opaque
Texture:	Heterogranular, fine-grained breccia Sub rounded to sub angular clasts Brecciated and dominated by zeolite
Mineral description:	
Laumontite:	Grain size: <mm. Found in open fractures and in matrix accompanied by saussuritized plagioclase. Some crystals can be identified – perfect cleavage
Quartz:	Grain size: 0.05-0.2mm. Occur in aggregates where grains have undulating extinction Amobidal with caries margins
Microcline:	Grain size: 0.1-0.5mm. Twinning. Anhedral.
Apatite:	Grain size: 0.1-1.5 mm. High relief, subhedral
Biotite:	Grain size: 0.05- 0.1mm. Lamellar appearance with straight grain boundaries.
Sphene:	Grain size: 0.05-0.1mm. Subhedral crystals with high relief.
Chlorite:	Pseudomorph from biotite and amphibole
Matrix:	Matrix consists of a mix of saussuritized plagioclase and columnar zeolite needles.
Classification:	Cohesive breccia from granitic gneiss

Sample: MBR03 Rød 2009	
Macroscopic description:	
Colour:	Pink zeolite material and light grey gneiss
Minerals:	Quartz, feldspar, amphibole, zeolite
Grain size:	Gneiss: ~1mm. zeolite: <0.5mm
Structure:	Foliation. Highly fractured with mineral growth in veins in diff. directions.
Other:	Zeolite is very sticky, like clay. It is all over your hands after touching it.
Microscopic description:	
Mineral content:	ze (40%), qz (30%), kfs (20%), bt (7%), sp (2%), gr (1%)
Texture:	Holocrystalline rock with xenoblastic crystal growth. The rock is crystalline fine-grained with grains of 0,1-1mm. It is heterogranular nematoblastic and gneissic. The dark/light layers show a clear foliation.
Mineral description:	
Quartz:	Grain size: 0.1-1mm. Amobidal crystal habit with caries grain boundaries. Undulating extinction. In aggregates.
Microcline:	Grain size: 0.2-1mm. Twins. Anhedral crystal habit.
Biotite:	Grain size: 0.2-0.4mm. Green colour. Parallel extinction. Lamellar with straight margins. 4th order interference colours
Garnet:	Grain size: 0.1mm. Round to subhedral (hexagonal). Isotropic. Light brown. Fractured and faulted.
Zeolite:	Grain size: <0.2mm. It has light brown colour. Crystals are euhedral. 1st order grey interference colour. High relief.
Matrix:	Difficult to see whether some of the material classified as zeolite is saussuritized plagioclase. This is due to the very fine grain size. More investigation on this in SEM and XRD.
Classification:	zeolite-breccia and granodioritic gneiss

Sample: MBR04 Rød 2009	
Macroscopic description:	
Colour:	Dark pink/brown with pink veins
Minerals:	Feldspar, quartz, biotite, amphibole, vein minerals: zeolite
Grain size:	1-2mm in the gneiss. The vein minerals are <0.1mm
Structure:	Foliation. Pink vein material
Microscopic description:	
Mineral content:	pl (40%), qz (25%), kfs (15%), abl (10%), bt (5%), sp (2%), ap (1%), cl (1%), ze
Texture:	Holocrystalline rock with xenoblastic crystal growth. The rock is crystalline medium to fine-grained with grains of 0.1-1.5mm. It is heterogranular and gneissic. The dark/light layers show a clear foliation.
Mineral description:	
Plagioclase:	Grain size: 0.4-1.5mm. Strongly saussuritized. Spot-antiperthite is seen. Anhedral crystals
Quartz:	Grain size: 0.1-1mm. Amobidal crystal habit with caries grain boundaries. Undulating extinction
Microcline:	Grain size: 0.2-1.5mm. Twins Spot-myrmekite and spot-perthite.
Biotite:	Grain size: 0.2-0.4mm. Green colour. Some crystals are kinked. Lamellar with straight margins. 4^{th} order interference colours
Apatite:	Grain size: 0.1-0.2mm. High relief. Not altered. Hexagonal or round crystals. 1^{st} order grey interference colours.
Amphibole:	Grain size: 0.2-3mm. Light green.
Chlorite:	Grain size: 0.1-0,2mm Green. Pseudomorf from Biotite.
Sphene:	Grain size: 0.2-0.4mm. Subhedral. High relief. 3^{rd} to 4^{th} order interference colours.
Zeolite:	Grain size: <0.2mm. Some have undulating extinction. It has light brown colour. Crystals are euhedral.
Classification:	Granodioritic gneiss and zeolite breccia

Sample MBR05, Rød, Tjelle 2009	
Macroscopic description:	
Colour:	Dark grey/green with pink areas and opaque stripes
Minerals:	Feldspar, quartz, amphibole, zeolite
Grain size:	3-6mm to fine-grained on slickenlines
Structure:	Foliation
Microscopic description:	
Mineral content:	qz (20-25%), pl (30-35%), bt (10%), kfs (5-10%) abl (10%), ep (1%), sp (1%), ze
Texture:	Medium grained, crystalline rock with heterogranular crystal assemblage of 0.2-0.4mm and 1-2mm. The fine-grained part crushed bedrock to micro-breccia. It is nematoblastic, gneissic and has a foliation. Opaque strings are present
Mineral description:	
Plagioclase:	Grain size: 0.5-2mm Saussuritizated, making it brown and altered. Remnants from albite twins can be seen Grains occur as tabular with straight to lobate margins
Quartz:	Grain size: 0.1-2mm Amoeboid with lobate grain-boundaries and big tabular grains
Amphibole:	Grain size: 0.1-2mm Prismatic with irregular, but straight margins
Chlorite:	Grain size: 0.2-0.4. Green colour, and with 3rd order interference colours. Often kinked Lamellar with straight margins
Zeolite:	Prismatic with the largest grains 0.2 mm long and 0.1 mm wide
Matrix:	Towards the gouge zone the rock is very fine-grained to a consolidated gouge. Some quartz grains are 0.1mm, but most grains are 0.01mm. In the transition from gneiss to gouge the amphibole is crushed and floats between other minerals as a very local matrix. Feldspar and quartz are intact.
Classification:	Tonalitic gneiss

Sample:MBR06, Rød, Tjelle 2009	
Macroscopic description:	
Colour:	1) Dark grey/black gneiss 2) Light pink gneiss with dark pink/red veins
Minerals:	Quartz, feldspar, amphibole, biotite, zeolite
Grain size:	0.5-1mm
Structure:	Foliation
Other characteristics: Mineral-filled fractures	
Microscopic description:	
Mineral content:	qz (50%), pl (40%), bt (5%), ep (1%), sp (1%), opaque
Texture:	Holocrystalline, fine-grained –microcrystalline rock with xenoblastic crystal limitations Heterogranular, gneissic with foliation particularly in the dark part Boundary between dark and light gneiss is marked with a brown/opaque string
Mineral description:	
Quartz:	Grain size: 0.1-0.3mm Amobidal with lobate margins
Epidote:	Grain size: 0.05-0.1mm Brown/yellow with high relief
Plagioclase:	Grain size: 0.2-1mm. Brown colour in PPL Saussuritizated Lack twins
Sphene:	Grain size: 0.2-0.5mm Subhedral with straight margins.
Biotite:	Grain size: 0.1-0.2mm Lamellar with straight margins. Colour is brown to beige. 3rd order interference colours.
Classification:	Amphibolitic gneiss (and tonalite gneiss)

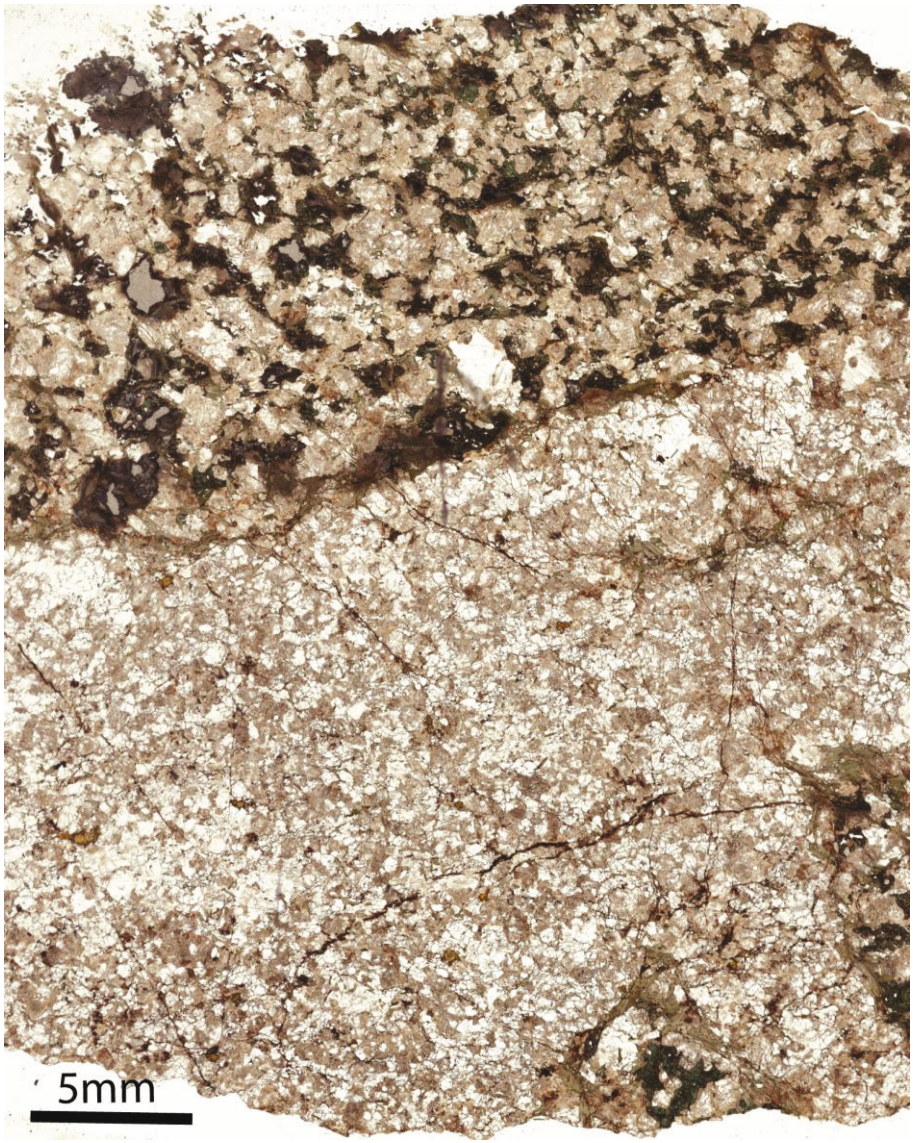

Sample:MBR07, Rød, Tjelle 2009 Host rock	
Macroscopic description:	
Colour:	Fresh fracture: pink to grey. Weathered surface: dark grey to yellow/green
Minerals:	Quartz, feldspar, amphibole, biotite
Grain size:	1mm
Structure:	Fractured
Microscopic description: Modal analysis (400 points)	
Mineral content:	qz (47.5%), pl (30.2%), kfs (20%), bt (1.2%), cl (0.7%) , ep (0.2%), sp (%), opaque (<1%)
Texture:	Holocrystalline, xenoblastic rock. Medium grained – microcrystalline. Gneissic, although the foliation is not very prominent.
Mineral description:	
Quartz:	Grain size: 0.1-1mm
Plagioclase:	Grain size: 0.1-2mm Saussuritizated, making it brown and rough Tabular with straight to lobate margins
Alkalifeldspar:	Grain size: 0.2-1mm Prominent twins Tabular with straight to lobate margins
Biotite:	Grain size: 0.2-0.4 mm Lamellar with straight margins
Chlorite:	Grain size: 0.2-0.5mm Lamellar with straight margins
Epidote:	Grain size: 0.2mm Yellow with high positive relief
Sphene:	Grain size: 0.1-0.2mm
Classification:	(Monzo-)granitic gneiss

VIK – Thin sections

Host rock: Granitic gneiss

Appendix 1 - Thin section descriptions, Vik

Sample: MBV01, Vik 2009	
Macroscopic description:	
Colour:	Light red to greyish green with pink/white Zeolite
Minerals:	Quartz, feldspar, zeolite
Grain size:	0.1-1mm
Structure:	Foliation. Opaque lineations. Both green and red breccia
Microscopic description:	
Mineral content:	ze (~90%) = matrix and veins. Clasts of qz, pl, kfs, abl, bt, opaque
Texture:	Bimodal grain size: Clasts: 0.1-0.2mm Matrix: <0.01mm = zeolite
Mineral description:	
Zeolite:	Grain size: 0.1 or smaller Perfect cleavage in {010}
Matrix:	It seems to have impacted and brecciated the ultracataclasite, making a micro-breccia with clasts of opaque coated ultracataclasites
Classification:	Micro ultra-cataclasite, brecciated in lower right part, close to a pocket of pseudotachylyte/ ultracataclasite

Vik 1

Sample: MBV02, Vik 2999	
Macroscopic description:	
Colour:	Green and pink in fresh fractures. Grey/green in weathered fractures.
Minerals:	Feldspar, amphibole, biotite, white zeolite
Grain size:	0.1-4mm
Structure:	Fractured fault rock
Microscopic description:	
Mineral content:	ze (~90%), ~10% clasts of cl, bt, abl, kfs, ap, zr, pl
Texture:	Red part: very fine grained zeolite bearing breccia Grain size up to 0.2mm. Sub rounded clasts Green part: very similar, but with more variations on the clasts.
Mineral description:	
Laumontite:	Grain size: < 0.2mm. Perfect cleavage in {010} and {110}
Microcline:	Grain size: < 0.4mm
Apatite:	Grain size: High relief
Zircon:	Grain size: < 0.1mm High relief. Subhedral crystal habit. Pleochroic halo. 3rd order interference colours.
Amphibole:	Grain size: Green and with 60-90° cleavage. Anhedral and sub angular.
Plagioclase:	Saussuritized
Classification:	Micro ultra-cataclasite – almost pure zeolite

Sample: MBV03, Vik 2999	
Macroscopic description:	
Colour:	Green matrix and pink clasts. Dark green mineral lineations.
Minerals:	Feldspar, quartz, amphibole and epidote.
Grain size:	Clasts: 0.5-10mm. Matrix: <1mm
Structure:	Clasts are of pink proto-breccia and older breccias
Microscopic description:	
Mineral content:	Matrix: (70%) The gneiss composition is: kfs (30%), qz (20%), pl (20%), ap (10%), abl (10%), bt (5%), sp (2%)
Texture:	Clast size is 0.2-10 mm Biotite, amphibole and zircon are aligned along foliation in gneiss clasts. Excluding the larger gneiss clasts this is a fine grained breccia of 0.02-0.2mm. Most of the clasts are isolated minerals like amphibole, zircon, quartz and microcline. Other clasts are aggregates if many minerals, but most of the clasts are remnants from an older breccia. This is bright zeolite aggregates mixed with other minerals.
Mineral description:	
Microcline:	Grain size: 0.3-4 mm
Apatite:	Grain size: 0.5-1.5 mm High relief
Sphene:	Grain size: <0.3 mm High relief. Subhedral crystal habit. Extreme interference colours.
Amphibole:	Grain size: 0.1-1.2 mm Green with 60-90° cleavage
Zircon:	Grain size: 0.05-0.4 mm Halo. 3rd order interference colours. Subhedral. High relief.
Matrix:	Zeolite
Classification:	Cataclasite with clasts • proto-breccia of granitic gneiss • micro-breccia

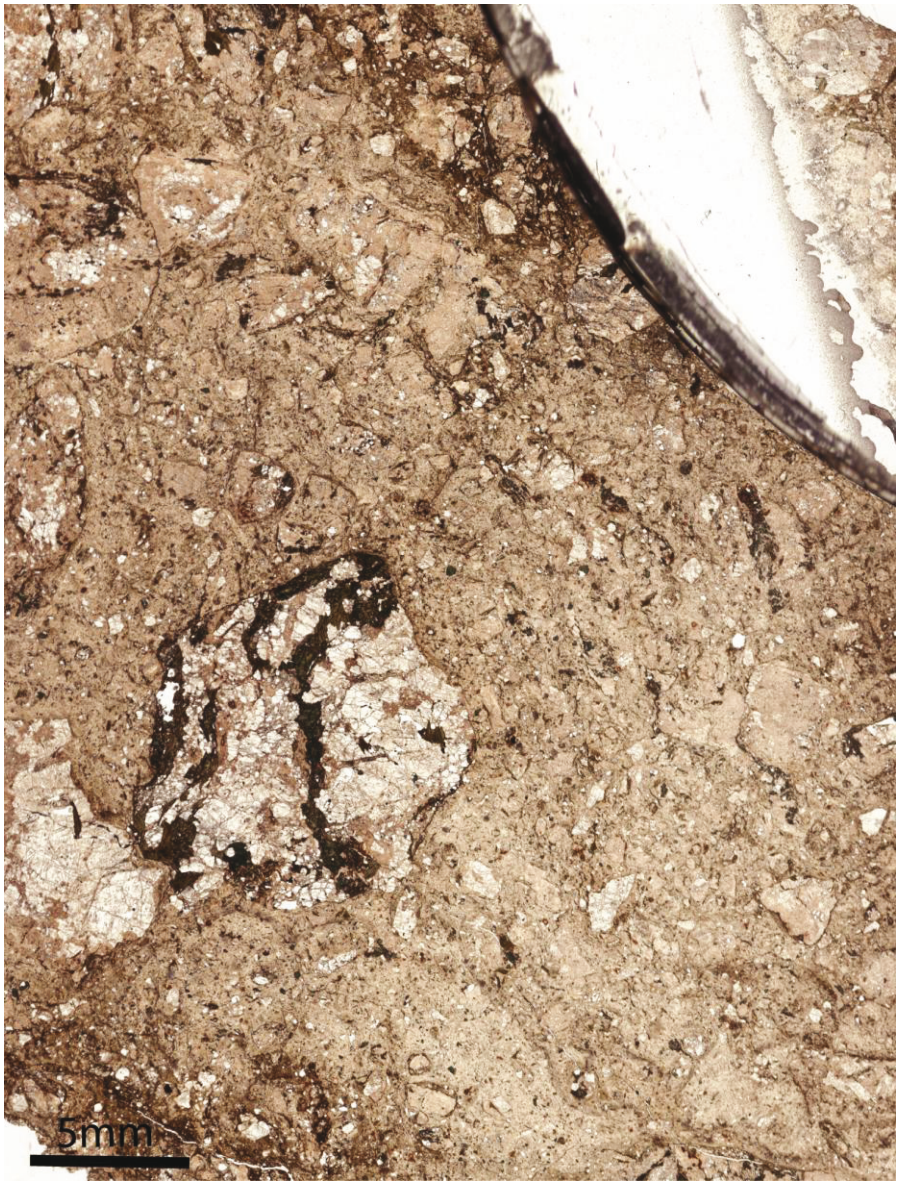

Sample: MBV04, Vik 2999	
Macroscopic description:	
Colour:	Light pink with white zeolite veins and light green (epidote) lineations
Minerals:	Quartz, feldspar, biotite, epidote, zeolite
Grain size:	0.1-1mm
Structure:	Zeolite veins
Microscopic description:	
Mineral content:	matrix (70%), kfs (15%), ap (10%), bt (2%), opaque (3%)
Texture:	Brecciated to a fine-grained to gougy breccia. Heterogranular with matrix <0,05mm. Clasts are sub-angular to sub rounded.
Mineral description:	
Microcline:	Grain size: 1mm. Anhedral
Apatite:	Grain size: 0.05-1mm. Anhedral to subhedral
Chlorite:	Grain size: 0.15mm. Pseudomorph from biotite. Green with high interference colours
Matrix:	Matrix consists of a mix of saussuritized plagioclase and zeolite
Classification:	Micro-breccia

Sample: MBU05, Vik 2009	
Macroscopic description:	
Colour:	Light pink/red
Minerals:	Alkali feldspar, quartz, amphibole
Grain size:	1-20mm Pegmatite
Structure:	Fractured
Microscopic description:	
Mineral content:	kfs (60%), pl (20%), qz (20%), bt (1%), cl (1%)
Texture:	Holocrystalline, xenoblastic, coarse, crystalline rock Comminuted between large grains of microcline.
Mineral description:	
Alkali feldspar:	Grain size: 0.4-20mm Microcline with well developed twins Tabular with straight to lobate margins. Subhedral
Quartz:	Grain size: 0.1-1mm Amobidal with straight to lobate/caries margins.
Plagioclase:	Grain size: 0.5-1mm Saussurite is common. Grains are anhedral and diffuse due to saussuritization. Remnants of albite twins are seen. Spot-antiperthite
Matrix:	Matrix consists of a mix of saussuritized plagioclase and zeolite
Classification:	Proto-brecciated pegmatitic quartz-syenite

Sample: MBV06, Vik 2999	
Macroscopic description:	
Colour:	Pink with black stripes
Minerals:	Feldspar, quartz, biotite, amphibole, zeolite
Grain size:	1-10mm
Structure:	Foliation and mineral veins
Microscopic description:	
Mineral content:	kfs (30-40%), pl (20-30%), la (10-20%), qz (5-10%), bt (5%), abl (5%), sp (5%), cl (3%), ep(2%)
Texture:	Holocrystalline rock with xenoblastic crystal growth. The rock is crystalline and medium-grained.
Mineral description:	
Alkali feldspar:	Grain size: 0.3-3 mm Microcline with some sericitization in two directions Tabular with straight to lobate margins. Anhedral.
Quartz:	Grain size: 0.2-0.4mm Undulating extinction. Highly fractured. Amobidal with straight to lobate/caries margins.
Plagioclase:	Grain size: diffuse grains Saussurite is common. Grains are anhedral and diffuse due to saussuritization. Remnants of grains are seen. Spot-antiperthite
Amphibole:	Grain size: 0.1-1mm 60-90 degrees cleavage Prismatic with straight to lobate margins. Colour is green.
Biotite:	Grain size: 0.1-0.5mm Brown to green with 4th order interference colours Parallel extinction Prismatic to lamellar with straight grain boundaries
Sphene:	Grain size: 0.1-0.2mm Pale brown, high relief. Associated with or reticent in biotite/amphibole. Anhedral crystals. Twins
Laumontite	Grain size: 0.2mm. Euhedral. Colour is light brown. Grown in veins.
Chlorite:	0.1-0.5mm. Pseudomorf from biotite
Classification:	Altered quartz-monzonite

Sample: MBV07, Vik 2009 Host rock	
Macroscopic description:	
Colour:	Fresh fracture: Grey with black stripes. Weathered surface: yellow-green
Minerals:	Quartz, feldspar, biotite, amphibole
Grain size:	0.5-2mm
Structure:	Foliation
Microscopic description: Modal analysis (400 points)	
Mineral content:	qz (41.2%), pl (23.7%), bt (14.5%), abl (12%), kfs (5.7%), sp (2.4%), ep (0.2%)
Texture:	Holocrystalline rock with xenoblastic crystal growth. The rock is crystalline medium-grained with grains of 0.5-2mm. It is heterogranular nematoblastic and gneissic. The dark/light layers show a clear foliation.
Mineral description:	
Quartz:	Grain size: 0.1-2mm Undulating extinction Myrmekite is common Amobidal with straight to lobate/caries margins.
Plagioclase:	Grain size: 0.5-2mm Saussurite is common Albite twins Tabular with straight to lobate grain boundaries
Alkali feldspar:	Grain size: 0.2-4mm Often in aggregates with myrmekite Tabular with straight to lobate grain boundaries
Amphibole:	Grain size: 0.2-1.5mm 60-90 degrees cleavage Prismatic with straight margins. Needle grooves
Biotite:	Grain size: 0.1-2mm Brown with 4th order interference colours Parallel extinction Prismatic with straight grain boundaries
Sphene:	Grain size: 0.2-0.4mm Pale brown, high relief. Associated with or reticent in biotite/amphibole
Classification:	Granitic gneiss

Appendix 2 – LIDAR models

Appendix 2 – LIDAR models

RØD

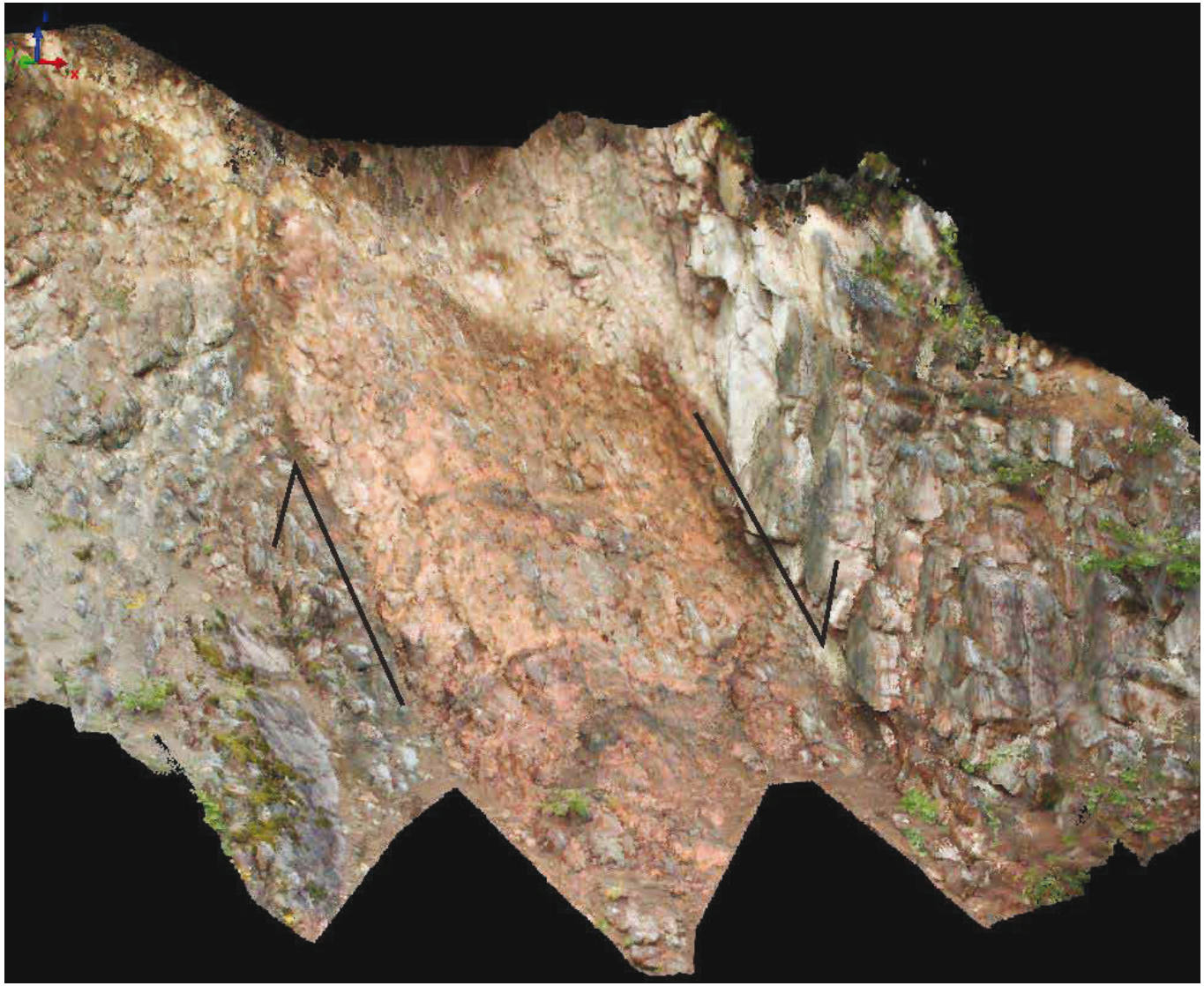

Appendix 2 – LIDAR models

VIK

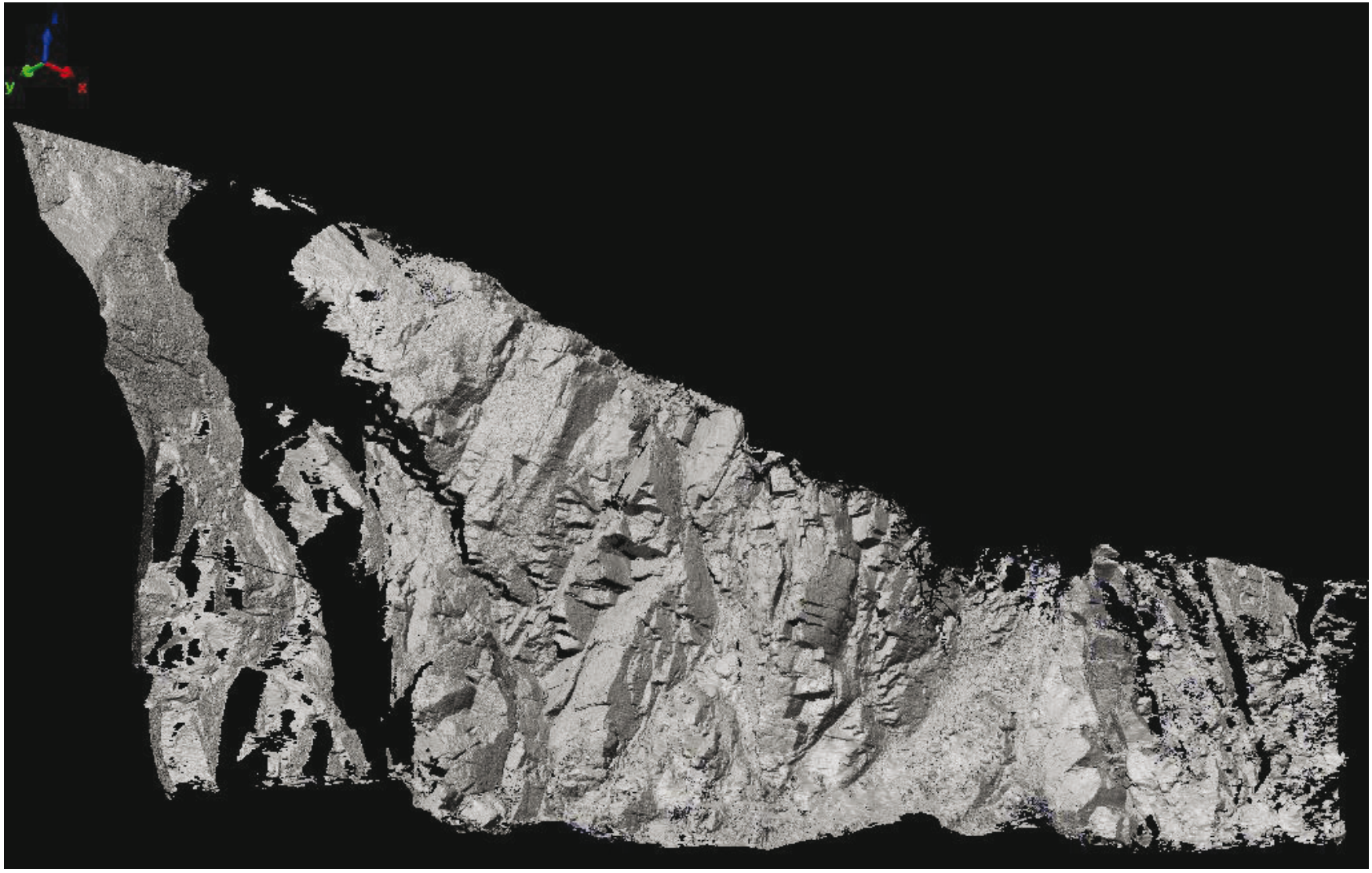

Appendix 2 – LIDAR models

VIK

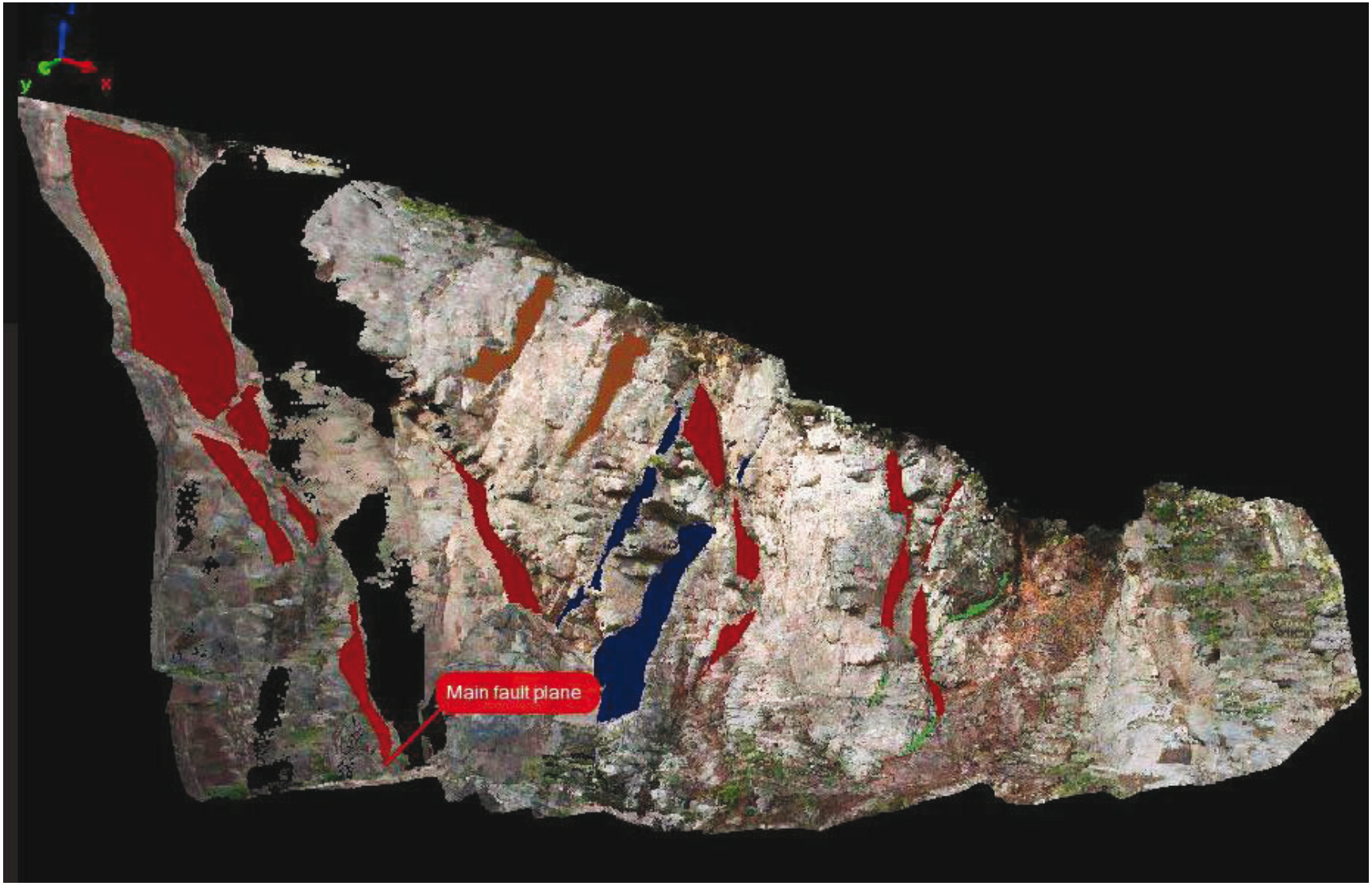

Appendix 3 – XRD analysis

Mulvik

MB02

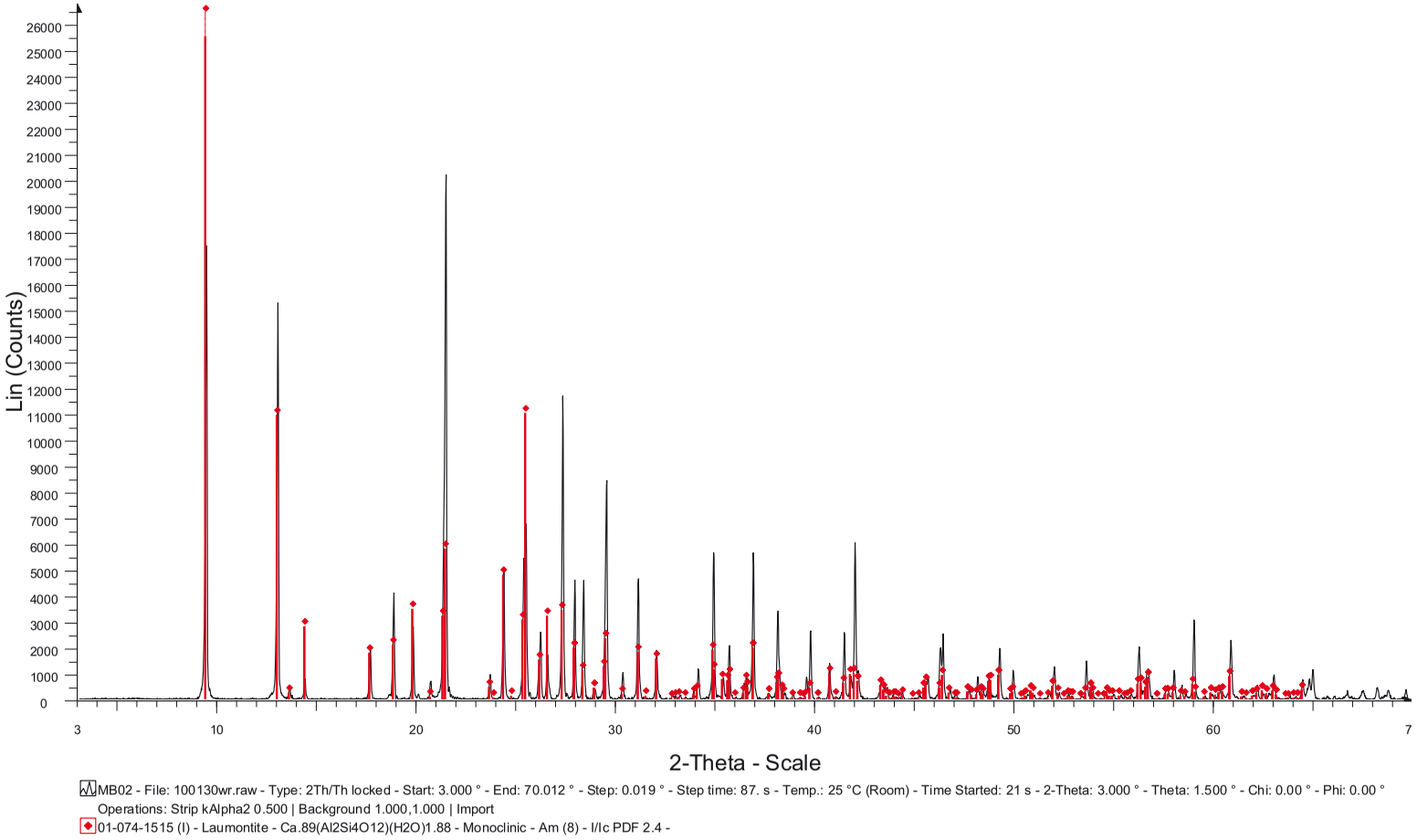
Lin (Counts)
26000
25000
24000
23000
22000
21000
20000
19000
18000
17000
16000
15000
14000
13000
12000
11000
10000
9000
8000
7000
6000
5000
4000
3000
2000
1000
0
3
10
20
30
40
50
60
7
2-Theta - Scale
MB02 - File: 100130wr.raw - Type: 2Th/Th locked - Start: 3.000 ° - End: 70.012 ° - Step: 0.019 ° - Step time: 87. s - Temp.: 25 °C (Room) - Time Started: 21 s - 2-Theta: 3.000 ° - Theta: 1.500 ° - Chi: 0.00 ° - Phi: 0.00 °
Operations: Strip kAlpha2 0.500 | Background 1.000,1.000 | Import
01-074-1515 (I) - Laumontite - Ca.89(Al2Si4O12)(H2O)1.88 - Monoclinic - Am (8) - I/Ic PDF 2.4 -

Rød

MBR01

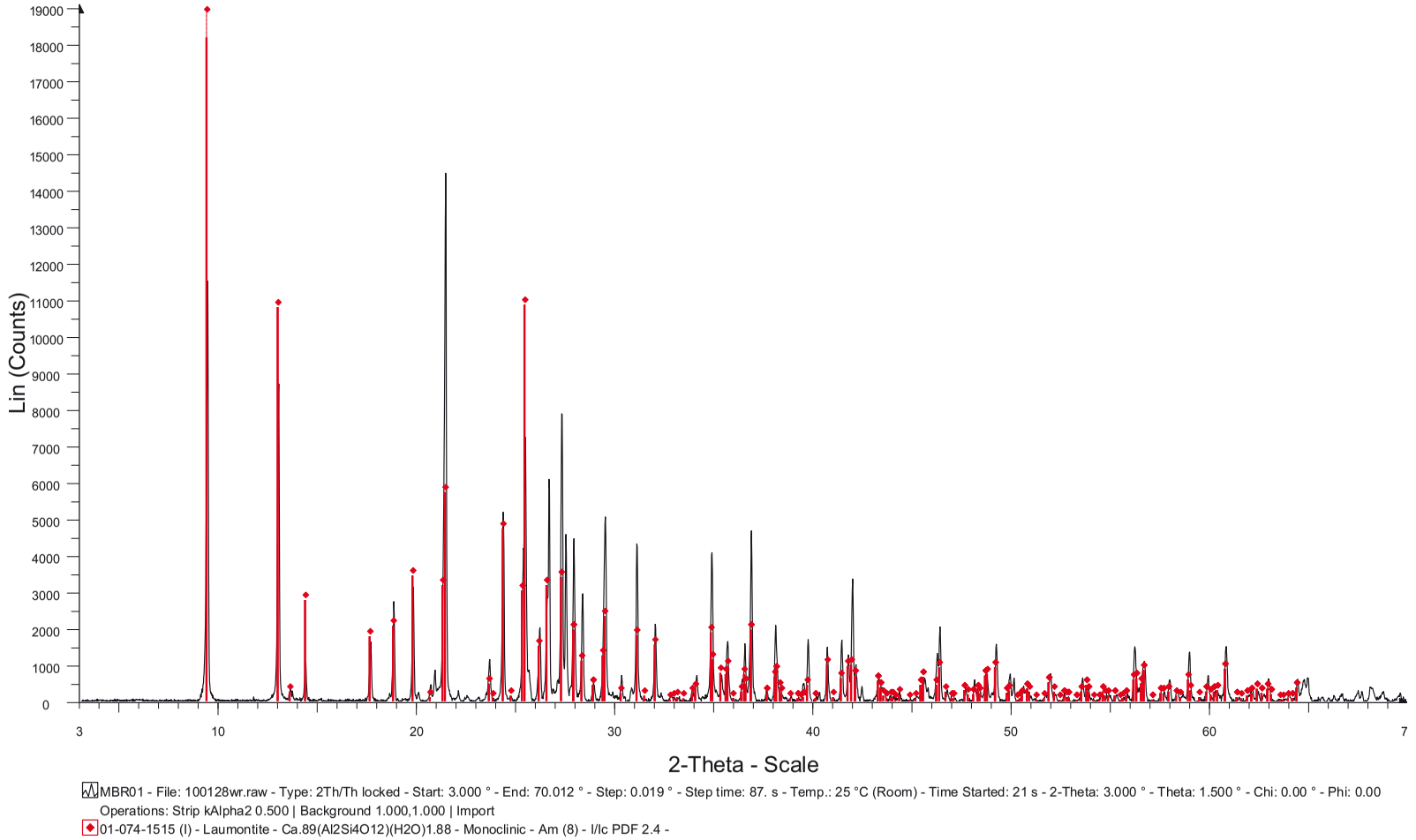
Lin (Counts)
19000
18000
17000
16000
15000
14000
13000
12000
11000
10000
9000
8000
7000
6000
5000
4000
3000
2000
1000
0
3
10
20
30
40
50
60
7
2-Theta - Scale
MBR01 - File: 100128wr.raw - Type: 2Th/Th locked - Start: 3.000 ° - End: 70.012 ° - Step: 0.019 ° - Step time: 87. s - Temp.: 25 °C (Room) - Time Started: 21 s - 2-Theta: 3.000 ° - Theta: 1.500 ° - Chi: 0.00 ° - Phi: 0.00
Operations: Strip kAlpha2 0.500 | Background 1.000,1.000 | Import
01-074-1515 (I) - Laumontite - Ca.89(Al2Si4O12)(H2O)1.88 - Monoclinic - Am (8) - I/Ic PDF 2.4 -

Vik

MBV06

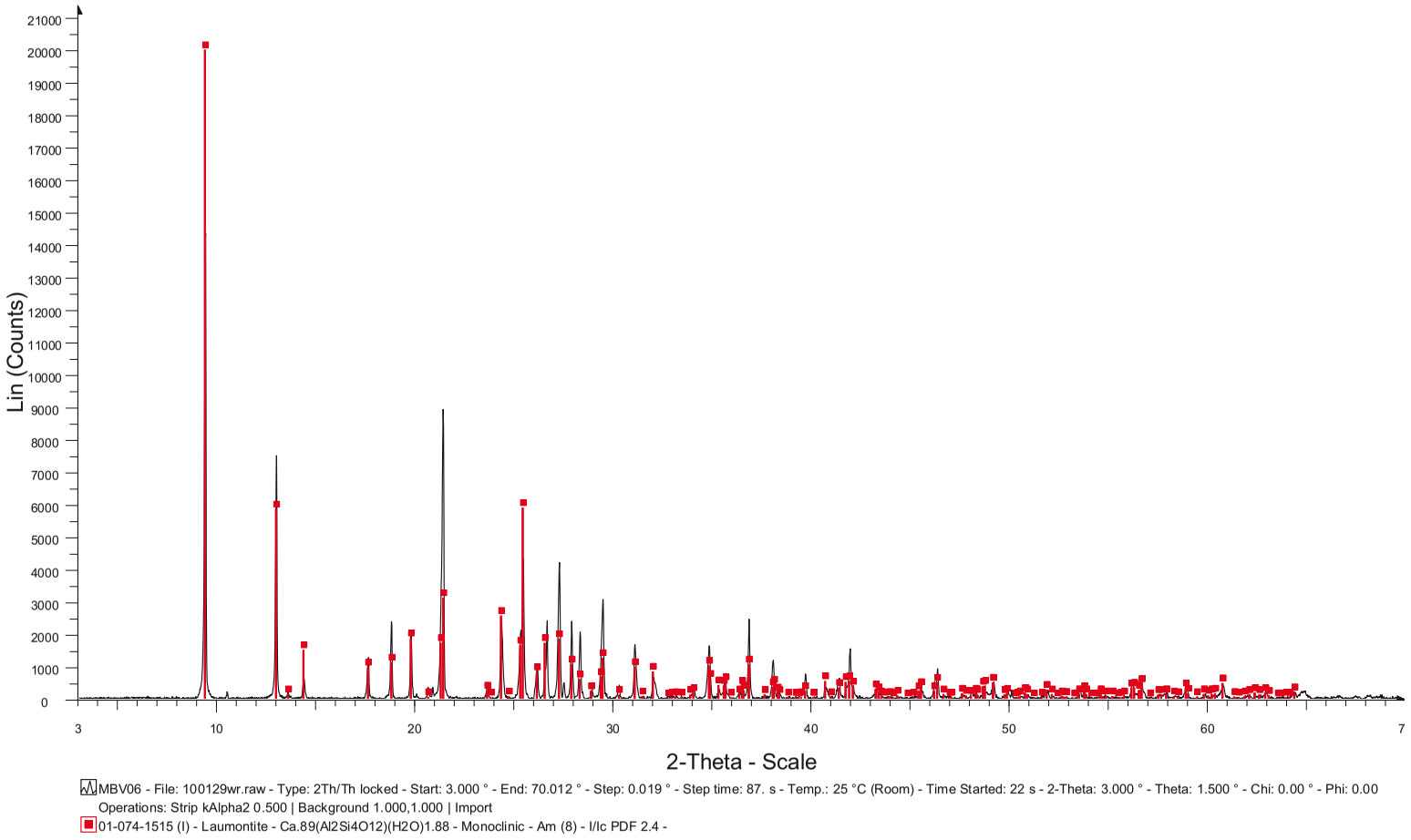
Lin (Counts)
21000
20000
19000
18000
17000
16000
15000
14000
13000
12000
11000
10000
9000
8000
7000
6000
5000
4000
3000
2000
1000
0
3
10
20
30
40
50
60
7
2-Theta - Scale
MBV06 - File: 100129wr.raw - Type: 2Th/Th locked - Start: 3.000 ° - End: 70.012 ° - Step: 0.019 ° - Step time: 87. s - Temp.: 25 °C (Room) - Time Started: 22 s - 2-Theta: 3.000 ° - Theta: 1.500 ° - Chi: 0.00 ° - Phi: 0.00
Operations: Strip kAlpha2 0.500 | Background 1.000,1.000 | Import
01-074-1515 (I) - Laumontite - Ca.89(Al2Si4O12)(H2O)1.88 - Monoclinic - Am (8) - I/Ic PDF 2.4 -